NASA CONTRACTOR REPORT

NASA CR-57

NASA CR-576

NONGREY RADIATION EFFECTS ON THE BOUNDARY LAYER OF AN ABSORBING GAS OVER A FLAT PLATE

by A. M. Smith and H. A. Hassan

Prepared by
RESEARCH TRIANGLE INSTITUTE
Durham, N. C.
for Langley Research Center

NATIONAL AERONAUTICS AND SPACE ADMINISTRATION • WASHINGTON, D. C. • SEPTEMBER 1966

NONGREY RADIATION EFFECTS ON THE BOUNDARY LAYER OF AN ABSORBING GAS OVER A FLAT PLATE

By A. M. Smith and H. A. Hassan

Prepared under Contract No. NAS 1-4270 by
RESEARCH TRIANGLE INSTITUTE
Durham, N.C.

for Langley Research Center

NATIONAL AERONAUTICS AND SPACE ADMINISTRATION

For sale by the Clearinghouse for Federal Scientific and Technical Information
Springfield, Virginia 22151 – Price $3.00

FOREWORD

This report was prepared for the Langley Research Center, National Aeronautics and Space Administration, under the contract entitled "A Research Study of Radiative Energy Transfer Considerations for a Reentry Vehicle with an Absorbing and Emitting Boundary Layer". The Contract No. was NAS1-4270. The technical monitor for NASA was W. B. Olstad of the Gas Physics Section, Aerophysics Division. The work documented herein was performed by A. M. Smith of the Research Triangle Institute with Dr. H. A. Hassan of North Carolina State University at Raleigh serving as a consultant.

NONGREY RADIATION EFFECTS ON THE BOUNDARY LAYER OF AN ABSORBING GAS OVER A FLAT PLATE

By A. M. Smith and H. A. Hassan*
Research Triangle Institute

SUMMARY

A study of the nongrey radiation effects on the laminar boundary layer of an absorbing gas over a flat plate is presented. The nongrey model employed assumes an absorption coefficient with a stepwise frequency dependence. Such a model gives a reasonable fit to the published data on monochromatic absorption coefficient for air.

Examination of the optical thicknesses corresponding to the various step functions shows that the maximum optical thickness based on boundary layer thickness and maximum absorption coefficient, from the data of Sewell, is less than unity in the boundary layer over a flat plate. This conclusion is based on a consideration of missions such as a reentry of a space probe from Mars.

For typical temperatures and Eckert numbers at the edge of the boundary layer, it is shown that, for high external flow emissivities the nongrey radiative flux to the wall is greater than the grey while the grey convective flux is greater than the nongrey. The total heat transfer, based on the nongrey model, is found to be greater than that based on the grey model, for a combination of high wall and high external flow emissivities or, low wall and low external flow emissivities. Also, for high external flow emissivities, the ratio of the radiative to the convective flux is always greater than unity; while for low external flow emissivities, the ratio is greater or less than unity depending on the wall emissivity and external flow Eckert number. These conclusions are based on numerical calculations for a temperature of 10 000° K and higher at the edge of the boundary layer.

INTRODUCTION

The advent of space flight at velocities greater than the escape velocities focused increased attention on the problem of radiative heating. For such velocities, the transfer of energy by radiation is

---

*Professor of Mechanical Engineering, N. C. State University, Raleigh, North Carolina.

comparable to that by convection and therefore, the coupling between the radiative transfer and other energy transport processes may have a large influence on the flow field around the reentry vehicle.

The object of this work is to consider the influence of the nongrey radiation effects on the heat transfer in the boundary layer of an absorbing gas over a flat plate. The wall and the external flow are not considered to be perfect absorbers and the influence of their optical properties on heat transfer is investigated. This study is motivated by the fact that results based on the grey approximation may, under certain conditions, be of little practical use as a result of the large variation of the absorption coefficient with frequency, especially at the higher temperatures of interest here.

An attempt at considering the effects of a nongrey model on the heat transfer of a boundary layer of an absorbing gas over a flat plate has been made by Cess (ref. 1). He ignored the viscous dissipation term in the energy equation and assumed, in addition to a Prandtl number of unity and the usual linear viscosity law, that the monochromatic absorption coefficient is independent of temperature and the Planck mean is a reciprocal function of temperature. His results for the nongrey model differed substantially from those for the grey model. Although the assumptions introduced by Cess regarding the temperature dependence of the monochromatic and total absorption coefficients are unrealistic for most gases, especially for air, his model, nevertheless, serves to illustrate the importance of nongrey effects.

A much improved nongrey model has been introduced by Olstad (ref. 2) in his analysis of the inviscid stagnation shock layer. He assumed an absorption coefficient with a stepwise dependence on the wavelength. To illustrate the importance of the nongrey effects, he assumed, for the sake of simplicity, that the pressure and temperature dependence in each wavelength interval is given by that of the Planck mean. His results also demonstrate the significance of the nongrey effects.

Examination of the data on monochromatic absorption coefficients given by Sewell (ref. 3) shows that it can be closely approximated by a stepwise frequency dependence. The pressure and temperature dependence in each frequency interval do not correspond, however, to that of the Planck mean or Rosseland mean. Using such a representation the divergence of the monochromatic radiative flux vector can be integrated in closed form to yield the divergence of the radiative flux vector. As a result of this, it is shown, in general, that the divergence of the radiative flux vector can be represented as a linear combination of terms corresponding to the usual thin, self-absorbing, and thick approximations. Using a reentry of a space probe from Mars and from the far solar system (ref. 4) as typical missions, it is shown that, under the most pessimistic estimates, the maximum optical thickness based on a characteristic length equal to the maximum boundary layer thickness on a ten meter plate is less than unity. It is concluded, therefore, that the boundary layer on a flat plate for such missions, is optically thin.

The thin approximation coupled with a two-step monochromatic absorption coefficient is employed in analyzing the boundary layer of an absorbing gas on a flat plate. The wall is assumed to be opaque, diffuse reflecting, and emitting; and the external flow is assumed to be emitting and nonreflecting. The wall is assumed to be grey and the emissivity of the external flow is assumed to be frequency dependent with the dependence being, for the sake of convenience, identical to that of the absorption coefficient.

Since the radiative flux is negligible for low external flow temperatures (ref. 5) the calculations were carried out for a $T_e = 10{,}000°K$. The results show that, for high external flow emissivities, the ratio of the radiative flux to the convective flux is always greater than unity. However, for low external flow emissivities, this ratio is influenced by the wall emissivity, being smaller than one for low wall emissivities and high Eckert numbers and about one or greater for high wall emissivities and low Eckert numbers.

For the higher Eckert numbers, the nongrey radiative flux is greater than the grey and the grey convective flux is greater than the nongrey if the external flow emissivity is large. When the external flow emissivity is low, the reverse is true. The total nongrey heat transfer is found to be greater than the grey for a combination of high wall and high external flow emissivities or, a combination of low wall and low external flow emissivities.

SYMBOLS

B_λ	Planck's distribution function (eq. (A11))
B_ν	Planck's distribution function (eq. (9))
Bo	Boltzmann number
c	speed of light
E	specific internal energy
F_i^R	radiation energy flux vector
$F_{\nu i,i}$	divergence of the monochromatic radiative flux vector
$g_m(\nu)$	function defined in eq. (11)
H_∞	freestream total enthalpy
h	specific enthalpy, Planck's constant or altitude
h_*	reference enthalpy in eq. (73)

$\bar{h}_o$	solution of eq. (70) in the absence of radiation
I_ν	specific intensity of radiation
J_λ	spectral radiance in eqs. (C8) and (C9)
J_T	total radiance in eqs. (C3), (C4), (C10), (C11), and (C12)
j_λ	spectral emission coefficient
K	mean linear absorption coefficient in eqs. (C7), (C10), and (C11)
K_ν, K_λ	linear spectral absorption coefficients
K_p	Planck mean linear absorption coefficient
K_R	Rosseland mean linear absorption coefficient
$K_m(x_i)$	height of the mth step function in eq. (11) (see fig. 2)
k	coefficient of conductivity or Boltzmann's constant
L	characteristic length
M_∞	freestream Mach number
P_{ij}	pressure tensor
P	pressure
Pr	Prandtl number
q_i	heat flux (other than radiative) vector
q_o^R	characteristic value of radiation energy flux vector
q_ν	spectral radiative flux
q_R	global radiative flux
q_{cw}	convective wall heat flux for a radiating gas
q_{cwo}	convective wall heat flux for a nonradiating gas
q_{tw}	total wall heat flux
Re_∞	freestream Reynolds number
r	reflectivity
T	temperature

T_s	stagnation temperature
u_i	velocity vector
u_e^2/h_e	Eckert number
Z	compressibility factor
α_j	function in eq. (13) and (A9)
$\alpha_j(\beta_j)$	function in eq. (A13)
Γ	radiation-convection parameter
Δ_m	frequency interval or intervals associated with $K_m(x_i)$ (see fig. 2)
δ	boundary layer thickness
ε	emissivity
ε/L	emissivity per cm
$\varepsilon_\nu, \varepsilon_\lambda$	spectral gas emissivity in eqs. (C2) and (C8)
κ_p	Planck mean mass absorption coefficient
κ_j	mass absorption coefficients in eqs. (D10) and (D11)
λ	wavelength
μ	coefficient of viscosity
ν	frequency
ρ	density
σ	Stefan-Boltzmann constant
τ_ℓ	characteristic optical thickness or Bouguer number for a grey gas
τ_{jo}	Bouguer number for a nongrey gas
τ'_{jo}	effective Bouguer number for optically thin nongrey gas
τ''_{jo}	effective Bouguer number for optically thick nongrey gas
ω	wavenumber or solid angle

Subscripts

e	external flow conditions
g	grey gas
o	reference state
s.l.	sea level conditions
w	wall conditions
ν	frequency dependent quantity

Superscripts

-	dimensionless or normalized quantity

ANALYSIS

The conservation equations for the laminar boundary layer of a radiating gas may be obtained from the general equations of radiation gas dynamics derived by Goulard (ref. 6), which can be expressed as

$$\frac{D\rho}{Dt} + \rho u_{i,i} = 0 \tag{1}$$

$$\rho \frac{Du_i}{Dt} + P_{ij,j} = 0 \tag{2}$$

$$\rho \frac{DE}{Dt} + q_{i,i} + F^R_{i,i} + P_{ij}\, u_{j,i} = 0 \tag{3}$$

where ρ, E, u_i, q_i, F^R_i, P_{ij} denote, respectively, the density, specific internal energy, velocity, heat flux (other than radiative) vector, radiation energy flux vector and pressure tensor. In writing eqs. (2) and (3) the radiation pressure tensor and the radiation energy density were ignored compared to the (molecular) pressure tensor and specific internal energy. As has been indicated by Goulard (ref. 7) this is justified except for temperatures greater than 10^7°K or particle densities approaching zero particles/cm^3.

Except for the term $F^R_{i,i}$ appearing in eq. (3), the conservation equations are identical with those of classical gas dynamics. As a

result of this, the boundary layer equations of a radiating gas are identical with the usual boundary layer equations except that an additional term $F^R_{i,i}$ appears in the energy equation. Thus, the boundary layer equations for a steady flow of a radiating gas over a flat plate can be written as

$$\frac{\partial}{\partial x}(\rho u) + \frac{\partial}{\partial y}(\rho v) = 0 \tag{4}$$

$$\rho u \frac{\partial u}{\partial x} + \rho v \frac{\partial u}{\partial y} = \frac{\partial}{\partial y}\left(\mu \frac{\partial u}{\partial y}\right) \tag{5}$$

$$\rho u \frac{\partial h}{\partial x} + \rho v \frac{\partial h}{\partial y} = \frac{\partial}{\partial y}\left(k \frac{\partial T}{\partial y}\right) + \mu\left(\frac{\partial u}{\partial y}\right)^2 - F^R_{i,i} \tag{6}$$

where u and v are the velocity components in the x and y directions, h is the specific enthalpy, T is the temperature, and μ and k are the coefficients of viscosity and conductivity. It should be pointed out that eqs. (4) through (6) assume a flow in chemical equilibrium and, in the case where Lewis number is different from unity, k is to be interpreted as the total heat conduction coefficient which includes the effects of both conduction and diffusion.

The general expression for $F^R_{i,i}$ can be obtained from the divergence of the monochromatic radiative flux vector as

$$F^R_{i,i} = \int_0^\infty F_{\nu i,i}\, d\nu \tag{7}$$

A general expression for $F_{\nu i,i}$ has been given by Goulard (ref. 6). For nonscattering gases in local thermodynamic equilibrium and perfectly absorbing surfaces, this relation can be expressed as (see Appendix A and fig. 1)

$$F_{\nu i,i}(x_i) = 4\pi\left[K_\nu(x_i)B_\nu(x_i) - K_\nu(x_i)\int_{4\pi}\int_{\eta_i}^{x_i} K_\nu(\xi_i)B_\nu(\xi_i)\exp\left(-\int_{\xi_i}^{x_i} K_\nu ds\right) ds\, \frac{d\omega}{4\pi}\right.$$
$$\left. - K_\nu(x_i)\int_{4\pi} B_\nu(\eta_i)\exp\left(-\int_{\eta_i}^{x_i} K_\nu ds\right)\frac{d\omega}{4\pi}\right] \tag{8}$$

where K_ν is the spectral linear absorption coefficient and B_ν is Planck's distribution function

$$B_\nu = \frac{2h\nu^3}{c^2} \frac{1}{\exp(h\nu/kT) - 1} \tag{9}$$

It is to be noted that the integral

$$\int K_\nu ds \tag{10}$$

which is usually referred to as the optical thickness (for frequency ν) is evaluated along a line $S(\ell_i)$ with direction cosines ℓ_i. It is evident from eq. (8) that, before one can carry out the integration in eq. (7) the frequency dependence of K_ν should be specified. The simplest case, where K_ν is independent of frequency, leads to the well-known grey case. In general, arbitrary dependence of K_ν on frequency leads to a rather complicated integration which would have to be carried out numerically. The desirability of choosing a K_ν which would represent a fair approximation to physical reality and which would make it possible to carry out the integration in closed form is evident. One way in which this can be achieved is to approximate K_ν by a number of step functions (see fig. 2), i.e.,

$$K_\nu(x_i,\nu) = \sum_{m=1}^{n} K_m(x_i) g_m(\nu)$$

where

$$g_m(\nu) = \begin{cases} 1 \text{ if } \nu \in \Delta_m \\ \\ 0 \text{ otherwise} \end{cases} \tag{11}$$

with Δ_m the frequency interval or intervals in which K_ν is $K_m(x_i)$. Substitution of eq. (11) into eq. (8), (see Appendix A), yields

$$F^R_{i,i} = 4\sigma \sum_{j=1}^{n} \left[K_j \alpha_j T^4 - K_j \int_{4\pi} \int_{\eta_i}^{x_i} K_j(\xi_i) \alpha_j(\xi_i) T^4(\xi_i) \exp\left(- \int_{\xi_i}^{x_i} K_j ds \right) ds \, \frac{d\omega}{4\pi} \right.$$

$$\left. - K_j \int_{4\pi} \alpha_j(\eta_i) T^4(\eta_i) \exp\left(- \int_{\eta_i}^{x_i} K_j ds \right) \frac{d\omega}{4\pi} \right] \tag{12}$$

where

$$\alpha_j = \frac{\int_{\Delta_j} B_\nu d\nu}{\sigma T^4/\pi} \quad ; \quad \sum_{j=1}^{n} \alpha_j = 1 \tag{13}$$

As a result of using the approximation indicated in eq. (11), it is seen from eq. (12) that the contributions of the various frequency intervals to the divergence of the radiative flux vector add up linearly. The implication of this interesting property will be discussed below.

The grey gas approximation follows from eq. (11) by choosing $n = 1$, $g_1 = 1$ and Δ_1 the frequency interval (o,∞). This rule is to be followed in reducing the nongrey expressions derived here to the corresponding grey expressions. In this connection, it is seen from eq. (12) that there is no grey equivalent to a nongrey model; this may be compared with eq. (4.23) of ref. 6 where such an equivalence is implied.

SIMILARITY PARAMETERS

Since eq. (6) is frequency independent, the similarity parameters which characterize radiation transfer in relation to other modes of energy transfer are identical with those derived by Goulard (ref. 7) for a grey gas. The dimensionless quantities appropriate for boundary layer analysis are

$$\bar{x} = \frac{x}{L} \; , \; \bar{y} = \frac{y}{\delta} \; , \; \bar{u} = \frac{u}{u_o} \; , \; \bar{v} = \frac{v}{u_o}\frac{L}{\delta} \; , \; \bar{h} = \frac{h}{h_o} \; ,$$

$$\bar{T} = \frac{T}{T_o} \; , \; \bar{\rho} = \frac{\rho}{\rho_o} \; , \; \bar{k} = \frac{k}{k_o} \; , \; \bar{\mu} = \frac{\mu}{\mu_o} \; , \; \bar{F}_i^R = \frac{F_i^R}{q_o^R} \tag{14}$$

where the subscript 'o' designates some reference state, δ is the boundary layer thickness and L is a characteristic length which may be chosen as the length of the plate. Introducing eq. (14) into eq. (6) one finds that the ratio of energy transfer by radiation to that by convection is characterized by the dimensionless number

$$\Gamma = \frac{q_o^R}{\rho_o u_o h_o}\frac{L}{\delta} \tag{15}$$

first introduced by Unsöld (ref. 8). If the characteristic value of the radiation energy flux vector can be chosen as

$$q_o^R = \sigma T_o^4 \tag{16}$$

Γ reduces to the inverse of the Boltzmann number Bo

$$\Gamma = \frac{\sigma T_o^4}{\rho_o u_o h_o} \frac{L}{\delta} = Bo^{-1} \tag{17}$$

In addition to the above "extrinsic" dimensionless parameters, there exists "intrinsic" dimensionless parameters which govern the structure of the radiation field. These can be deduced from examination of the various forms of $F^R_{i,i}$. It may be recalled that, for a grey gas, the appropriate intrinsic parameter is the optical thickness or Bouguer number, τ_ℓ, defined as the product of a characteristic absorption coefficient and a characteristic length. In the presence of nongrey radiation, it is very difficult to define a characteristic absorption coefficient. In this connection, it may be mentioned that Olstad (ref. 2) employed a nongrey absorption coefficient given by

$$K_\nu = \gamma_j K_p \; ; \; \nu_j \leq \nu \leq \nu_{j+1} \; ; \; j = 1, \ldots, m \tag{18}$$

where the constants γ satisfy the relation

$$\sum_{j=1}^{m} \gamma_j b_j = 1$$

with

$$b_j = \frac{\int_{\nu_j}^{\nu_{j+1}} B_\nu d\nu}{\int_0^\infty B_\nu d\nu} \; , \; T = T_o \tag{19}$$

and defined an optical thickness based on K_p where K_p is the Planck mean. Using the same idea, one can define

$$K_\nu = \delta_j K_R \; ; \; \nu_j \leq \nu \leq \nu_{j+1} \; ; \; j = 1, \ldots, m \tag{20}$$

with K_R being the Rosseland mean, and employ an optical thickness based on K_R. In this case, the δ_j's satisfy the relation

$$\sum_{j=1}^{m} \frac{a_j}{\delta_j} = 1$$

with

$$a_j = \int_{\nu_j}^{\nu_{j+1}} \frac{dB_\nu}{dT}\, d\nu \Bigg/ \int_o^\infty \frac{dB_\nu}{dT}\, d\nu \; , \; T = T_o \tag{21}$$

As has been recognized in ref. 2, definitions like eqs. (18) and (20), have one drawback in common, namely the K_ν dependence on pressure and temperature is the same as that of the respective mean which, in a true nongrey representation, is not the case. Because of such difficulties, the concept of a representative or an effective optical thickness for nongrey representations, other than the ones mentioned above, is not feasible.

Writing eq. (12) in dimensionless form shows that one can define a characteristic optical thickness for each frequency interval Δ_j. Thus, letting

$$\bar{x}_i = \frac{x_i}{d} \; , \; \bar{s} = \frac{s}{d} \; , \; \bar{\omega} = \frac{\omega}{4\pi} \; , \; \bar{T} = \frac{T}{T_o}$$

$$\bar{F}_i^R = \frac{F_i^R}{4\sigma T_o^4} \; , \; \bar{K}_j = \frac{K_j}{K_{jo}} \; , \; \bar{\alpha}_j = \frac{\alpha_j}{\alpha_{jo}} \tag{22}$$

and substituting into eq. (12), one finds

$$\bar{F}_{i,\bar{i}}^R = \sum_{j=1}^{n} \tau_{jo}\alpha_{jo}\bar{K}_j(\bar{x}_i)\left[\bar{\alpha}_j\bar{T}^4 - \tau_{jo}\int_o^1\int_{\bar{\eta}_i}^{\bar{x}_i} \bar{K}_j\bar{\alpha}_j\bar{T}^4 \exp\left(-\tau_{jo}\int_{\bar{\xi}}^{\bar{x}_i}\bar{K}_j d\bar{s}\right) d\bar{s}d\bar{\omega} \right.$$
$$\left. - \int_o^1 \bar{\alpha}_j\bar{T}^4 \exp\left(-\tau_{jo}\int_{\bar{\eta}_i}^{\bar{x}_i}\bar{K}_j d\bar{s}\right) d\bar{\omega}\right] \tag{23}$$

where

$$\tau_{jo} = K_{jo} d \tag{24}$$

is the Bouguer number for the interval Δ_j and d is a characteristic geometric length of the radiating gas. Since τ_{jo} may have different values for different Δ_j, it is possible that in some Δ_j, $\tau_{jo} < 1$, while in another Δ_j, τ_{jo} may be of order unity and finally, in still another Δ_j, it is possible that $\tau_{jo} > 1$. The fact that τ_{jo} can have arbitrary values shows the difficulty of defining an effective optical thickness.

The role played by τ_{jo} in determining the asymptotic form of the jth bracket of eq. (23) is identical to the role played by the optical thickness in the case of grey radiation (ref. 7). Thus, for the thin case, where $\tau_{jo} < 1$, the jth bracket reduces to

$$\alpha_{jo}\tau_{jo}\left[\bar{\alpha}_j \bar{K}_j \bar{T}^4 - \bar{K}_j \int_o^1 \bar{\alpha}_j(\bar{\eta}_i)\bar{T}^4(\bar{\eta}_i)\,d\bar{\omega}\right] \tag{25}$$

It is seen from eq. (25) that an effective Bouguer number can be defined, for the thin case, by the relation

$$\tau'_{jo} = \alpha_{jo}\tau_{jo} \tag{26}$$

Since $o \leq \alpha_{jo} \leq 1$, this means that the gas may be optically thinner in this Δ_j than actually indicated by τ_{jo}.

In the case where τ_{jo} is of order unity, all the terms of the jth bracket should be retained. For the thick case, where $\tau_{jo} > 1$, it is shown in Appendix B that the jth bracket reduces to

$$-\frac{1}{3}\frac{\alpha_{jo}}{\tau_{jo}} \sum_{i=1}^{3} \frac{\partial}{\partial \bar{x}_i}\left\{\frac{1}{\bar{K}_j}\frac{\partial}{\partial \bar{x}_i}\left[\bar{\alpha}_j \bar{T}^4\right]\right\} \tag{27}$$

Similar to eq. (26), an effective Bouguer number τ''_{jo} can be defined by the relation

$$\tau''_{jo} = \frac{\tau_{jo}}{\alpha_{jo}} \geq \tau_{jo} \tag{28}$$

Thus the gas is optically thicker than indicated by τ_{jo}.

The above discussion shows that, in general, eq. (23) can be written as

$$\bar{F}^{R}_{i,\bar{i}} = \sum_{j=1}^{p} \alpha_{jo}\tau_{jo}\left[\bar{\alpha}_j\bar{K}_j\bar{T}^4 - \bar{K}_j\int_0^1 \bar{\alpha}_j\bar{T}^4 d\bar{\omega}\right] + \sum_{j=1}^{q} \tau_{jo}\alpha_{jo}\bar{K}_j\left[\bar{\alpha}_j\bar{T}^4 - \tau_{jo}\int_0^1\int_{\bar{\eta}_i}^{\bar{x}_i} \bar{K}_j\bar{\alpha}_j\bar{T}^4 \exp\left(-\tau_{jo}\int_{\bar{\xi}_i}^{\bar{x}_i}\bar{K}d\bar{s}\right)d\bar{s}d\bar{\omega} - \int_0^1 \bar{\alpha}_j\bar{T}^4\exp\left(-\tau_{jo}\int_{\bar{\eta}_i}^{\bar{x}_i}\bar{K}_j d\bar{s}\right)d\bar{\omega}\right]$$
$$- \frac{1}{3}\sum_{j=1}^{r}\left[\frac{\alpha_{jo}}{\tau_{jo}}\sum_{i=1}^{3}\frac{\partial}{\partial\bar{x}_i}\left\{\frac{1}{\bar{K}_j}\frac{\partial}{\partial\bar{x}_i}(\bar{\alpha}_j\bar{T}^4)\right\}\right] \tag{29}$$

where

$$p + q + r = n \tag{30}$$

Equation (29) shows a basic difference between grey and nongrey radiation. Since there is one characteristic optical thickness for a grey gas, it is possible to characterize the whole flow field as thin, self-absorbing or thick depending on whether $\tau_\ell \lessgtr 1$. On the other hand, in the nongrey case, such characterization is, in general, not possible unless $\tau_{jo} < 1$, $\tau_{jo} \simeq 1$ or $\tau_{jo} > 1$ for all j.

ESTIMATE OF τ_{jo} FOR RADIATING AIR IN THE BOUNDARY LAYER

To determine p, q, and r in eq. (29), it is necessary to estimate the order of magnitude of the various Bouguer numbers for the radiating boundary layer on a flat plate. The characteristic geometric length of the radiating gas may be taken as the boundary layer thickness δ and, therefore, τ_{jo} can be expressed as

$$\tau_{jo} = K_{jo}\delta$$

Since it is expected that most of the τ_{jo}'s will be much less than unity for the radiating air boundary layer, the maximum value of τ_{jo} will be estimated for a set of representative flight conditions encountered upon reentry into the earth's atmosphere. The reentry flight paths chosen are those given by Howe and Viegas (ref. 4) for reentry from a Mars mission and reentry from a far solar system mission (see fig. 3).

To estimate $(\tau_{jo})_{max}$ one needs to estimate the maximum K_{jo} and δ for the flight conditions existing along these reentry trajectories. From the calculations of Van Driest (ref. 9) and for the range of Mach numbers considered there, the correlation

$$\frac{\delta}{x}\sqrt{Re_\infty} = 2.1(M_\infty - 15) + 28 \quad , \quad M_\infty \geq 15 \tag{32}$$

may be used to calculate an upper limit for the boundary layer thickness on a flat plate for $M_\infty \geq 15$ and all calculated wall to free stream temperature ratios. Another method for estimating the boundary layer thickness can be inferred from the usual order of magnitude analysis employed in deriving the boundary layer equations. As a result of such analysis, one finds

$$\frac{\delta}{x}\sqrt{Re_x} = O(1)$$

or

$$\frac{\delta}{x} = O(\sqrt{\mu_a/\rho_a u_e x}) \tag{33}$$

where μ_a and ρ_a are representative average values of the viscosity and density in the boundary layer while u_e is the velocity at the edge of the boundary layer. Letting

$$\frac{\mu_a}{\mu_\infty} = \frac{T_a}{T_\infty} \quad , \quad \rho = \frac{P}{ZRT} \tag{34}$$

where P is the pressure, Z the compressibility factor and R is the gas constant, and assuming weak interactions, i.e.,

$$u_e \simeq u_\infty \quad , \quad P_e \simeq P_\infty$$

one finds that eq. (33) reduces to

$$\frac{\delta}{x} = 0\left(\sqrt{\frac{Z_a}{Re_\infty}}\,\frac{T_a}{T_\infty}\right) \tag{35}$$

Comparison of eqs. (32) and (35) shows that the two equations give similar results. For a given freestream total enthalpy H_∞ and pressure P_∞, all that is necessary to calculate the boundary layer thickness is a knowledge of the plate length and flight conditions. These conditions were determined from the altitude-velocity curves of fig. 3 in conjunction with the standard atmospheric data presented by COESA (ref. 10). The data of Neel and Lewis (ref. 11) for high temperature air was used in calculating the various thermodynamic properties for a given H_∞ and P_∞. As suggested by Dorrance (ref. 12) and others, T_a is usually taken as the stagnation temperature, T_s.

The maximum K_{jo} occurring at flight conditions corresponding to the trajectories of fig. 3 were calculated from the data of Sewell (ref. 3) which give the spectral emission coefficient of air versus wave number for a wide range of temperature and density. The maximum K_{jo} were calculated using the values of T_s and ρ_a (see eq. (34)) corresponding to (H_∞, P_∞) for equilibrium air. Now choosing $T_a = T_s$ underestimates ρ_a because, for a boundary layer along a flat plate,

$$P = \text{const or } Z\rho T = \text{const or } \rho T \simeq \text{const} \tag{36}$$

Since $K_j = K_j(\rho, T)$, the question arises whether such choice of temperature would lead to $(K_{jo})_{max}$. This can be seen from the consideration that K_j can be approximated as (ref. 13)

$$\begin{aligned} K_j &= c_j \rho^{\alpha} T^{\beta} \quad , \; c_j, \; \alpha, \; \beta = \text{consts} \; , \; \beta > \alpha \\ &= c_j (\rho T)^{\alpha} T^{\beta - \alpha} \end{aligned} \tag{37}$$

It is seen from eq. (36) that using $T = T_s$ in eq. (37) results in the highest value of K_j for a flat plate.

Knowing δ and $(K_{jo})_{max}$, it is possible to estimate $(\tau_{jo})_{max}$ which occurs in the boundary layer during reentry into the earth's atmosphere along the flight paths shown in fig. 3. The results for a plate three meters long are shown in fig. 4. For a plate of length L meters, the ordinate should be multiplied by $\sqrt{L/3}$. It is seen that $(\tau_{jo})_{max} < 1$. Therefore, $p \equiv n$ in eqs. (29) and (30) and the flat plate laminar boundary layer of radiating air is optically thin.

The expression for $F^{R}_{i,i}$ given in eq. (8) assumes that the external flow and the wall are perfect absorbers. A relaxation of this restriction requires replacing the last integral of eq. (8) by

$$K_\nu(x_i)\int_{4\pi} I_\nu(\eta_i)\exp\left(-\int_{\eta_i}^{x_i} K_\nu ds\right)\frac{d\omega}{4\pi} \tag{38}$$

or, B_ν is replaced by I_ν, where I_ν is the specific intensity of radiation. A general expression for I_ν can be derived from the general transfer equation. For a nonscattering medium in local thermodynamic equilibrium, the transfer equation can be written as

$$\frac{1}{K_\nu}\frac{dI_\nu}{ds} = -I_\nu + B_\nu \tag{39}$$

Integration of eq. (39) yields (ref. 6)

$$I_\nu(x_i,\eta_i) = \int_{\eta_i}^{x_i} B_\nu(\xi_i)\exp\left(-\int_{\xi_i}^{x_i} K_\nu ds\right)K_\nu(\xi_i)ds + I_\nu(\eta_i)\exp\left(-\int_{\eta_i}^{x_i} K_\nu ds\right) \tag{40}$$

or

$$I_\nu(x_i,\zeta_i) = \int_{\zeta_i}^{x_i} B_\nu(\xi_i)\exp\left(-\int_{\xi_i}^{x_i} K_\nu ds\right)K_\nu(\xi_i)ds + I_\nu(\zeta_i)\exp\left(-\int_{\zeta_i}^{x_i} K_\nu ds\right) \tag{41}$$

when η_i refers to the wall surface and ζ_i to the edge of the boundary layer.

A general treatment of eq. (38) is extremely difficult. However, since it has been established that the air boundary layer on a flat plate is optically thin, a treatment of eq. (38) is possible by utilizing the fact that second order terms in optical thickness can be ignored. Thus, for an optically thin gas, one may write

$$\exp\left(-\int_{\eta_i}^{x_i} K_\nu ds\right) = 1 - \int_{\eta_i}^{x_i} K_\nu ds \tag{42}$$

Hence, keeping first order terms in the optical thickness, eq. (38) reduces to

$$K_\nu(x_i)\int_{4\pi} I_\nu(\eta_i)\,\frac{d\omega}{4\pi} \tag{43}$$

A general expression for the radiation intensity at an interface has been given by Goulard (eq. (4.16) of ref. 6). Assuming that the interface properties are independent of direction and, diffuse reflection, one finds, at an interface

$$I_\nu = \varepsilon_\nu B_\nu + r_\nu \int_{2\pi} I_\nu' \,\frac{\cos\theta' d\omega'}{\pi} \tag{44}$$

where ε_ν and r_ν are the emissivity and reflectivity. Thus, assuming an emitting but nonreflecting external flow and a reflecting opaque wall, one obtains

$$I_{\nu,e} = I_\nu(\zeta_i) = \varepsilon_{\nu,e} B_\nu(T_e)$$

and

$$I_{\nu,w} = I_\nu(\eta_i) = \varepsilon_{\nu,w} B_\nu(T_w) + (1 - \varepsilon_{\nu,w})\int_{2\pi} I_\nu(\eta_i,\zeta_i')\,\frac{\cos\theta' d\omega'}{\pi} \tag{45}$$

Keeping first order terms in the optical thickness, $I_\nu(\eta_i,\zeta_i)$ is calculated from eqs. (41) and (45) as

$$I_\nu(\eta_i,\zeta_i) = \varepsilon_{\nu,e} B_\nu(T_e) + \int_{\zeta_i}^{\eta_i} (B_\nu(\xi_i) - \varepsilon_{\nu,e} B_\nu(T_e)) K_\nu(\xi_i) ds \tag{46}$$

Substituting eqs. (45) and (46) into eq. (43) and retaining first order terms, one finds, for a grey wall

$$K_\nu(x_i)\int_{4\pi} I_\nu(\eta_i)\,\frac{d\omega}{4\pi} = K_\nu(x_i)\left[\frac{\varepsilon_w}{2} B_\nu(T_w) + \left(\frac{2 - \varepsilon_w}{2}\right)\varepsilon_{\nu,e} B_\nu(T_e)\right] \tag{47}$$

Thus, using eq. (8) and (47), $F_{\nu i,i}$ for an optically thin gas reduces to

$$F_{\nu i,i} = 4\pi K_\nu \left[B_\nu(x_i) - \frac{\varepsilon_w}{2} B_\nu(T_w) - \left(\frac{2 - \varepsilon_w}{2}\right) \varepsilon_{\nu,e} B_\nu(T_e) \right] \tag{48}$$

Assuming that $\varepsilon_{\nu,e}$ has the same frequency dependence as $K_\nu(x_i, \nu)$ (eq. (11)) and integrating over the entire frequency spectrum, one obtains

$$F^R_{i,i} = 4\sigma \left[K_p(x_i) T^4(x_i) - \frac{\varepsilon_w}{2} T_w^4 \sum_{j=1}^{n} K_j(x_i) \alpha_j(T_w) - \left(\frac{2 - \varepsilon_w}{2}\right) T_e^4 \sum_{j=1}^{n} \varepsilon_{je} \alpha_j(T_e) K_j(x_i) \right] \tag{49}$$

where

$$K_p = \sum_{j=1}^{n} \alpha_j(x_i) K_j(x_i)$$

is the Planck's mean, and

$$\alpha_j(T_t) = \int_{\Delta_j} B_\nu(T_t) d\nu \Big/ (\sigma T_t^4/\pi) \quad , \; t = w, \; e \tag{50}$$

If the contribution of the wall and external flow to the divergence of the flux vector is ignored, then eq. (49) reduces to

$$F^R_{i,i} = 4\sigma K_p(x_i) T^4(x_i) \tag{51}$$

Thus, grey heat transfer calculations for an optically thin gas with the absorption coefficient equal to the Planck's mean are identical to the nongrey calculations regardless of the frequency dependence of $K_\nu(x_i, \nu)$.

The grey equivalent of eq. (49) can be written as

$$F^R_{i,i} = 4\sigma K_p T_e^4 \left[\left(\frac{T}{T_e}\right)^4 - \frac{\varepsilon_w}{2} \left(\frac{T_w}{T_e}\right)^4 - \varepsilon_e \left(\frac{2 - \varepsilon_w}{2}\right) \right] \tag{52}$$

THE RADIATIVE HEAT FLUX AT THE WALL

The radiative heat flux at the wall can be derived from the general relations given by Goulard (ref. 6) for the radiation flux at an arbitrary point in a radiating gas. These relations are the expression for the spectral radiative flux crossing a surface of unit normal vector n_i at the point ξ_i,

$$q_\nu(\xi_i, n_i) = \int_{4\pi} I_\nu \cos\theta d\omega \tag{53}$$

where θ is the angle between n_i and the ray cone specified by ω (see fig. 1), and the definition of global radiative flux

$$q_R = \int_o^\infty q_\nu d\nu \tag{54}$$

The radiative flux at an arbitrary surface x_i between η_i and ζ_i can be calculated from the radiation intensity directed upwards $I_\nu(x_i, \eta_i)$ and the radiation intensity directed downward $I_\nu(x_i, \zeta_i)$ as

$$q_\nu = \int_o^{2\pi}\int_o^{\pi/2} I_\nu(x_i, \zeta_i)\cos\theta\sin\theta d\theta d\phi + \int_o^{2\pi}\int_{\pi/2}^{\pi} I_\nu(x_i, \eta_i)\cos\theta\sin\theta d\theta d\phi \tag{55}$$

where, in writing eq. (55), $d\omega$ was replaced by

$$d\omega = \sin\theta d\theta d\phi \tag{56}$$

In particular, eq. (55) shows that the radiative heat flux at the wall where $x_i = \eta_i$ is given by

$$q_{\nu w} = \int_o^{2\pi}\int_o^{\pi/2} I_\nu(\eta_i, \zeta_i)\cos\theta\sin\theta d\theta d\phi + \int_o^{2\pi}\int_{\pi/2}^{\pi} I_\nu(\eta_i)\cos\theta\sin\theta d\theta d\phi \tag{57}$$

Now $I_\nu(\eta_i)$ is independent of θ and ϕ as a result of assuming diffuse reflection. If it is assumed further that $I_\nu(\eta_i, \zeta_i)$ is independent of ϕ, eq. (57) reduces to

$$q_{\nu w} = 2\pi\int_o^{\pi/2} I_\nu(\eta_i, \zeta_i)\cos\theta\sin\theta d\theta - \pi I_\nu(\eta_i) \tag{58}$$

For an optically thin gas, $I_\nu(\eta_i,\zeta_i)$ is given by eq. (46). Substitution of eq. (46) into eqs. (45) and (58) yields, for a grey wall

$$q_{\nu w} = \pi\varepsilon_w\left\{\varepsilon_{\nu,e}B_\nu(T_e) - B_\nu(T_w) + 2\int_o^{\pi/2}\int_{\zeta_i}^{\eta_i}\left[\left(B_\nu(\xi_i) - \varepsilon_{\nu,e}B_\nu(T_e)\right)K_\nu(\xi_i)ds\right]\cos\theta\sin\theta d\theta\right\} \tag{59}$$

The spectral radiative flux at a given x on a flat plate can be obtained from eq. (59) by letting

$$ds = -\cos\theta dy\ ,\ \zeta_i = \delta\ ,\ \eta_i = 0 \tag{60}$$

The resulting expression can be written as

$$q_{\nu w} = \pi\varepsilon_w\left\{\varepsilon_{\nu,e}B_\nu(T_e) - B_\nu(T_w) + 2\int_o^{\pi/2}\int_o^{\delta}\left[B_\nu(\theta,y) - \varepsilon_{\nu,e}B_\nu(T_e)\right]K_\nu(\theta,y)\sin\theta dy d\theta\right\} \tag{61}$$

The global radiative flux to the surface is

$$\begin{aligned} q_{Rw} &= \int_o^\infty q_{\nu w}d\nu \\ &= \sigma\varepsilon_w\left\{\sum_{j=1}^{n}\alpha_j(T_e)\varepsilon_{je}T_e^4 - T_w^4 + 2\int_o^{\pi/2}\int_o^{\delta}\left[K_pT^4 - \sum_{j=1}^{n}K_j\alpha_j(T_e)\varepsilon_{je}T_e^4\right]\sin\theta dy d\theta\right\} \end{aligned} \tag{62}$$

where, again, the frequency dependence of $\varepsilon_{\nu,e}$ was assumed identical to that of K_ν.

TRANSFORMATION OF THE GOVERNING EQUATIONS

The governing equations are equations (4) through (6) with $F^R_{i,i}$ given by eq. (49). The appropriate boundary conditions can be written as

$$\begin{aligned} &u = v = 0 \ , \ h = h_w \text{ at } y = 0 \\ &u \to u_e \ , \ h \to h_e \text{ as } y \to \infty \ ^{1} \\ &u = u_e \ , \ h = h_e \text{ at } x = 0 \end{aligned} \tag{63}$$

where u_e, h_e, and h_w are assumed to be constants. The continuity equation is satisfied identically if one introduces the stream function ψ defined by

$$\rho u = \frac{\partial \psi}{\partial y} \ , \ \rho v = - \frac{\partial \psi}{\partial x} \tag{64}$$

The momentum and energy equations will now be transformed from the x-y to an s-η coordinate system. Letting

$$s = \rho_e \mu_e u_e x \ , \ \eta = \frac{\rho_e u_e}{\sqrt{Cs}} \int_o^y \bar{\rho} dy \ , \ \psi = \sqrt{Cs}\ f(s,\eta) \tag{65}$$

with

$$\bar{h} = \frac{h}{h_e} \ , \ \bar{\rho} = \frac{\rho}{\rho_e} \ , \ C = \frac{\mu \rho}{\mu_e \rho_e} = \text{const.} \tag{66}$$

eqs. (5) and (6) reduce to, respectively.

$$\frac{\partial^3 f}{\partial \eta^3} + \frac{f}{2} \frac{\partial^2 f}{\partial \eta^2} = s\left(\frac{\partial f}{\partial \eta} \frac{\partial^2 f}{\partial \eta \partial s} - \frac{\partial f}{\partial s} \frac{\partial^2 f}{\partial \eta^2} \right) \tag{67}$$

and

---

[1] See Appendix F.

$$\frac{1}{Pr}\frac{\partial^2 \bar{h}}{\partial \eta^2} + \frac{f}{2}\frac{\partial \bar{h}}{\partial \eta} + \frac{u_e^2}{h_e}\left(\frac{\partial^2 f}{\partial \eta^2}\right)^2 = s\left[\frac{\partial f}{\partial \eta}\frac{\partial \bar{h}}{\partial s} - \frac{\partial f}{\partial s}\frac{\partial \bar{h}}{\partial \eta}\right] + \frac{\bar{x}L}{\rho_e u_e h_e \bar{\rho}} F^R_{i,i} \tag{68}$$

where $\bar{x} = x/L$ and it has been assumed that the Prandtl number Pr = const. As is seen from eqs. (49) and (68), true similarity does not exist in the boundary layer of an optically thin gas.

In order to simplify the numerical calculations, the assumption of local similarity will be introduced. Thus, eqs. (67) and (68) reduce to, respectively,

$$f''' + \frac{f}{2} f'' = 0 \tag{69}$$

and

$$\bar{h}'' + Pr\,\frac{f}{2}\,\bar{h}' = - Pr\,\frac{u_e^2}{h_e} f''^2 + \frac{Pr\,\bar{x}L}{\rho_e u_e h_e \bar{\rho}} F^R_{i,i} \tag{70}$$

where the prime denotes differentation with respect to η. Equation (69) is the well-known Blasius equation. Therefore, the solution of the problem reduces to the solution of eq. (70) with the boundary conditions

$$\bar{h} = \bar{h}_w \text{ at } \eta = 0 \text{ and } \bar{h} \to 1 \text{ as } \eta \to \infty \tag{71}$$

The convective heat transfer at the wall q_{cw} is given by

$$q_{cw} = - k_w\left(\frac{\partial T}{\partial y}\right)_{y=0} = - \frac{\mu_w}{Pr}\left(\frac{\partial h}{\partial y}\right)_{y=0}$$

$$= - \sqrt{\frac{C\rho_e \mu_e u_e}{L\bar{x}}}\,\frac{h_e}{Pr}\left(\frac{\partial \bar{h}}{\partial \eta}\right)_{\eta=0} \tag{72}$$

where C is evaluated, as suggested by Eckert (ref. 14), at the reference enthalpy h_* which, for Pr = 0.70, can be written as

$$\bar{h}_* = \frac{1}{2}(1 + \bar{h}_w) + .092\,\frac{u_e^2}{h_e} \tag{73}$$

The radiative heat flux at a given station x is obtained from eq. (62) as

$$q_{Rw} = \varepsilon_w \sigma T_e^4 \left\{ \sum_{j=1}^{n} \alpha_j(T_e)\,\varepsilon_{je} - \bar{T}_w^4 \right.$$

$$\left. + 2\,\frac{\sqrt{Cs}}{u_e} \int_o^{\eta_\delta} \left[\frac{K_p(T_e,P_e)}{\rho_e} \frac{\bar{K}_p}{\bar{\rho}}\,\bar{T}^4 - \sum_{j=1}^{n} \frac{K_j(P_e,T_e)}{\rho_e} \frac{\bar{K}_j}{\bar{\rho}}\,\alpha_j(T_e)\varepsilon_{je} \right] d\eta \right\} \qquad (74)$$

where η_δ is the value of η at which $f'(\eta) = 0.9999$. The corresponding grey expression can be expressed as

$$q_{Rw,g} = \varepsilon_w \sigma T_e^4 \left\{ \varepsilon_e - \bar{T}_w^4 + 2\,\frac{\sqrt{Cs}}{u_e} \int_o^{\eta_\delta} \left[\frac{K_{pe}}{\rho_e} \frac{\bar{K}_p}{\bar{\rho}} (\bar{T}^4 - \varepsilon_e) \right] d\eta \right\} \qquad (75)$$

Method of Solution

The method of solution to be employed here is to transfer the differential eq. (70) into an integral equation and to solve the resulting integral equation by iteration. A formal integration of eq. (70) yields

$$\bar{h} = \bar{h}_w + C_1 g_1(\eta) - Pr\,\frac{u_e^2}{h_e}\,g_2(\eta) + \lambda g_3(\eta) \qquad (76)$$

where

$$g_1(\eta) = \int_o^{\eta} \exp\left(-\frac{Pr}{2} \int_o^{\eta_1} f\,d\eta_2 \right) d\eta_1$$

$$g_2\,,\ g_3 = \int_o^{\eta} \left\{ \exp\left(-\frac{Pr}{2} \int_o^{\eta_1} f\,d\eta_2 \right) \left[\int_o^{\eta_1} \chi \exp\left(\frac{Pr}{2} \int_o^{\eta_2} f\,d\eta_3 \right) d\eta_2 \right] \right\} d\eta_1 \ ;$$

$$\chi = f''^2 \ ,\ W$$

$$W = \frac{F^R_{i,i}}{\rho_e \bar{\rho} 4\sigma T_e^4} = \frac{K_p(T_e,P_e)}{\rho_e} \frac{\bar{K}_p}{\bar{\rho}}\,\bar{T}^4 - \sum_{j=1}^{n} \frac{K_{je}}{\rho_e} \frac{\bar{K}_j}{\bar{\rho}} \left[\frac{\varepsilon_w}{2}\,\bar{T}_w^4 \alpha_j(T_w) + \frac{(2-\varepsilon_w)}{2}\,\varepsilon_{je}\alpha_j(T_e) \right]$$

and

$$\lambda = \frac{4Pr\sigma T_e^4 L\bar{x}}{u_e h_e} \tag{77}$$

C_1 is a "constant" determined from the condition that

$$\bar{h} = 1 \text{ when } \eta = \eta_\delta \tag{78}$$

The resulting expression for C_1 is

$$C_1 = \left[1 - \bar{h}_w + Pr \frac{u_e^2}{h_e} g_2(\eta_\delta) - \lambda g_3(\eta_\delta)\right] \Big/ g_1(\eta_\delta) \tag{79}$$

It is seen from eqs. (76) and (77) that, in order to calculate $g_3(\eta)$ one needs to know the temperature or enthalpy distribution in the boundary layer at a given $\bar{x}$. In the scheme employed here, the iteration has been started by assuming that the enthalpy distribution needed to calculate W and g_3 is given by the solution of eq. (70) for the case of no radiation. This enables one to calculate g_3 and an improved value of $\bar{h}$. This improved value of $\bar{h}$ is employed in calculating g_3 and so on.

Designating the solution of eq. (70) in the absence of radiation by $\bar{h}_o$, one obtains

$$\bar{h}_o = \bar{h}_w + C_o g_1(\eta) - Pr \frac{u_e^2}{h_e} g_2(\eta) \tag{80}$$

where C_o is determined from eqs. (78) and (80) as

$$C_o = \left[1 - \bar{h}_w + Pr \frac{u_e^2}{h_e} g_2(\eta_\delta)\right] \Big/ g_1(\eta_\delta) \tag{81}$$

Examination of eqs. (79) and (81) shows that

$$C_1 = C_o - \lambda \frac{g_3(\eta_\delta)}{g_1(\eta_\delta)} \tag{82}$$

and therefore,

$$\bar{h} = \bar{h}_o + \lambda g_3(\eta_\delta)\left[\frac{g_3(\eta)}{g_3(\eta_\delta)} - \frac{g_1(\eta)}{g_1(\eta_\delta)}\right] \tag{83}$$

The calculations were carried out for values of $\bar{x}$ ranging from 0.1 to 1.0. The function for $\bar{h}_o$ was employed to start the iteration scheme for the case where $\bar{x} = 0.1$. For other values of $\bar{x}$ the calculated value of $\bar{h}$ at the preceding $\bar{x}$ station was employed to start the iteration. In the course of the calculations, it was noticed that convergence is achieved rapidly if one chooses for the input of the nth iteration the mean of the input and output of the previous iteration, i.e.,

$$(\bar{h}_{in})_n = \frac{(\bar{h}_{in})_{n-1} + (\bar{h}_{out})_{n-1}}{2} \tag{84}$$

The ratio of the convective heat flux with radiation q_{cw} to that without radiation q_{cwo} follows from eqs. (72), (76), (80), and (82) as

$$\frac{q_{cw}}{q_{cwo}} = \frac{C_1}{C_o} = 1 - \frac{\lambda}{C_o}\frac{g_3(\eta_\delta)}{g_1(\eta_\delta)} \tag{85}$$

RESULTS AND DISCUSSION

The influence of the nongrey radiation effects on the air boundary layer over a flat plate has been investigated. The monochromatic absorption coefficient employed assumes a stepwise frequency dependence; as a result of this assumption it is shown that the contributions of the various frequency intervals to the divergence of the radiative flux vector add up linearly. This marks a departure from the grey case in the sense that for certain conditions the various contributions to the divergence of the radiative flux vector may be a combination of the usual thin, self-absorbing and thick contributions. Because of this it is not possible to define an effective optical thickness for the whole flow field and hence there is no grey equivalent to a nongrey flow model.

It is shown that for a typical reentry mission from Mars and other similar missions, the air boundary layer over a flat plate is optically thin. Therefore the results presented here are for an optically thin boundary layer on a flat plate. The calculations were carried out for Eckert numbers, u_e^2/h_e, of approximately 16, 10, 1 and 0.7; external flow

temperatures of 2000°, 4000°, 10 000°, and 12 000° K; external flow velocities of 32, 24.4 and 7.7 Km/sec; wall temperatures of 1000°, 2000° and 3000° K; pressures of 1.0 and 0.1 atmospheres; and plate lengths of 3 and 10 meters. The Prandtl number was chosen as 0.7. The monochromatic absorption coefficient model employed is shown in fig. 5 with K_1 and K_2 given, respectively, by eqs. (D2) and (D5). The Planck mean absorption coefficient employed in the grey calculations is given by eq. (D4). The calculations are aimed at providing an increased knowledge of the physical effects of radiation (and the various parameters which characterize the nature of that radiation) on the behavior of the boundary layer.

The calculated results presented are for the cases of high and low Eckert number. The specific results given do not pertain to a particular reentry vehicle or trajectory but serve only as examples. However, in order to better illustrate the meaning of these results it is worthwhile to make some connection between the Eckert number and a vehicle geometry with specified freestream flight conditions. For example, the Eckert number for a wedge with a semi-apex angle of 53° traveling at 45 000 ft/sec at an altitude of 150 000 ft is about 0.7 while the Eckert number for a wedge of 28° semi-apex angle moving at a velocity of 39 000 ft/sec at an altitude of 150 000 ft is around 7.0 (ref. 28).

Figures 6(a) and 6(b) show the effects of grey radiation on the boundary layer enthalpy distribution for high and low Eckert numbers, respectively. The $\bar{h}_o$ profile refers to the similar enthalpy distribution for a non-radiating gas; the other profiles are for a grey radiating gas at $\bar{x} = 1.0$. From fig. 6(a) it is seen that for high Eckert number flows and all values of wall and external flow emissivities the energy loss by emission significantly reduces the boundary layer enthalpy below its value for a non-radiating gas. In particular the peak enthalpy is reduced a considerable amount. The results in fig. 6(a) also indicate that the enthalpy profile for a high Eckert number flow is relatively insensitive to the magnitude of the wall and external flow emissivities. This may be explained by the fact that for the high Eckert number case the enthalpy in the boundary layer exceeds that in any other region of the flow by a considerable amount and, consequently, the gas in the boundary layer will emit energy at a much greater rate than it will absorb. Thus, the amount of radiant energy incident on the boundary layer, which depends on the magnitude of the external flow and wall emissivities, is of secondary importance in determining the boundary layer enthalpy profile.

From fig. 6(b) the results indicate that the enthalpy distribution for low Eckert number flows is affected considerably different by radiation than is the enthalpy distribution for high Eckert number flows. In particular, the magnitudes of the wall and external flow emissivities influence the enthalpy distribution in such a manner that the boundary layer enthalpy may be greater or less than its value for a nonradiating gas in some or all parts of the boundary layer. For instance, the results given in fig. 6(b) indicate that for a combination of high external flow and low wall emissivity the enthalpy is somewhat greater than its value for a nonradiating gas in that part of the boundary layer nearest the wall. This sensitivity of the enthalpy profile to the external flow and wall emissivities is due to the fact that for the low Eckert number case the enthalpy in the boundary layer

is equal or less than that in any other portion of the flow and hence the gas in the boundary layer absorbs energy at approximately the same rate as it emits. Thus the amount of radiant energy incident on the boundary layer, which is governed by the magnitude of the wall and external flow emissivities, strongly influences the enthalpy distribution in the boundary layer.

From fig. 6(b) it is noted that there is no appreciable effect of the magnitude of the wall emissivity on the boundary layer enthalpy distribution for a low external flow emissivity but a quite significant effect for a high external flow emissivity. These results point out the fact that the photons emitted by the relatively cold wall have a negligible influence on the boundary layer enthalpy profile and emphasize that the major effect of the wall emissivity on the enthalpy profiles is due to reflection from the surface of incident photons which originated in the radiating external flow.

Plots of $\bar{h}/\bar{h}_o$ and $\bar{h}_g/\bar{h}_o$ vs. η for high Eckert number flow are shown in figs. 7(a) and 7(b) for various wall and external flow emissivities. It is seen that the nongrey effects are more pronounced at the high external flow emissivity and/or low wall emissivity. The results also indicate that the nongrey profiles are less sensitive than the corresponding grey profiles to the various values of external flow and wall emissivities. In general the results of fig.7 show that the enthalpy profiles for a nongrey gas are not significantly different from those for a grey gas. This is explained by the combination of facts that for high Eckert number flows the radiation process is emission dominated and the Planck mean absorption coefficient used for the grey gas is the proper mean absorption coefficient for the nongrey emission process.

Plots of grey and nongrey enthalpy profiles for the low Eckert number case are presented in figs. 8(a) and 8(b). It is seen that for all combinations of wall and external flow emissivities the enthalpy for a nongrey gas significantly exceeds its value for a grey gas. The curves in figs. 8(a) and 8(b) also indicate that for low Eckert number flows the nongrey enthalpy profiles are more sensitive to the wall and external flow emissivities than the grey profiles. Both results are explained by noting that absorption is always more significant for a nongrey gas than for a grey gas. In fact, it is observed from fig. 8(a) that at a high external flow emissivity the effect of absorption in a nongrey gas is so significant that the geometrical boundary layer thickness is markedly reduced below its value for a nonradiating gas.

Figures 9(a) and 9(b) show a comparison of the grey convective heat flux and the convective heat flux in the absence of radiation for high and low Eckert numbers, respectively. The results presented indicate that the ratio of these two fluxes increases with an increase in the external flow emissivity and/or decrease in the wall emissivity. From fig. 9(a) it is seen that for a high Eckert number flow the convective heat flux is reduced appreciably below its value for a nonradiating gas and also there is little influence of the wall or external flow emissivities on the heat flux. Both results, of course, are explained by the previous discussion pertaining to the enthalpy profiles for high Eckert number flows. For low Eckert number flows the results in fig. 9(b) indicate that the effect of radiation on the

grey convective heat flux is quite significant and is strongly influenced by the magnitude of the wall and external flow emissivities. In particular, for the combination of high external flow and low wall emissivities, the grey convective heat flux exceeds the convective heat flux for a nonradiating gas. This result is explained by the fact that near the wall the absorption of radiant energy incident on the boundary layer exceeds the energy loss by emission and hence the enthalpy gradient near the wall increases over its nonradiating value.

The ratio of the nongrey convective heat flux to the corresponding grey heat flux is shown in figs. 10(a) and 10(b) for high and low Eckert numbers, respectively. This ratio is generally greater than unity except for a combination of high Eckert number and high external flow emissivity. The high Eckert number results in fig. 10(a) indicate that the convective heat fluxes for a nongrey gas are not significantly different from those for a grey gas. The previous discussion on nongrey enthalpy profiles for high Eckert numbers explains these results. For low Eckert number flows the results in fig. 10(b) show that the effect of nongrey absorption on the convective heat flux is quite significant. In particular, the nongrey convective heat flux is appreciably greater (up to 27%) than the grey convective heat flux. Also, the influence of the wall emissivity on the results is so strong that the ratio of the nongrey to grey convective heat flux is greater for a combination of low wall and low external flow emissivity than for a combination of high wall and high external flow emissivity.

In figs. 11(a) and 11(b) the nongrey radiative heat flux is compared to the corresponding grey radiative heat flux for high and low Eckert numbers, respectively. The ratio of these two fluxes is generally less than unity except for the combination of a high Eckert number and high external flow emissivity. An analysis of the numerical results from which fig. 11 was derived indicates that for high Eckert number flows the effect of the optically thin boundary layer on the radiative wall heat flux is to reinforce the radiant heat flux directed from the inviscid flow to the wall. This result is explained by noting that the boundary layer in a high Eckert number flow emits more energy than it absorbs and hence increases the total radiant heat transfer. However, this increase in the radiative wall heat flux is negligible except for low values of external flow emissivity where the boundary-layer contribution to the radiative wall heat flux is a maximum of 17% of the external flow contribution. For these low values of external flow emissivity, the nongrey absorption effect on the boundary-layer contribution is found to be small (less than 6%). At low Eckert number flow conditions, the numerical results indicate that the effect of the optically thin boundary layer on the radiant heat flux directed from the external flow to the wall is to inhibit it for a high external flow emissivity and reinforce it for a low external flow emissivity. This reduction (increase) of the total radiant heat transfer is explained by noting that the low Eckert number boundary layer will absorb (emit) more energy than it emits (absorbs) for a high (low) external flow emissivity. However, from the numerical results for low Eckert number, it is found that the reduction in radiant wall heat flux at high external flow emissivities is negligible while the increase in radiant wall heat flux at low external flow emissivities is small (less than 2.5%).

The radiative heat flux and the convective heat flux are compared in figs. 12(a) and 12(b). It is seen that, for the high external flow temperatures considered here, 10 000° and 12 000° K, the radiative heat flux is larger than the convective heat flux with the ratio of the two fluxes increasing with an increase in the external flow and/or wall emissivities and a decrease in the Eckert number. The results also show that the ratio of the radiative to convective heat flux increases with an increase in the external flow temperature and plate length and a decrease in the external flow pressure and wall temperature.

The ratio of the total (convective + radiative) heat flux to the heat flux in the absence of radiation is shown in figs. 13(a) and 13(b) for high and low Eckert numbers, respectively. This ratio, which is always greater than unity, increases with an increase in wall and/or external flow emissivities with the influence of the external flow emissivity being more pronounced. It is also seen that a significant reduction in the total heat flux can be achieved by a reduction in both wall and external flow emissivities.

Figures 14(a) and 14(b) compare the nongrey total heat flux to the grey total heat flux. From the high Eckert number results in fig. 14(a), it is seen that the nongrey heat flux is slightly larger than the grey heat flux for a combination of low external flow and low wall or high external flow and high wall emissivities. For low Eckert number flow conditions, the results in fig. 14(b) indicate that the nongrey heat flux exceeds the grey heat flux for the lower wall emissivities. However, in either the high or low Eckert number case, the results show that the difference between the grey and nongrey total heat flux is small regardless of the values of the wall and external flow emissivities.

It is noticed from the results that the differences between the various grey and the nongrey heat fluxes are small except for the convective heat flux at low Eckert number where the dominant heat flux is radiative. It follows from eqs. (65), (74), and (75) that for given external flow emissivity and wall temperature the dimensionless radiative heat flux depends explicitly on the effective Bouguer numbers (for an optically thin gas) τ'_{je} where the τ'_{je} are related to the grey Bouguer number $\tau_{pe}(= K_{pe}\delta)$ by the expression

$$\tau_{pe} = \sum_{j=1}^{n} \tau'_{je}$$

The difference between the nongrey and grey radiative heat flux is proportional to the τ'_{je} and they are small (of the order of 10^{-2}) for the cases under consideration.

CONCLUSIONS

The analysis carried out here shows that in the presence of nongrey radiation it is not, in general, possible to define an effective optical thickness for the whole flow field. This, in turn, suggests that there is no grey equivalent to a nongrey flow field.

Optical thickness estimates for a typical reentry mission from Mars suggest that the boundary layer over a flat plate is optically thin. The results obtained in the analysis of the optically thin boundary layer indicate that the effect of radiative transfer on the boundary-layer characteristics depends primarily on the Bouguer-Boltzmann number ratio as appropriately defined for boundary-layer flow geometry. From the numerical results for air, it is found that the effect of radiative transfer on the boundary-layer enthalpy profile and convective heat flux becomes quite significant when the Bouguer-Boltzmann number ratio is of the order of magnitude of 0.1. Other explicit parameters found to appreciably influence the effect of radiation on the enthalpy profile and dimensionless convective heat flux are the Eckert number, the wall emissivity, and the emissivity of the external flow. The numerical results also indicate that the optically thin boundary layer has little influence on the radiative wall heat flux except for low values of external flow emissivity at high Eckert number where the boundary-layer contribution to the radiative wall heat flux is roughly 15% of the external flow contribution. Thus, by far the major portion of the radiative wall heat flux comes from the external flow region of the shock layer.

The nongrey heat flux results obtained in the optically thin boundary-layer calculations show that the total nongrey heat flux for Eckert numbers of interest is greater than the corresponding grey heat flux for a combination of high external flow and high wall or low external flow and low wall emissivities. These results also indicate that the differences between the various grey and nongrey heat fluxes are small except for the convective heat flux at low Eckert number where the nongrey heat flux is up to 27% greater than the grey heat flux. The numerical results also show that the total wall heat flux may be drastically reduced by lowering both wall and external flow emissivities. This suggests a scheme for decreasing the total heat flux to the wall. It should be noted, however, that the emissivity of the external flow depends on the optical properties of the gases in the shock layer.

Since the pressure in the boundary layer over a flat plate is constant, the dependence of the absorption coefficient on temperature and density should be consistent with the requirement that $\rho T \simeq$ const. Thus, it is not possible to simultaneously have both high temperature and high density in the flat plate boundary layer. This is why the air boundary layer over a flat plate is optically thin. In the stagnation point region no such restriction exists. Therefore, it is expected that the various contributions to the divergence of the radiation flux vector in the stagnation point region are a combination of the usual thin, self-absorbing and thick contributions.

APPENDIX A

THE DIVERGENCE OF THE RADIATION ENERGY FLUX VECTOR FOR NONGREY GASES

The general expression for $F_{\nu i,i}(x_i)$, the divergence of the spectral radiation energy flux vector $F_{\nu i}$ at the point x_i, has been formulated previously by Goulard (ref. 6). For nonscattering gases in local thermodynamic equilibrium and perfectly absorbing surfaces, this relation is

$$F_{\nu i,i}(x_i) = 4\pi K_\nu(x_i)B_\nu(x_i) - K_\nu(x_i)\int_V K_\nu(\xi_i)B_\nu(\xi_i)\exp\left[-\int_{\xi_i}^{x_i} K_\nu ds\right]\frac{dV(\xi_i)}{\sum_i\left[x_i - \xi_i\right]^2}$$

$$- K_\nu(x_i)\int_A B_\nu(\eta_i)\exp\left[-\int_{\eta_i}^{x_i} K_\nu ds\right]\frac{\cos\theta dA(\eta_i)}{\sum_i\left[x_i - \eta_i\right]^2} \qquad \text{(A1)}$$

where $K_\nu(x_i)$ is the spectral linear absorption coefficient which is related to the spectral mass absorption coefficient $\kappa_\nu(x_i)$ by the relation

$$K_\nu(x_i) = \rho(x_i)\kappa_\nu(x_i)$$

The physical meaning of the three terms on the right hand side of eq. (A1) are illustrated most easily by use of fig. 1 which depicts a volume V of radiating gas enclosed in the boundary surface A. The first term represents the radiation energy emitted by the gas at point x_i where $B_\nu(x_i)$ is the well-known Planck distribution function

$$B_\nu(x_i) = \frac{2h\nu^3}{c^2}\frac{1}{\exp\left(\frac{h\nu}{kT(x_i)}\right) - 1} \qquad \text{(A2)}$$

The second term represents that energy emitted by the gas in all the elementary volumes $dV(\xi_i)$ around the points ξ_i in the entire volume V which is absorbed by the gas at point x_i. In this term the point ξ_i is a "running" point moving along the directed line $S(\ell_i)$ from the point η_i on the elemental surface area $dA(\eta_i)$ to the point x_i. The angle between the unit normal vector n_i of $dA(\eta_i)$ and the directed line $S(\ell_i)$ is θ. It should be noted that the integral

$$\int_{\xi_i}^{x_i} K_\nu ds$$

which is called the optical length from ξ_i to x_i, is evaluated by integrating along the directed line $S(\ell_i)$ whose direction cosines are ℓ_i. Hence the optical length from ξ_i to x_i is a function of direction $S(\ell_i)$. Finally the third term in eq. (A1) represents that energy emitted by all the elemental surfaces $dA(\eta_i)$ around the points η_i on the boundary A which is absorbed by the gas at point x_i. Here the optical length from η_i to x_i,

$$\int_{\eta_i}^{x_i} K_\nu ds$$

is evaluated by integrating along $S(\ell_i)$ and hence it is a function of the direction $S(\ell_i)$.

Now eq. (A1) can be simplified by introducing the relations

$$dV(\xi_i) = \sum_i [x_i - \xi_i]^2 \, d\omega ds$$

$$dA(\eta_i) = \frac{\sum_i [x_i - \eta_i]^2 \, d\omega}{\cos \theta}$$

derived from the geometry of fig. 1, and applying the appropriate integration limits. Thus $F_{\nu i,i}(x_i)$ becomes

$$F_{\nu i,i}(x_i) = 4\pi \left\{ K_\nu(x_i) B_\nu(x_i) - K_\nu(x_i) \int_{4\pi} \int_{\eta_i}^{x_i} K_\nu(\xi_i) B_\nu(\xi_i) \exp\left[- \int_{\xi_i}^{x_i} K_\nu ds \right] ds \, \frac{d\omega}{4\pi} \right.$$
$$\left. - K_\nu(x_i) \int_{4\pi} B_\nu(\eta_i) \exp\left[- \int_{\eta_i}^{x_i} K_\nu ds \right] \frac{d\omega}{4\pi} \right\} \quad \text{(A3)}$$

where $\int_{4\pi}$ denotes integration over a solid angle of 4π steradians and the $\int_{\eta_i}^{x_i}$ is carried out along the directed line $S(\ell_i)$.

Now it is necessary to integrate $F_{\nu i,i}$ over frequency ν to obtain the divergence of the radiation flux vector $F^R_{i,i}$ which appears in the general energy equation of radiation gas dynamics. Thus

$$F^{R}_{i,i} \equiv \int_{o}^{\infty} F_{\nu i,i} d\nu \tag{A4}$$

can be evaluated by integrating eq. (A3) over ν. However, before this integration can be carried out it is necessary that the frequency dependence of K_ν be specified. As has been indicated in the analysis, this has been chosen as

$$K_\nu(x_i,\nu) = \sum_{m=1}^{n} K_m(x_i) g_m(\nu) \tag{A5}$$

with

$$g_m(\nu) \equiv \begin{cases} 1 \text{ if } \nu \in \Delta_m \\ \\ 0 \text{ otherwise} \end{cases}$$

where Δ_m corresponds to the frequency interval or intervals in which the value of K_ν is $K_m(x_i)$. The Δ_m do not overlap and the $K_m(x_i)$ are not functions of frequency. Hence the frequency and position dependence of K_ν is assumed to be separable. An example of a nongrey absorption coefficient model which might be specified by eq. (A5) is shown in fig. 2.

If the absorption coefficient model of eq. (A5) is now introduced into the $F_{\nu i,i}$ of eq. (A3) the resulting first term on the right hand side of eq. (A4) becomes

$$4\pi \int_{o}^{\infty} K_\nu(x_i) B_\nu(x_i) d\nu = 4\pi \sum_{j=1}^{n} \int_{\Delta_j} \sum_{m=1}^{n} K_m(x_i) g_m(\nu) B_\nu(x_i) d\nu$$

$$= 4\pi \sum_{j=1}^{n} K_j(x_i) \int_{\Delta_j} B_\nu(x_i) d\nu$$

since by definition of g_j the sum

$$\sum_{m=1}^{n} K_m(x_i) g_m(\nu)$$

reduces to $K_j(x_i)$ as the integration on Δ_j is carried out. If the definition

$$\int_{\Delta_j} B_\nu(x_i)d\nu \equiv \alpha_j[T]\int_o^\infty B_\nu(x_i)d\nu = \alpha_j[T(x_i)]\,\frac{\sigma T^4(x_i)}{\pi} = \alpha_j(x_i)\,\frac{\sigma T^4(x_i)}{\pi}$$

is now employed the first term takes the final form

$$4\pi\int_o^\infty K_\nu(x_i)B_\nu(x_i)d\nu = 4\sigma T^4(x_i)\sum_{j=1}^{n} K_j(x_i)\alpha_j(x_i) \tag{A6}$$

It should be noted at this point that $\int_{\Delta_j} B_\nu d\nu$ may actually represent a sum of integrals as, for example, in the case of Δ_1 in fig. 2 where

$$\int_{\Delta_1} B_\nu d\nu = \int_{\nu_1}^{\nu_2} B_\nu d\nu + \int_{\nu_5}^{\nu_6} B_\nu d\nu + \int_{\nu_9}^{\nu_{10}} B_\nu d\nu$$

since Δ_1 contains the frequency intervals (ν_1,ν_2), (ν_5,ν_6) and (ν_9,ν_{10}). It is also obvious that from the definition of $\alpha_j[T(x_i)]$ that

$$\sum_{j=1}^{n} \alpha_j(x_i) \equiv 1 \tag{A7}$$

Employing similar techniques as above the second term on the right-hand side of eq. (A4) becomes

$$-4\pi\int_o^\infty K_\nu(x_i)\int_{4\pi}\int_{\eta_i}^{x_i} K_\nu(\xi_i)B_\nu(\xi_i)\exp\left[-\int_{\xi_i}^{x_i} K_\nu ds\right]ds\,\frac{d\omega}{4\pi}\,d\nu$$

$$= -4\pi\sum_{j=1}^{n}\int_{\Delta_j}\sum_{m=1}^{n} K_m(x_i)g_m(\nu)\int_{4\pi}\int_{\eta_i}^{x_i}\sum_{m=1}^{n} K_m(\xi_i)g_m(\nu)B_\nu(\xi_i)$$

$$\times\exp\left[-\int_{\xi_i}^{x_i}\sum_{m=1}^{n} K_m g_m ds\right]ds\,\frac{d\omega}{4\pi}\,d\nu$$

$$= - 4\pi \sum_{j=1}^{n} K_j(x_i) \int_{4\pi} \int_{\eta_i}^{x_i} K_j(\xi_i) \int_{\Delta_j} B_\nu(\xi_i) d\nu \exp\left[- \int_{\xi_i}^{x_i} ds \right] ds \frac{d\omega}{4\pi}$$

$$= - 4\sigma \sum_{j=1}^{n} K_j(x_i) \int_{4\pi} \int_{\eta_i}^{x_i} K_j(\xi_i) \alpha_j(\xi_i) T^4(\xi_i) \exp\left[- \int_{\xi_i}^{x_i} K_j ds \right] ds \frac{d\omega}{4\pi}$$

Finally the third term of eq. (A4) becomes

$$- 4\pi \int_{o}^{\infty} K_\nu(x_i) \int_{4\pi} B_\nu(\eta_i) \exp\left[- \int_{\eta_i}^{x_i} K_\nu ds \right] \frac{d\omega}{4\pi} d\nu$$

$$= - 4\pi \sum_{j=1}^{n} \int_{\Delta_j} \sum_{m=1}^{n} K_m(x_i) g_m(\nu) \int_{4\pi} B_\nu(\eta_i) \exp\left[- \int_{\eta_i}^{x_i} \sum_{m=1}^{n} K_m g_m ds \right] \frac{d\omega}{4\pi} d\nu$$

$$= - 4\pi \sum_{j=1}^{n} K_j(x_i) \int_{4\pi} \int_{\Delta_j} B_\nu(\eta_i) d\nu \exp\left[- \int_{\eta_i}^{x_i} K_j ds \right] \frac{d\omega}{4\pi}$$

$$= - 4\sigma \sum_{j=1}^{n} K_j(x_i) \int_{4\pi} \alpha_j(\eta_i) T^4(\eta_i) \exp\left[- \int_{\eta_i}^{x_i} K_j ds \right] \frac{d\omega}{4\pi}$$

Thus when the absorption coefficient model of eq. (A5) is substituted into the $F_{\nu i,i}$ of eq. (A3) and the indicated integration over frequency is carried out, $F^R_{i,i}$ of eq. (A4) takes the final form

$$F^R_{i,i}(x_i) = 4\sigma \left\{ \sum_{j=1}^{n} K_j(x_i) \alpha_j(x_i) T^4(x_i) \right.$$

$$- \sum_{j=1}^{n} K_j(x_i) \int_{4\pi} \int_{\eta_i}^{x_i} K_j(\xi_i) \alpha_j(\xi_i) T^4(\xi_i) \exp\left[- \int_{\xi_i}^{x_i} K_j ds \right] ds \frac{d\omega}{4\pi}$$

$$\left. - \sum_{j=1}^{n} K_j(x_i) \int_{4\pi} \alpha_j(\eta_i) T^4(\eta_i) \exp\left[- \int_{\eta_i}^{x_i} K_j ds \right] \frac{d\omega}{4\pi} \right\} \qquad \text{(A8)}$$

When the function α_j applies to a single frequency interval (ν_j, ν_{j+1}) it may be written as

$$\alpha_j = \frac{\int_{\nu_j}^{\nu_{j+1}} B_\nu d\nu}{\int_0^\infty B_\nu d\nu} \tag{A9}$$

Introducing the wavelength λ by the relation

$$\nu = c/\lambda$$

eq. (A9) reduces to

$$\alpha_j = \frac{\int_{\lambda_j}^{\lambda_{j+1}} B_\lambda d\lambda}{\int_0^\infty B_\lambda d\lambda} \tag{A10}$$

where

$$B_\lambda = \frac{2hc^2}{\lambda^5} \frac{1}{\exp(hc/\lambda kT) - 1} \tag{A11}$$

Letting

$$\beta = \frac{hc}{k\lambda T}$$

and replacing the definite integral in the denominator of eq. (A10) by its value of $\pi^4/15$, eq. (A10) reduces to

$$\alpha_j = \frac{15}{\pi^4} \int_{\beta_j}^{\beta_{j+1}} \frac{\beta^3}{\exp(\beta) - 1} d\beta \tag{A12}$$

or, by defining $\alpha_j(\beta_j)$ as

$$\alpha_j(\beta_j) = \frac{15}{\pi^4} \int_{\beta_j}^{\infty} \frac{\beta^3}{\exp(\beta) - 1} \, d\beta \tag{A13}$$

eq. (A12) reduces to

$$\alpha_j = \alpha_j(\beta_j) - \alpha_j(\beta_{j+1}) \tag{A14}$$

A plot of $\alpha_j(\beta_j)$ vs $\lambda_j T$ is shown in fig. 15 using the tabulated data given in Tribus (ref. 15).

APPENDIX B

ASYMPTOTIC FORM OF $F^{R}_{i,i}$ FOR LARGE τ_{jo}

Factoring τ_{jo} outside of the jth bracket of eq. (23), the remaining terms can be expressed as

$$\left\{\bar{\alpha}_j(\bar{x}_i)\bar{K}_j(\bar{x}_i)\bar{T}^4(\bar{x}_i)\right.$$

$$- \tau_{jo}\bar{K}_j(\bar{x}_i)\int_o^1\int_{\bar{\eta}_i}^{\bar{x}_i}\bar{\alpha}_j(\bar{\xi}_i)\bar{T}^4(\bar{\xi}_i)\exp\left[-\tau_{jo}\left(\int_o^{\bar{x}_i}\bar{K}_j d\bar{s} - \int_o^{\bar{\xi}_i}\bar{K}_j d\bar{s}\right)\right]\bar{K}_j(\bar{\xi}_i)d\bar{s}d\bar{\omega}$$

$$\left. - \bar{K}_j(\bar{x}_i)\int_o^1\bar{\alpha}_j(\bar{\eta}_i)\bar{T}^4(\bar{\eta}_i)\exp\left[-\tau_{jo}\left(\int_o^{\bar{x}_i}\bar{K}_j d\bar{s} - \int_o^{\bar{\eta}_i}\bar{K}_j d\bar{s}\right)\right]d\bar{\omega}\right\}$$

Now if the following change of variables

$$t_j \equiv \int_o^{\bar{x}_i}\bar{K}_j d\bar{s}\ ,\quad t_{j1} \equiv \int_o^{\bar{\eta}_i}\bar{K}_j d\bar{s}\ ,\quad t_j' \equiv \int_o^{\bar{\xi}_i}\bar{K}_j d\bar{s}$$

are introduced into the last two terms of the jth bracket above the resulting equation is

$$\left\{\bar{\alpha}_j(\bar{x}_i)\bar{K}_j(\bar{x}_i)\bar{T}^4(\bar{x}_i) - \tau_{jo}\bar{K}_j(\bar{x}_i)\int_o^1\int_{t_{j1}}^{t_j}\bar{\alpha}_j(t_j')\bar{T}^4(t_j')\exp[-\tau_{jo}(t_j - t_j')]dt_j'd\bar{\omega}\right.$$

$$\left. - \bar{K}_j(\bar{x}_i)\int_o^1\bar{\alpha}_j(t_{j1})\bar{T}^4(t_{j1})\exp[-\tau_{jo}(t_j - t_{j1})]\,d\bar{\omega}\right\} \quad \text{(B1)}$$

From this relation it is seen that the exponential term,

$$\exp[-\tau_{jo}(t_j - t_j')]$$

in the integrand of the second term is the governing factor for the case of $\tau_{jo} > 1$. For the points $\bar{\xi}_i$ removed from the neighborhood of point

$\bar{x}_i$, $(t_j - t_j')$ has a finite value. Hence if τ_{jo} increases indefinitely this exponential term approaches zero faster than τ_{jo} approaches infinity, so that the second term tends to zero. The same argument applies to the third term except that it approaches zero much faster than the second term as τ_{jo} is increased since it is not multiplied by τ_{jo}. Thus the third term in the jth bracket can be omitted. Hence, for $\tau_{jo} > 1$ the only radiation energy contributions to the point $\bar{x}_i$ come from points $\bar{\xi}_i$ that are very close to $\bar{x}_i$. Thus the lower integration limit t_{j1} in the second term may be replaced by $-\infty$ since the points $\bar{\eta}_i$ behave like points at $-\infty$ with respect to $\bar{x}_i$ in terms of their radiation energy contributions to $\bar{x}_i$. (This argument breaks down if $\bar{x}_i$ is very close to $\bar{\eta}_i$, i.e., in the immediate vicinity of the wall.)

Now since the only radiation energy contributions to the point $\bar{x}_i$ come from the points $\bar{\xi}_i$ that are very close to it the variation of $\bar{\alpha}_j\bar{T}^4$ between these points $\bar{\xi}_i$ and point $\bar{x}_i$ cannot be too large and hence $\bar{\alpha}_j(\bar{\xi}_i)\bar{T}^4(\bar{\xi}_i)$ in the integrand of the second term of eq. (23) can be replaced by the Taylor series expansion around its value at $\bar{x}_i$, $\bar{\alpha}_j(\bar{x}_i)\bar{T}^4(\bar{x}_i)$. Thus, $\bar{\alpha}_j(t_j')\bar{T}^4(t_j')$ in the integrand of the second term of eq. (B1) can be replaced by its Taylor series expansion around t_j

$$\bar{\alpha}_j(t_j')\bar{T}^4(t_j') = \bar{\alpha}_j(t_j)\bar{T}^4(t_j) + (t_j' - t_j)\frac{d}{dt_j}\left[\bar{\alpha}_j(t_j)\bar{T}^4(t_j)\right] + \frac{(t_j' - t_j)}{2!}\frac{d^2}{dt_j^2}\left[\bar{\alpha}_j(t_j)\bar{T}^4(t_j)\right] + \cdots$$

Then the integration over t_j' in the second term of eq. (B1) becomes

$$\int_{-\infty}^{t_j}\bar{\alpha}_j(t_j')\bar{T}^4(t_j')\exp[-\tau_{jo}(t_j - t_j')]\,dt_j' = \bar{\alpha}_j(t_j)\bar{T}^4(t_j)\int_{-\infty}^{t_j}\exp[\tau_{jo}(t_j' - t_j)]\,dt_j'$$
$$+ \frac{d}{dt_j}\left[\bar{\alpha}_j(t_j)\bar{T}^4(t_j)\right]\int_{-\infty}^{t_j}(t_j' - t_j)\exp[\tau_{jo}(t_j' - t_j)]\,dt_j'$$
$$+ \frac{1}{2!}\frac{d^2}{dt_j^2}\left[\bar{\alpha}_j(t_j)\bar{T}^4(t_j)\right]\int_{-\infty}^{t_j}(t_j' - t_j)^2\exp[\tau_{jo}(t_j' - t_j)]\,dt_j' + \cdots \quad \text{(B2)}$$

Introducing the change of variable

$$Y = t_j' - t_j$$

into this expression, and using the relations

$$\frac{1}{b!}\int_{-\infty}^{o} Y^b \exp(\tau_{jo} Y)\,dY = (-1)^b/(\tau_{jo})^{b+1} \quad , \; b = 0, 1, 2, \ldots$$

and

$$\frac{\partial}{\partial t_j} = \frac{1}{\bar{K}_j} \sum_{i=1}^{3} \ell_i \frac{\partial}{\partial \bar{x}_i}$$

the resulting eq. (B2) reduces to

$$\int_{-\infty}^{t_j} \bar{\alpha}_j(t_j')\bar{T}^4(t_j')\exp[-\tau_{jo}(t_j - t_j')]\,dt_j'$$

$$= \frac{\bar{\alpha}_j(\bar{x}_i)\bar{T}^4(\bar{x}_i)}{\tau_{jo}} - \frac{1}{\tau_{jo}^2 \bar{K}_j} \sum_{m=1}^{3} \ell_m \frac{\partial}{\partial \bar{x}_m}\left[\bar{\alpha}_j(\bar{x}_i)\bar{T}^4(\bar{x}_i)\right]$$

$$+ \frac{1}{\tau_{jo}^3 \bar{K}_j} \sum_{p=1}^{3} \ell_p \frac{\partial}{\partial \bar{x}_p}\left\{\frac{1}{\bar{K}_j} \sum_{m=1}^{3} \ell_m \frac{\partial}{\partial \bar{x}_m}\left[\bar{\alpha}_j(\bar{x}_i)\bar{T}^4(\bar{x}_i)\right]\right\} \quad \ldots, \; \tau_{jo} > 1 \qquad \text{(B3)}$$

is obtained where the ℓ_i are the direction cosines of the directed line $S(\ell_i)$. If eq. (B3) is now substituted into the second term of eq. (B1) and the integration over the solid angle carried out the resulting expression can be written as

$$\tau_{jo}\bar{K}_j(\bar{x}_i)\int_0^1\int_{-\infty}^{t_j} \bar{\alpha}_j(t_j')\bar{T}^4(t_j')\exp[-\tau_{jo}(t_j - t_j')]\,dt_j'd\bar{\omega}$$

$$= \bar{K}_j(\bar{x}_i)\bar{\alpha}_j(\bar{x}_i)\bar{T}^4(\bar{x}_i) + \frac{1}{3\tau_{jo}^2} \sum_{m=1}^{3} \frac{\partial}{\partial \bar{x}_m}\left\{\frac{1}{\bar{K}_j}\frac{\partial}{\partial \bar{x}_m}\left[\bar{\alpha}_j(\bar{x}_i)\bar{T}^4(\bar{x}_i)\right]\right\}$$

$$+ \text{terms } O\left(1/\tau_{jo}^4\right) + \cdots \qquad \text{(B4)}$$

In obtaining this expression the properties

$$\int_o^1 \ell_i d\bar{\omega} = 0 \ , \ \int_o^1 \ell_i \ell_j d\bar{\omega} = \delta_{ij}/3 \ , \ \sum_{j=1}^{3} \ell_j \ell_{i,j} = 0 \ , \ i,j = 1, 2, 3$$

were employed where δ_{ij} is Kronecker's delta.

Now if terms of $0\left(1/\tau_{jo}^4\right)$ and lower are neglected in eq. (B4) and eq. (B4) is then substituted into eq. (B1) the resulting experession inside the jth bracket is

$$-\frac{1}{3\tau_{jo}^2} \sum_{j=1}^{3} \frac{\partial}{\partial \bar{x}_i} \left\{ \frac{1}{\bar{K}_j} \frac{\partial}{\partial \bar{x}_i} \left[\bar{\alpha}_j \bar{T}^4 \right] \right\} \tag{B5}$$

Thus the form of $\bar{F}^R_{i,\bar{i}}$ for a Δ_j where $\tau_{jo} > 1$ is given by the relation

$$-\frac{1}{3} \frac{\alpha_{jo}}{\tau_{jo}} \sum_{i=1}^{3} \frac{\partial}{\partial \bar{x}_i} \left\{ \frac{1}{\bar{K}_j} \frac{\partial}{\partial \bar{x}_i} \left[\bar{\alpha}_j \bar{T}^4 \right] \right\} \tag{B6}$$

which is a diffusion-type expression.

APPENDIX C

REVIEW OF THE AVAILABLE ABSORPTION PROPERTY DATA FOR HIGH-TEMPERATURE AIR

In the course of the research reported here, a survey of the data available for the absorption properties of high-temperature air was conducted and a brief evaluation of this data was carried out with regard to its extensiveness over wide ranges of frequency, temperature, and density and hence its usefulness in radiation gas dynamics.

Kivel and Bailey (ref. 16) were probably the first to present extensive data on the radiative properties of high-temperature air. They presented graphical and tabular data on the emissivity per cm, ε/L, of optically thin air in a temperature range from 1000° to 18 000° K and a density range from 10^{1} to 10^{-6} of normal sea level density. However, very little data was presented on the frequency dependence of the radiative properties. It should be noted that the data given for ε/L in this reference can be converted to a Planck mean linear absorption coefficient by the relation

$$K_p = \frac{1}{2}\frac{\varepsilon}{L} \tag{C1}$$

Armstrong et.al., (ref. 17) presented graphical data for the linear spectral absorption coefficient of air at 12 000° K and sea level density over a wavelength range of 1167 to 19 837 Å. Other graphical data on the frequency dependence of the absorption coefficient was given at a pressure of 1 atm for kT ranging from 2 to 20 ev and $h\nu$ from 1 to 1000 ev. Armstrong et. al., also plotted the absorption coefficient at a wavelength of 3967 Å over the temperature range 3000° to 13 000° K for sea level density and 10^{-6} of sea level density. Tabular data was also presented for the Planck mean linear absorption coefficient over a range of temperature from 1000° to 18 000° K and a range of densitites from 10^{1} to 10^{-6} of sea level density This data has been displayed graphically by Davis (ref. 18). Graphical data for the Planck mean linear absorption coefficient was also given by Armstrong et.al., for densities ranging from 10^{1} to 10^{-6} of sea level density and temperatures ranging from approximately 6000° to 250 000° K. The preceding reference is a good survey article on the absorption coefficients of high temperature air. However, little data is given on the frequency dependence of the absorption coefficient for the temperature and pressure ranges of interest in reentry calculations.

Breene and Nardone (ref. 19) have presented curves of the total spectral emissivity for a 1 cm thick isothermal layer of air. The wave number range covered is from 1000 to 62 000 cm^{-1} while the density ranges from 10^{-3} to 10^{2} of normal sea level density for temperatures of 3000° to 9000° K.

The emissivity data of this reference can be converted to linear absorption coefficient data by use of the relation

$$\varepsilon_\nu = 1 - \exp(-\alpha K_\nu x) \tag{C2}$$

where $x = 1$ cm and α is a geometrical factor taken as 1.8.

Breene and Nardone also presented data on the total radiance of air for the same temperature and density ranges considered in the case of the spectral emissivity. The quantity plotted is apparently derived from the relation

$$J_T = [1 - \exp(-\alpha K x)] \frac{\sigma T^4}{\pi} \tag{C3}$$

with x taken as unity. For an optically thin layer, where $[1 - \exp(-\alpha K x)] < 0.1$, eq. (C3) reduces to

$$J_T = \alpha K x \frac{\sigma T^4}{\pi} \tag{C4}$$

with x equal unity. The major drawbacks of the radiative property data given by Breene and Nardone are that temperatures higher than 9000° K are not considered and also the data is presented in a form which is difficult to use in general radiation gas dynamics where the absorption coefficient is the radiative property of primary interest.

Thomas (ref. 20) presented graphical data on the total emissivity per cm, ε/L, for high-temperature air. The range of temperatures covered was 6000° to 23 000° K and the range of density levels was 10^{-6} to 10^{1} of sea level density. This emissivity data can be converted to Planck mean linear absorption coefficients by eq. (C1). The data in this reference would be quite useful in obtaining the Planck mean absorption coefficient. Its main limitation is that no data was given on the frequency dependence of the absorption coefficient.

Sewell (ref. 3) has presented graphical data on the spectral emission coefficient of air over a wave number range of 6000 to 202 000 cm^{-1}, a density range of 10^{1} to 10^{-6} of sea level density and a temperature range of 4000° to 20 000° K. The linear spectral absorption coefficient K_λ can be calculated from the emission coefficient j_λ by use of the simple relation

$$K_\lambda = \frac{j_\lambda}{B_\lambda} \tag{C5}$$

where

$$B_\lambda = \frac{2hc^2}{\lambda^5} \frac{1}{\exp(hc/k\lambda T) - 1} \tag{C6}$$

Sewell has also presented graphical data on the mean linear absorption coefficient K for the same temperature and density ranges as those mentioned earlier in the case of the spectral emission coefficient. It should be noted that the Planck mean absorption coefficient K_p may be related to mean absorption coefficient of Sewell by the expression

$$K_p = \pi K \tag{C7}$$

The data on the absorption coefficient of air which is given in this reference is much more extensive than that of any other reference reviewed during this survey. Also the data is presented in a form from which the spectral and Planck mean absorption coefficients can be obtained with ease. Hence Sewell's absorption coefficient data for air should be quite usable and useful in radiation gas dynamics problems.

Nardone et.al. (ref. 21) have presented graphically the spectral radiance J_λ for a 1 cm thick slab of equilibrium air over a wavelength range of 600 to 100 000 Å at a density of 10^{-1} of sea level density for temperatures of 3000°, 10 000°, and 25 000° K. The quantity plotted was

$$J_\lambda = \varepsilon_\lambda B_\lambda = [1 - \exp(- K_\lambda L)]B_\lambda \tag{C8}$$

where L = 1 cm. For an optically thin layer, where $[1 - \exp(- K_\lambda L)] < 0.1$, eq. (C8) becomes

$$J_\lambda = K_\lambda L B_\lambda \tag{C9}$$

with L = 1 cm.

Nardone et. al., also presented graphical data for the total radiance of a 1 cm slab of air over a density range of 10^{-4} to 10^2 of sea level density and a temperature range from 3000° to 25 000° K. In this case the quantity plotted was

$$J_T = [1 - \exp(- KL)] \frac{\sigma T^4}{\pi} \tag{C10}$$

where L = 1 cm. For an optically thin layer, where [1 - exp(- KL)] < 0.1, eq. (C10) reduces to

$$J_T = KL \frac{\sigma T^4}{\pi} \qquad (C11)$$

with L = 1 cm.

The spectral radiative property data given in this reference extends over a wide wavelength range but is restricted to a single density level and three different temperatures. It is also presented in a form which is difficult to use in general radiation gas dynamics where the absorption coefficient K_λ is of primary interest. The frequency averaged radiative property data given by Nardone et.al., is quite extensive with regard to the density and temperature ranges covered. However it is also presented in a form which is difficult to use when the Planck mean absorption coefficient is of primary interest.

Archer (ref. 22) has presented tabular data for the spectral distribution of energy radiated by equilibrium air in the temperature range from 3000° to 9000° K for densities of 10^{-4}, 10^{-5}, and 10^{-6} of sea level density. These results for the spectral radiant emission are an extension of the work of Breene and Nardone (ref. 19) to the lower density levels and cover the wave number range from 1250 to 56 000 cm^{-1}. The data given in this reference are presented in a form from which it would be difficult to obtain the spectral absorption coefficient K_λ. Thus its usefulness in general radiation gas dynamics is limited.

Churchill et.al., (ref. 23) defined an average absorption coefficient for an isothermal, homogeneous, gas layer of thickness x. Graphical results for heated air were plotted versus wavenumber with temperature, density, and thickness x as parameters. The wavenumber range covered was 21 500 to 49 000 cm^{-1} while the temperature range was 1000° to 8000° K and the density range was 10^0 to 10^{-4} of sea level density.

Gilmore (ref. 24) presented tabular data for the linear spectral absorption coefficient of air over a wavelength range of 0.1167 to 1.9836 microns. The temperature range covered was 2000° to 8000° K and the density range was 10^1 to 10^{-4} of sea level density. Gilmore also presented tabular data on the Planck mean absorption coefficient for the same temperature and density range. The absorption coefficient data given in this reference is considered to be quite accurate but its usefulness in radiation gas dynamics is limited by the fact that temperatures above 8000° K are not considered.

Bowen (ref. 25) presented graphical data on the spectral radiance of high-temperature air over a wavelength range of 0.2 to 1.0 micron for density levels from 10^{-6} to 10^0 of sea level density and temperatures from 3000° to 12 000° K. The quantity plotted is apparently derived from eq. (C8) with L taken as unity. Bowen also presented graphical data on the total radiance of air for the wavelength interval $\delta\lambda$ of 0.35 to 0.55

microns over the same temperature and density ranges as those of the spectral data. The quantity plotted is apparently

$$J_T = \int_{\delta\lambda} J_\lambda d\lambda \tag{C12}$$

where $\delta\lambda$ is 0.35 to 0.55 microns and J_λ is given by eq. (C8). The total radiance of air for the wavelength interval of 0.35 to 0.75 microns was also given over the same temperature and density ranges as those above. The quantity plotted is apparently the same as that given by eq. (C12) except $\delta\lambda$ is 0.35 to 0.75 microns.

Ashley (ref. 26) has presented graphical data on the linear spectral absorption coefficient of high-temperature equilibrium air for optical wavelengths within the range of 3800 to 6500 Å. The temperature range covered was 1000° to 24 000° K while the density levels ranged from 10^{-6} to 10^0 of sea level density. The mean linear absorption coefficient averaged over the wavelength interval $\delta\lambda$ from 3800 to 6500 Å, $\mu_{\delta\lambda}$, where

$$\mu_{\delta\lambda} \equiv \frac{\int_{\delta\lambda} \mu_\lambda d\lambda}{\delta\lambda}$$

has also been presented for the same temperature and density ranges. Tabular data has also been given over the same wavelength, temperature, and density ranges for the apparent spectral absorption coefficient which is the true absorption coefficient corrected for induced emission. The absorption coefficient data given in the above reference is quite extensive over large temperature and density ranges. However the wavelength range considered is limited to the optical band of 0.38 to 0.65 microns.

Gilmore (ref. 27) gives graphical data on the linear absorption coefficient of air at a wavelength of 1270 Å for a temperature range of 2000° to 8000° K and density levels of 10^{-3} and 10^0 of sea level density. Graphical data is also presented on the mean absorption coefficients in the spectral regions of 4100 to 4500 Å and 5500 to 6200 Å for the same temperature range and density levels.

In the calculations reported here, Sewell's data was employed because it is extensive and is presented in a form suitable for nongrey calculation.

APPENDIX D

NONGREY ABSORPTION COEFFICIENT MODEL AND THERMODYNAMIC RELATIONS FOR HIGH-TEMPERATURE AIR

In Appendix C it was concluded that the data presented by Sewell (ref. 3) for the absorption properties of air was the most extensive with respect to the frequency, temperature, and density and was in a form from which both the spectral and Planck mean absorption coefficients could be obtained with ease. Hence Sewell's data has been used to determine the linear spectral absorption coefficient of air for several representative combinations of density level and temperature. These results have been plotted versus wavenumber and are given in fig. 16.

For comparison purposes the spectral absorption coefficient of optically thin air has also been determined using the spectral radiance data at 10 000° K and a density of 10^{-1} normal sea level density given by Nardone et.al., (ref. 21). The results have been plotted versus wavelength and are shown in fig. 17 along with the spectral absorption coefficient derived from Sewell's data for the same temperature and density condition. It is seen from fig. 17 that Sewell's spectral absorption coefficient data and the data of Nardone et.al., are in fair agreement with regard to order of magnitude and gross spectral behavior.

From the curves of spectral absorption coefficient in figs. 16 and 17 with particular emphasis on those curves displayed in fig. 17 it is seen that the nongrey absorption coefficient of air could be mathematically represented with substantial accuracy by the step function model shown in fig. 5.

The step function model in fig. 5 appears to be a quite reasonable mathematical representation of the spectral absorption coefficient of air for most thermodynamic conditions except combinations of high temperatures on the order of 18 000° to 20 000° K and low densities of 10^{-3} to 10^{-6} of sea level density such as those of figs. 16(f) and 16(i). However at these thermodynamic conditions of low density and high temperature the assumption of local thermodynamic equilibrium which applies throughout the analysis presented here is probably invalid (ref. 27).

Now the nongrey absorption coefficient model in fig. 5 represents quite well the spectral absorption coefficient data for air as given in fig. 17 at a temperature of 10 000° K and a density of 10^{-1} of sea level density which are typical of thermodynamic conditions expected to exist in the boundary layer when the effect of energy transfer by air radiation is appreciable. Thus the temperature and density dependence used for $K_1(T,\rho)$ in fig. 5 will be obtained by first determining from Sewell's data the average absorption coefficient for the spectral interval associated with

K_1 and then correlating this average absorption coefficient as a function of temperature and density.

Using Sewell's graphical data and the relation

$$K_1 = \frac{\int_{\delta\omega} K_\lambda d\omega}{\delta\omega} , \quad \omega = 1/\lambda \tag{D1}$$

the average absorption coefficient K_1 for the wavenumber interval $\delta\omega$ of 74 000 cm^{-1} to 122 000 cm^{-1} has been determined first for temperature of 8000°, 10 000°, 12 000°, and 14 000° K at a density of 10^{-1} of sea level density and then for densities of 10^{-4}, 10^{-3}, 10^{-2}, 10^{-1}, and 10^{0} of sea level density at a temperature of 10 000° K. Next assuming that the functional dependence of K_1 on temperature T and density ρ can be expressed in power law form (see eq. (37)) the aforementioned temperature and density data for the average absorption coefficient has been correlated using the least-mean-square method to obtain the following relation for $K_1(\rho,T)$

$$K_1(\rho,T) = 4.370\left(\rho/\rho_{s.l.}\right)^{1.009}(T/10^4)^{2.850} \tag{D2}$$

where $\rho_{s.l.}$ is the normal sea level density of 1.225×10^{-3} gm·cm^{-3}.

Once $K_1(\rho,T)$ is obtained the relation $K_2(\rho,T)$ for the mean absorption coefficient associated with the other spectral interval of fig. 5 may be determined from the following expression for the Planck mean absorption coefficient

$$K_p(\rho,T) = K_1(\rho,T)\alpha_1(T) + K_2(\rho,T)\alpha_2(T) \tag{D3}$$

provided $K_p(\rho,T)$ and the $\alpha_j(T)$, $j = 1, 2,$ are known. The $\alpha_j(T)$ for the spectral intervals of fig. 5 can be determined at any given temperature from fig. 15 by use of eq. (A14). The functional relation used for $K_p(\rho,T)$ is the correlation formula determined by Olstad (ref. 28) for Planck mean absorption coefficient data derived from the results of Kivel and Bailey (ref. 16), Sewell (ref. 3) and Nardone et.al. (ref. 21). This relation is

$$K_p(\rho,T) = 7.943 \times 10^{-2}\left(\rho/\rho_{s.l}\right)^{1.10}(T/10^4)^{6.95} \tag{D4}$$

It should be noted that the density and temperature dependence of K_p in

eq. (D4) is in excellent agreement with that proposed by Goulard (ref. 13) for the grey absorption coefficient of high-temperature air.

Numerical values of $K_2(\rho,T)$ have been determined from eq. (D3) for temperatures ranging from 4000° to 14 000° K and densities ranging from 10^{-4} to 10^{0} of sea level density. These data for $K_2(\rho,T)$ were then correlated as a function of temperature and density in the same manner as that employed for $K_1(\rho,T)$. The resulting correlation formula for $K_2(\rho,T)$ is

$$K_2(\rho,T) = 4.985 \times 10^{-2}\left(\rho/\rho_{s.l.}\right)^{1.205}(T/10^4)^{5.47} \tag{D5}$$

Now the linear absorption coefficients $K_p(\rho,T)$, $K_1(\rho,T)$, and $K_2(\rho,T)$ given respectively by eqs. (D4), (D2), and (D5) may be expressed as mass absorption coefficients $\kappa_p(T,P)$, $\kappa_1(T,P)$, and $\kappa_2(T,P)$ by using the relation between linear and mass absorption coefficient

$$K = \rho\kappa \tag{D6}$$

and then employing the equation of state for a perfect gas

$$\rho = \frac{P}{ZRT} \tag{D7}$$

where Z is expressed as a function of temperature and pressure by the correlation formula

$$Z = 2.11(T/10^4)^{0.775}(P/P_o)^{-0.065} \tag{D8}$$

This correlation formula for Z was determined by Olstad (ref. 28) from the thermodynamic data of high-temperature air given by Ahyte and Peng (ref. 29). The resulting equations for κ_p, κ_1, and κ_2 are, respectively,

$$\kappa_p(T,P) = 42.22(T/10^4)^{6.772}(P/P_o)^{0.1065} \tag{D9}$$

$$\kappa_1(T,P) = 3.431 \times 10^3(T/10^4)^{2.834}(P/P_o)^{0.0096} \tag{D10}$$

and

$$\kappa_2(T,P) = 16.89(T/10^4)^{5.106}(P/P_o)^{0.2182} \qquad \text{(D11)}$$

where T is in °K and P is in atm with P_o equal 1 atm. The units of κ_p, κ_1, and κ_2 are $cm^2 \cdot gm^{-1}$.

It is necessary to know the enthalpy as a function of temperature and pressure, $h(T,P)$, before the solution to the integral form of the energy equation can be obtained. The functional relation used for $h(T,P)$ was

$$h(T,P) = 5.201 \times 10^{11}(T/10^4)^{1.7699}(P/P_o)^{-0.0920} \qquad \text{(D12)}$$

which is a modified form of a correlation formula determined by Olstad (ref. 28) from the high-temperature air data of Ahyte and Peng (ref. 29). The units of $h(T,P)$ in eq. (D12) are $erg \cdot gm^{-1}$.

If eq. (D12) is written for external flow conditions the resulting relation is

$$h_e = 5.201 \times 10^{11}(T_e/10^4)^{1.7699}(P_e/P_o)^{-0.0920} \qquad \text{(D13)}$$

Then from eqs. (D12) and (D13) the expression for $\bar{h} \equiv h/h_e$ is

$$\bar{h} = \bar{T}^{1.7699} \qquad \text{(D14)}$$

where the boundary layer condition of P/P_e equal to unity has been employed. Equation (D14) is the $\bar{h} = \bar{h}(\bar{T})$ relation employed in the calculation.

The only remaining property value needed for the calculation of eq. (76) is the Prandtl number of air. This has been taken as 0.70.

Once the solution $\bar{h}(\bar{x},\eta)$ for the energy equation, eq. (70), is obtained the convective and radiative wall heat fluxes may be calculated using eqs. (72) and (74) provided that the values of $\rho_e\mu_e$ and C are known. The values of $\rho_e\mu_e$ can be determined from the relation

$$\rho_e\mu_e = \frac{2.80 \times 10^{-4}(P_e)^{0.992}}{(h_e)^{0.3329} - 119.9} \qquad \text{(D15)}$$

which was derived from the correlation formulas given by Cohen (refs. 30, 31) for high-temperature air. The units of $\rho_e\mu_e$ in eq. (D15) are $gm^2 \cdot cm^{-4} \cdot sec^{-1}$ when h_e is expressed in $erg \cdot gm^{-1}$ and P_e in atm. The values of C may be determined from the relation

$$C = \frac{\rho_*\mu_*}{\rho_e\mu_e} = \frac{(h_e)^{0.3329} - 119.9}{(h_*)^{0.3329} - 119.9} \tag{D16}$$

where h_* is the reference enthalpy given by eq. (73).

APPENDIX E

COMPUTER PROGRAM FOR SOLVING THE BOUNDARY LAYER ENERGY EQUATION AND SUBSEQUENT CALCULATION OF THE CONVECTIVE AND RADIATIVE WALL HEAT FLUXES

The solution to the boundary layer energy equation has been determined by the method described previously using an IBM 7072 digital computer. From these results the computer subsequently calculated both the convective and radiative wall heat fluxes. The computer program necessary to make the computer carry out these actions was written in FORTRAN II programming language. The variable names which were assigned to the mathematical relations and symbols used in the text and appendices are presented below immediately preceding the program listing.

ALPHA	$\alpha_j(\bar{T}T_e)$ as given by eq. (A12)
BE2	β_{j+1} in eq. (A12)
BE1	β_j in eq. (A12)
N	number of intervals used in subroutine for α_j
ETA	η as given by eq. (65)
W	W as given by eq. (77)
AMESS	integrand of eq. (A12)
MMN	number of η's used
PR	Pr
UE	u_e , $cm \cdot sec^{-1}$
TE	T_e , °K
PE	P_e , atm
TBARW	$\bar{T}_w$
EPSW	ε_w
EPS	a predetermined small number used in the convergence test

SIGMA	Stefan-Boltzmann constant, $erg \cdot cm^{-2} \cdot sec^{-1} \cdot {}^{\circ}K^{-4}$
FPP1	$f''(\eta)$ at $\eta = 0.05$
FPP2	$f''(\eta)$ at $\eta = 0.10$
XL	L , cm
POW1	the exponent on $(T/10^4)$ in the relation for $\kappa_p(T,P)$
POW2	the exponent on (P/P_o) in the relation for $\kappa_p(T,P)$
CE	the coefficient of $(T/10^4)^{POW1}(P/P_o)^{POW2}$ in the relation for $\kappa_p(T,P)$
C	C as given by eq. (D16)
FA(I)	the values of $f(\eta)$ at $\eta = \eta(I)$
ETA(I)	the values of $\eta = \eta(I)$
FPP(I)	the values of $f''(\eta)$ at $\eta = \eta(I)$
FFA(I)	the values of $f(\eta)$ at $\eta = 0, 0.025, 0.05, 0.10, 0.20$
X(I)	the values of $\bar{x}$
E1E(I)	the values of ε_{je}
POWER(I)	the exponents on $(T/10^4)$ in the relations for $\kappa_j(T,P)$
POW(I)	the exponents on (P/P_o) in the relations for $\kappa_j(T,P)$
CON(I)	the coefficients of $(T/10^4)^{POWER(I)}(P/P_o)^{POW(I)}$ in the relations for $\kappa_j(T,P)$
JUNK	variable which equals zero for grey case and unity for nongrey case
ALAM1(I)	λ_j used in eq. (A10), microns
ALAM2(I)	λ_{j+1} used in eq. (A10), microns
A1E(K)	$\alpha_j(T_e)$
A1W(K)	$\alpha_j(\bar{T}_w T_e)$
BET1(K)	β_j for $\alpha_j(T_e)$ calculation
BET2(K)	β_{j+1} for $\alpha_j(T_e)$ calculation

BETW1(K)	β_j for $\alpha_j(\bar{T}_w T_e)$ calculation
BETW2(K)	β_{j+1} for $\alpha_j(\bar{T}_w T_e)$ calculation
XKPE	$\kappa_p(T_e,P_e)$, $cm^2 \cdot gm^{-1}$
FACT	$\varepsilon_w \sigma T_e^4$, $erg \cdot cm^{-2} \cdot sec^{-1}$
ACT	$\sum_{j=1}^{n} \varepsilon_{je} \alpha_j(T_e) - \bar{T}_w^4$
TEMP1(K)	$- \alpha_j(T_e) \varepsilon_{je}$
TEMP2(K)	$- 0.5\left[\varepsilon_w \alpha_j(\bar{T}_w T_e)\bar{T}_w^4 + (2 - \varepsilon_w)\varepsilon_{je}\alpha_j(T_e)\right]$
AA1	1/0.565
AHE	h_e as given by eq. (D13), $erg \cdot gm^{-1}$
RHOMU	$\rho_e \mu_e$ as given by eq. (D15) , $gm^2 \cdot cm^{-4} \cdot sec^{-1}$
AA2	$Pr\ u_e^2/h_e$
APOWR	POWER(K)
APOW	POW(K)
XK(K)	$\kappa_j(T_e,P_e)$, $cm^2 \cdot gm^{-1}$
AHBRW	$\bar{h}_w$
G1(1)	$\int_o^\eta f d\eta_1$ at $\eta = 0.0$
G1(2)	$\int_o^\eta f d\eta_1$ at $\eta = 0.2$
G1(I)	$\int_o^\eta f d\eta_1$ at $\eta = \eta(I)$
PR2	$\frac{Pr}{2}$
G2(1)	$\exp\left[-\frac{Pr}{2} G1(1)\right]$
G2(I)	$\exp\left[-\frac{Pr}{2} G1(I)\right]$
G4(1)	G2(1)
G	$\int_o^\eta f d\eta_1$ at $\eta = 0.1$
G4(2)	$\exp\left[-\frac{Pr}{2} G\right]$
G4(3)	$\exp\left[-\frac{Pr}{2} G1(2)\right]$ at $\eta = 0.2$

G3(1)	$\int_o^{\eta} G4(\eta_1)d\eta_1$ at $\eta = 0$
G3(2)	$\int_o^{\eta} G4(\eta_1)d\eta_1$ at $\eta = 0.2$
G3(I)	$\int_o^{\eta} G2(\eta_1)d\eta_1$ at $\eta = \eta(I)$
G5(1)	$\exp\left[\frac{Pr}{2}\ G1(1)\right]$ at $\eta = 0$
G5(I)	$\exp\left[\frac{Pr}{2}\ G1(I)\right]$
G6(1)	$\left[f''(\eta)\right]^2 G5(1)$ at $\eta = 0$
GG	$\int_o^{\eta} f d\eta_1$ at $\eta = 0.05$
G6(2)	$\left\{\left[f''(\eta)\right]^2 \exp\left(\frac{Pr}{2}\ GG\right)\right\}$ at $\eta = 0.05$
G6(3)	$\left\{\left[f''(\eta)\right]^2 \exp\left(\frac{Pr}{2}\ G\right)\right\}$ at $\eta = 0.1$
G7(1)	$\int_o^{\eta} G6(\eta_1)d\eta_1$ at $\eta = 0$
G7(2)	$\int_o^{\eta} G6(\eta_1)d\eta_1$ at $\eta = 0.1$
G8(1)	G6(1)
G8(2)	G6(3)
G8(3)	$\left\{\left[f''(\eta)\right]^2 \exp\left[\frac{Pr}{2}\ G1(2)\right]\right\}$ at $\eta = 0.2$
G7(3)	$\int_o^{\eta} G8(\eta_1)d\eta_1$ at $\eta = 0.2$
G9(1)	G4(1)G7(1)
G9(2)	G4(2)G7(2)
G9(3)	G4(3)G7(3)
G12(I)	$\left[f''(\eta)\right]^2 G5(I)$ at $\eta = \eta(I)$
G11(1)	G9(1)
G11(2)	G9(3)
G13(1)	G7(1)
G13(2)	G7(3)
G13(I)	$\int_o^{\eta} G12(\eta_1)d\eta_1$ at $\eta = \eta(I)$
G11(I)	G13(I)G2(I)

G10(1)	$\int_o^\eta G9(\eta_1)d\eta_1$ at $\eta = 0.0$
G10(2)	$\int_o^\eta G9(\eta_1)d\eta_1$ at $\eta = 0.2$
G10(I)	$\int_o^\eta G11(\eta_1)d\eta_1$ at $\eta = \eta(I)$
CZERO	C_o as given by eq. (81)
G10(MMN)	G10(I) at $\eta = \eta_\delta$
G3(MMN)	G3(I) at $\eta = \eta_\delta$
AHBR1(I)	$(\bar{h}_{in})_n$ in eq. (84) , $\eta = \eta(I)$
AHBRO(I)	$\bar{h}_o(\eta)$ as given by eq. (80) , $\eta = \eta(I)$
CONST	$-4Pr\sigma T_e^4 L/u_e h_e$
CONS	CONST$\cdot\kappa_p(T_e,P_e)$
TBAR(I)	$\left[(\bar{h}_{in})_n\right]^{1/AA1}$, $\eta = \eta(I)$
TO(I)	$(\bar{h}_o)^{1/AA1}$, $\eta = \eta(I)$
DONST	CONST$\cdot\kappa_j(T_e,P_e)\alpha_j(T_e)$
ABC(I)	CONST$\cdot$G3(I)/G3(MMN)
APOWR	POWER(K)
XK1(I,K)	$\bar{\kappa}_j(\bar{T})$ at $\eta = \eta(I)$
AB(I)	ABC(I)X(J)
XKP(I)	$\bar{\kappa}_p(\bar{T})$ at $\eta = \eta(I)$
W(I)	W of eq. (77) at $\eta = \eta(I)$
QW(I)	the integrand of the integral in eq. (74) at $\eta = \eta(I)$
G15(I)	W(I)G5(I)
XT	$\bar{T}$ at $\eta = 0.1$
XK1A(K)	$\bar{\kappa}_j(\bar{T})$ at $\eta = 0.1$
XKP1	$\bar{\kappa}_p(\bar{T})$ at $\eta = 0.1$
WT	W at $\eta = 0.1$

QT	QW at $\eta = 0.1$
AGAIN(1)	$\int_o^{\eta} QW(\eta_1)d\eta_1$ at $\eta = 0$
AGAIN(2)	$\int_o^{\eta} QW(\eta_1)d\eta_1$ at $\eta = 0.2$
AGAIN(I)	$\int_o^{\eta} QW(\eta_1)d\eta_1$ at $\eta = \eta(I)$
G17(1)	$\int_o^{\eta} G15(\eta_1)d\eta_1$ at $\eta = 0$
G17(2)	$\int_o^{\eta} W(\eta_1)\exp\left(\frac{Pr}{2}\int_o^{\eta_1} f d\eta_2\right)d\eta_1$ at $\eta = 0.2$
G17(I)	$\int_o^{\eta} G15(\eta_1)d\eta_1$ at $\eta = \eta(I)$
G19(I)	G17(I)G2(I)
G19(1)	G17(1)G2(1)
G19(2)	G17(2)G2(2)
G20(1)	G19(1)
G20(3)	G19(2)
XT1	$\bar{T}$ at $\eta = 0.05$
XK1B(K)	$\bar{\kappa}_j(\bar{T})$ at $\eta = 0.05$
XKP11	$\bar{\kappa}_p(\bar{T})$ at $\eta = 0.05$
WT1	W at $\eta = 0.05$
WTG1	$WT1\ \exp\left(\frac{Pr}{2}\ GG\right)$
GTX	$\int_o^{\eta} W(\eta_1)\exp\left(\frac{Pr}{2}\int_o^{\eta_1} f d\eta_1\right)d\eta_2$ at $\eta = 0.1$
G20(2)	G4(2)GTX
TERM2(1)	$\int_o^{\eta} G19(\eta_1)d\eta_1$ at $\eta = 0$
TERM2(2)	$\int_o^{\eta} G20(\eta_1)d\eta_1$ at $\eta = 0.2$
CX	CONST·X(J)
TERM2(I)	$\int_o^{\eta} G19(\eta_1)d\eta_1$ at $\eta = \eta(I)$
AHBR2(I)	$(\bar{h}_{out})_n$ in eq. (84)
SS	$\sum_{I=1}^{MMN}\left[AHBR2(I) - AHBR1(I)\right]$

SUMA	$\sum_{I=1}^{MMN} \left\lvert \left[AHBR2(I) - AHBR1(I) \right] \right\rvert$
AHBAR(I,J)	the solution for $\bar{h}$, $\eta = \eta(I)$, $\bar{x} = X(J)$
T(I,J)	the solution for $\bar{T}$, $\eta = \eta(I)$, $\bar{x} = X(J)$
C1(J)	C_1 as given by eq. (82), $\bar{x} = X(J)$
TERM2(MMN)	TERM2(I) at $\eta = \eta_\delta$
S(J)	s as given by eq. (65) , $\bar{x} = X(J)$
QWR(J)	q_{Rw} as given by eq. (74) , $\bar{x} = X(J)$
AGAIN(MMN)	AGAIN(I) at $\eta = \eta_\delta$
QWCO(J)	q_{cwo} as given by eq. (72) , $\bar{x} = X(J)$
QWC1(J)	q_{cw} as given by eq. (72) , $\bar{x} = X(J)$

```
      PROGRAM WITH EXPANDED ETA AND EXPANDED W
      SUBROUTINE ALPHA(BE2,BE1,N,VALUE)
      DIMENSION AMESS(400),Z(400)
      DO 1 I = 1,400
      AMESS(I) = 0.0
      Z(I) = 0.0
    1 CONTINUE
      AN = N
      NN = N + 1
      Z(1) = BE1
      IF(BE1) 6,3,7
    6 STOP
    3 AMESS(1) = 0.0
      GO TO 5
    7 IF(Z(1) - 112.) 16,16,17
   16 AMESS(1) = (Z(1)**3)/(EXPF(BE1) - 1.)
      GO TO 18
   17 VALUE = 0.0
      RETURN
   18 CONTINUE
    5 CONTINUE
      IF(BE2 - 112.) 19,19,20
   20 DZ = (112. - BE1)/AN
      GO TO 21
   19 DZ = (BE2 - BE1)/AN
   21 CONTINUE
      DO 10 JJ = 2,NN
      Z(JJ) = Z(JJ - 1) + DZ
   11 AMESS(JJ) = (Z(JJ)**3)/(EXPF(Z(JJ)) - 1.)
   10 CONTINUE
      NM = N - 2
      NM = NM
      SA = 0.0
      SB = 0.0
      DO 4 L = 2,NM,2
      SA = SA + AMESS(L)
      SB = SB + AMESS(L + 1)
    4 CONTINUE
      SA = SA + AMESS(N)
      VALUE = (.15398)*(DZ/3.)*(AMESS(1) + 4.*SA + 2.*SB + AMESS(NN))
      VALUE = VALUE
      RETURN
      END
  700 DIMENSION G1(45),FFA(5),G2(45),G3(45),G4(3),FA(45),ETA(45),G5(45),
  7001G6(3),G7(3),G8(3),G9(3),G10(45),G11(45),G12(45),G13(45),AHBR0(45),
  7002AHBR1(45),TBAR(45),AB(45),G15(45),G17(45),G19(45),G20(3),TERM2(45)
  7003,AHBR2(45),X(10),AHBAR(45,10),ABC(45),W(45),FPP(45),XK1B(10),ALAM1
  7004(10),ALAM2(10),POWER(10),POW(10),CON(10),A1E(10),A1W(10),E
  70051E(10),TEMP2(10),XK(10),BET1(10),BET2(10),BETW1(10),XKP(45),QWR(10
  7006)
      DIMENSION TEMP1(10),C1(10),QW(45),AGAIN(45),S(10),QWC0(10),QWC1(10
     1)
      DIMENSION T(45,10),T0(45),BETW2(10),XK1(45,10),DONST(10),XK1A(10)
  701 READ 20,NUM
      PRINT 21,NUM
      NUM = NUM
      READ 20,MMN
      PRINT 136,MMN
      READ 100, PR,UE,TE,PE,TBARW,EPSW,EPS
```

```
  490 READ 100, SIGMA,FPP1,FPP2,XL
      READ 100, POW1,POW2,CE
      POW1 = POW1
      POW1 = POW1
      POW2 = POW2
      READ 100,C
  702 READ 101,(FA(I), I = 1,MMN)
  703 READ 101,(ETA(I), I = 1,MMN)
  704 READ 101,(FPP(I), I = 1,MMN)
  705 READ 101,(FFA(I),I=1,5)
  706 READ 101,(X(I), I = 1,10)
      READ 100,(E1E(I), I = 1,NUM)
      READ 100,(POWER(I), I = 1,NUM)
      READ 100,(POW(I), I = 1,NUM)
      READ 100,(CON(I), I = 1,NUM)
      READ 55, JUNK
IF JUNK = 0, GREY CASE, IF JUNK = 1, NON-GREY CASE
      IF(JUNK)56,56,57
   57 READ 100,( ALAM1(I), I = 1,NUM)
      READ 100,( ALAM2(I), I = 1,NUM)
      GO TO 58
   56 PRINT 59
   58 CONTINUE
  970 PRINT 920,PR
  971 PRINT 921,UE
  972 PRINT 922,TE
  973 PRINT 923,PE
  974 PRINT 924,TBARW
  975 PRINT 925,EPSW
  978 PRINT 928,EPS
  979 PRINT 929,XL
      PRINT 50, POW1
      PRINT 51, POW2
      PRINT 52, CE
  977 PRINT 927,(E1E(I), I = 1,NUM)
  980 PRINT 930,(POWER(I), I = 1,NUM)
      PRINT 450,( POW(I), I = 1,NUM)
      PRINT 451,( CON(I), I = 1,NUM)
      PRINT 32, C
      IF(JUNK)60,60,62
   62 PRINT 926,(ALAM1(I), I = 1,NUM)
      PRINT 976,( ALAM2(I) , I = 1,NUM)
   60 CONTINUE
      IF(JUNK) 63,63,64
   63 DO 65 K = 1,NUM
      A1E(K) = 1.0
      A1W(K) = 1.0
   65 CONTINUE
      GO TO 66
   64 DO 150 K = 1,NUM
      BET1(K) = (14388.)/(TE*ALAM1(K))
      BET2(K) = (14388.)/(TE*ALAM2(K))
      BETW1(K) = BET1(K)/TBARW
      BETW2(K) = BET2(K)/TBARW
      BAT1 = BET1(K)
      BAT2 = BET2(K)
      CALL ALPHA(BAT2,BAT1,398,ANS)
      A1E(K) = ANS
      BAT1 = BETW1(K)
```

```
      BAT2 = BETW2(K)
      CALL ALPHA(BAT2,BAT1,398,ANS)
      A1W(K) = ANS
  150 CONTINUE
   66 CONTINUE
  454 PRINT 404,(A1E(K), K = 1,NUM)
  455 PRINT 405,(A1W(I), I = 1,NUM)
      XKPE = CE*((TE/10000.)**POW1)*(PE**POW2)
      PRINT 71, XKPE
      FACT = EPSW*(TE**4)*SIGMA
      ACT = 0.0
      DO 41 K = 1,NUM
      ACT = ACT + E1E(K)*A1E(K)
   41 CONTINUE
      ACT = ACT - TBARW**4
      DO 151 K = 1,NUM
      TEMP1(K) = - E1E(K)*A1E(K)
      TEMP2(K) = -(.5)*(EPSW*A1W(K)*(TBARW**4) + (2. - EPSW)*E1E(K)*A1E(
     1K))
  151 CONTINUE
      PRINT 360, FACT
      PRINT 361, ACT
      PRINT 179,(TEMP1(K), K = 1,NUM)
  456 PRINT 406,(TEMP2(K), K = 1,NUM)
  714 AA1 = 1./(.565)
  715 AHE = ((TE/.002401)**AA1)*(PE**(-AA1*.052))
  457 PRINT 407,AHE
      RHOMU = (.0002796)*(PE**(.992))/(AHE**(.3329) - 119.9526)
      PRINT 33, RHOMU
  716 AA2 = (PR*(UE**2))/AHE
      PRINT 67, AA2
      DO 152 K = 1,NUM
      APOWR = POWER(K)
      APOW = POW(K)
      APOWR = APOWR
      APOW = APOW
      XK(K) = CON(K)*((TE/10000.)**APOWR)*(PE**APOW)
  152 CONTINUE
  458 PRINT 408,(XK(I), I = 1,NUM)
  718 AHBRW = TBARW**AA1
  459 PRINT 409, AHBRW
  690 G1(1) = 0.0
  720 G1(2) = (.03333333)*(FA(1) + 4.*FFA(4) + FA(2))
  721 DO 202 I = 3,MMN
  722 G1(I) = (.06666667)*(FA(I-2) + 4.*FA(I-1) + FA(I)) + G1(I-2)
  202 CONTINUE
  724 G2(1) = 1.0
  725 PR2 = PR/2.
  726 DO 203 I = 2,MMN
  727 G2(I) = EXPF(-PR2*G1(I))
  203 CONTINUE
  729 G4(1) = G2(1)
  730 G = (.05/3.)*(FA(1) + 4.*FFA(3) + FFA(4))
  731 G4(2) = EXPF(-PR2*G)
  732 G4(3) = G2(2)
  735 G3(1) = 0.0
  736 G3(2) = (.03333333)*(G4(1) + 4.*G4(2) + G4(3))
  737 DO 204 I = 3,MMN
  738 G3(I) = (.06666667)*(G2(I-2) + 4.*G2(I-1) + G2(I)) + G3(I-2)
```

```
204 CONTINUE
740 G5(1) = 1.0
    DO 205 I = 2,MMN
742 G5(I) = EXPF(PR2*G1(I))
205 CONTINUE
744 G6(1) = FPP(1)**2
745 GG = (.025/3.)*(FFA(1) + 4.*FFA(2) + FFA(3))
746 G6(2) = (FPP1**2)*EXPF(PR2*GG)
747 G6(3) = (FPP2**2)*EXPF(PR2*G)
750 G7(1) = 0.0
751 G7(2) = (.05/3.)*(G6(1) + 4.*G6(2) + G6(3))
752 G8(1) = G6(1)
753 G8(2) = G6(3)
 54 G8(3) = (FPP(2)**2)*G5(2)
756 G7(3) = (.03333333)*(G8(1) + 4.*G8(2) + G8(3))
758 G9(1) = 0.0
759 G9(2) = G4(2)*G7(2)
760 G9(3) = G2(2)*G7(3)
764 DO 206 I = 1,MMN
765 G12(I) = (FPP(I)**2)*G5(I)
206 CONTINUE
767 G11(1) = 0.0
768 G11(2) = G9(3)
769 G13(1) = 0.0
770 G13(2) = G7(3)
771 DO 207 I = 3,MMN
772 G13(I) = (.06666667)*(G12(I-2) + 4.*G12(I-1) + G12(I)) + G13(I-2)
773 G11(I) = G13(I)*G2(I)
207 CONTINUE
776 G10(1) = 0.0
777 G10(2) = (.03333333)*(G9(1) + 4.*G9(2) + G9(3))
778 DO 208 I = 3,MMN
779 G10(I) = (.06666667)*(G11(I-2) + 4.*G11(I-1) + G11(I)) + G10(I-2)
208 CONTINUE
781 CZERO = (1. - AHBRW + AA2*G10(MMN))/G3(MMN)
782 DO 209 I = 1,MMN
783 AHBR1(I) = AHBRW + CZERO*G3(I) - AA2*G10(I)
784 AHBRO(I) = AHBR1(I)
209 CONTINUE
785 CONST = - 4.*PR*SIGMA*(TE**4)*XL/(UE*AHE)
788 PRINT 117,CZERO
789 PRINT 142, CONST
    CONS = CONST*XKPE
    PRINT 70, CONS
    CONS = CONS
    DO 115 I = 1,MMN
    TBAR(I) = AHBRO(I)**.565
    TO(I) = TBAR(I)
115 CONTINUE
    DO 153 K = 1,NUM
    DONST(K) = CONST*XK(K)*A1E(K)
153 CONTINUE
    PRINT 102,(DONST(K), K = 1,NUM)
790 DO 300 I = 1,MMN
791 ADC(I) = CONST*G3(I)/G3(MMN)
300 CONTINUE
900 DO 250 J = 1,10
907 MM = 1
291 CONTINUE
```

```
796 DO 211 I = 1,MMN
    DO 154 K = 1,NUM
    APOWR = POWER(K)
    XK1(I,K) = TBAR(I)**APOWR
154 CONTINUE
602 AB(I) = ABC(I)*X(J)
    XKP(I) = TBAR(I)**POW1
211 CONTINUE
    DO 156 I = 1,MMN
    W(I) = XKPE*XKP(I)*(TBAR(I)**4)
    QW(I) = XKPE*XKP(I)*(TBAR(I)**4)
156 CONTINUE
    DO 157 I = 1,MMN
    DO 157 K = 1,NUM
    W(I) = W(I) + XK(K)*XK1(I,K)*TEMP2(K)
    QW(I) = QW(I) + XK(K)*XK1(I,K)*TEMP1(K)
157 CONTINUE
    DO 159 I = 1,MMN
    G15(I) = W(I)*G5(I)
159 CONTINUE
623 XT = (TBAR(2) + TBAR(1))*(.5)
    DO 160 K = 1,NUM
    APOWR = POWER(K)
    XK1A(K) = XT**APOWR
160 CONTINUE
    XKP1 = XT**POW1
    WT = XKPE*XKP1*(XT**4)
    QT = XKPE*XKP1*(XT**4)
    DO 161 K = 1,NUM
    WT = WT + XK(K)*XK1A(K)*TEMP2(K)
    QT = QT + XK(K)*XK1A(K)*TEMP1(K)
161 CONTINUE
    AGAIN(1) = 0.0
    AGAIN(2) = (.03333333)*(QW(1) + 4.*QT + QW(2))
    DO 48 I = 3,MMN
    AGAIN(I) = (.06666667)*(QW(I - 2) + 4.*QW(I - 1) + QW(I)) + AGAIN(
   1I - 2)
 48 CONTINUE
615 G17(1) = 0.0
635 G17(2) = (.03333333)*(G15(1) + 4.*WT*EXPF(G*PR2) + G15(2))
616 DO 212 I = 3,MMN
618 G17(I) = (.06666667)*(G15(I-2) + 4.*G15(I-1) + G15(I)) + G17(I-2)
620 G19(I) = G17(I)*G2(I)
212 CONTINUE
637 G19(1) = 0.0
638 G19(2) = G17(2)*G2(2)
640 G20(1) = G19(1)
641 G20(3) = G19(2)
642 XT1 = (XT + TBAR(1)) *(.5)
    DO 162 K = 1,NUM
    APOWR = POWER(K)
    XK1B(K) = XT1**APOWR
162 CONTINUE
    XKP11 = XT1**POW1
    WT1 = XKP11*XKPE*(XT1**4)
    DO 163 K = 1,NUM
    WT1 = WT1 + XK(K)*XK1B(K)*TEMP2(K)
163 CONTINUE
648 WTG1 = WT1*EXPF(PR2*GG)
```

```
650 GTX = (.05/3.)*(G15(1) + 4.*WTG1 + WT*EXPF(PR2*G))
651 G20(2) = G4(2)*GTX
666 TERM2(1) = 0.0
    TERM2(2) = (.03333333)*(G20(1) + 4.*G20(2) + G20(3))
668 CX = CONST*X(J)
669 DO 260 I = 3,MMN
670 TERM2(I) = (.06666667)*(G19(I-2) + 4.*G19(I-1) + G19(I)) + TERM2(I
6701-2)
260 CONTINUE
    DO 672 I = 1,MMN
671 AHBR2(I) = AHBR0(I) + AB(I)*TERM2(MMN) - CX*TERM2(I)
    IF(AHBR2(I)) 844,846,846
844 STOP
846 CONTINUE
672 CONTINUE
    SS = 0.0
676 SUMA = 0.0
677 DO 261 I = 1,MMN
    SS = SS + (AHBR2(I) - AHBR1(I))
    SUMA = SUMA + ABSF(AHBR2(I) - AHBR1(I))
261 CONTINUE
981 PRINT 932,MM
    PRINT 673,SS
679 PRINT 931,SUMA
680 IF(SUMA-EPS) 280,280,281
281 CONTINUE
681 DO 282 I = 1,MMN
    AHBR1(I) = (AHBR1(I) + AHBR2(I))*(.5)
683 TBAR(I) = AHBR1(I)**(.565)
282 CONTINUE
904 MM = MM + 1
684 GO TO 291
280 CONTINUE
685 DO 285 I = 1,MMN
686 AHBAR(I,J) = AHBR2(I)
    TBAR(I) = AHBAR(I,J)**(.565)
688 AHBR1(I) = AHBR2(I)
    T(I,J) = TBAR(I)
285 CONTINUE
983 PRINT 933,MM
    C1(J) = CZERO + CONST*X(J)*TERM2(MMN)/G3(MMN)
    S(J) = RHOMU*UE*X(J)*XL
    QWR(J) = FACT*(ACT + (2.*SQRTF(C*S(J))/(UE))*AGAIN(MMN))
    QWR(J) = QWR(J)
    QWC0(J) = -(SQRTF((C*RHOMU*UE)/(XL*X(J))))*AHE*CZERO/PR
    QWC1(J) = -(SQRTF((C*RHOMU*UE)/(XL*X(J))))*AHE*C1(J)/PR
250 CONTINUE
    DONST(1) = DONST(1)
    PRINT 170
    PRINT 171
    PRINT 170
    PRINT 174
    PRINT 173,(ETA(I),AHBR0(I),(AHBAR(I,J),J=1,10),I=1,MMN)
    PRINT 170
    PRINT 170
    PRINT 172
    PRINT 170
    PRINT 175
    PRINT 173,(ETA(I),T0(I),(T(I,J),J=1,10),I=1,MMN)
```

```
      PRINT 170
      PRINT 170
      PRINT 177
      PRINT 176,(X(J),C1(J),S(J),QWC0(J),QWC1(J),QWR(J),J=1,10)
      PRINT 170
      PRINT 170
      GO TO 701
   20 FORMAT(I2)
   21 FORMAT(29H THE NUMBER OF TERMS IN W IS I4)
   32 FORMAT(5H C = E16.8)
   33 FORMAT(9H RHOMU = E16.8)
   50 FORMAT(8H POW1 = E16.8)
   51 FORMAT(8H POW2 = E16.8)
   52 FORMAT(6H CE = E16.8)
   55 FORMAT(I1)
   59 FORMAT(10H GREY CASE)
   67 FORMAT(15H PR*UE**2/HE = E16.8)
   70 FORMAT(8H CONS = E16.8)
   71 FORMAT(7H KPE = E16.8)
  100 FORMAT (E14.8)
  101 FORMAT( 5E14.8)
  102 FORMAT(9H DONST = E16.8)
  117 FORMAT(9H CZERO = E16.8)
  136 FORMAT(28H THE NUMBER OF ETAS USED IS I4)
  142 FORMAT(9H CONST = E16.8)
  170 FORMAT(2H  )
  171 FORMAT(54H                                                      HBAR)
  172 FORMAT(54H                                                      TBAR)
  173 FORMAT(F4.1,11F10.6)
  174 FORMAT(114H ETA     HBARO    XBAR =.1  XBAR =.2  XBAR =.3  XBAR =.4
 1741 XBAR =.5  XBAR =.6  XBAR =.7  XBAR =.8  XBAR =.9  XBAR=1.0)
  175 FORMAT(114H ETA     TBARO    XBAR =.1  XBAR =.2  XBAR =.3  XBAR =.4
 1751 XBAR =.5  XBAR =.6  XBAR =.7  XBAR =.8  XBAR =.9  XBAR=1.0)
  176 FORMAT(F5.1,5E16.8)
  177 FORMAT(86H XBAR        C1              S              QWC0
 1771   QWC1             QWR        )
  179 FORMAT(12H TEMP1(K) = E16.8)
  360 FORMAT(8H FACT = E16.8)
  361 FORMAT(7H ACT = E16.8)
  404 FORMAT(7H A1E = E16.8)
  405 FORMAT(7H A1W = E16.8)
  406 FORMAT(9H TEMP2 = E16.8)
  407 FORMAT(7H AHE = E16.8)
  408 FORMAT(6H XK = E16.8)
  409 FORMAT(9H AHBRW = E16.8)
  450 FORMAT(7H POW = E16.8)
  451 FORMAT(7H CON = E16.8)
  673 FORMAT(6H SS = E16.8)
  920 FORMAT(6H PR = E16.8)
  921 FORMAT(6H UE = E16.8)
  922 FORMAT(6H TE = E16.8)
  923 FORMAT(6H PE = E16.8)
  924 FORMAT(9H TBARW = E16.8)
  925 FORMAT(8H EPSW = E16.8)
  926 FORMAT(9H ALAM1 = E16.8)
  927 FORMAT(7H E1E = E16.8)
  928 FORMAT(7H EPS = E16.8)
  929 FORMAT(6H XL = E16.8)
  930 FORMAT(9H POWER = E16.8)
  931 FORMAT(8H SUMA = E16.8)
  932 FORMAT(26H THESE ARE THE RESULTS OF I4,11H ITERATIONS)
  933 FORMAT(28H CONVERGENCE OBTAINED AFTER I4, 11H ITERATIONS)
  976 FORMAT(9H ALAM2 = E16.8)
      END
```

APPENDIX F

THE OUTER-EDGE BOUNDARY CONDITION FOR THE ENTHALPY

In previous investigations dealing with the radiating boundary layer on a flat plate the enthalpy boundary condition which has generally been specified for the outer-edge of the boundary layer is the one given in eq. (63),

$$h \to h_e \text{ as } y \to \infty$$

However, there appears to be some question as to whether this is the proper outer-edge boundary condition for the enthalpy. A brief study of this outer-edge boundary condition problem indicates that it is not sufficient to only require that the enthalpy in the outer part of the boundary layer be asymptotic to some arbitrary value of the external flow enthalpy h_e. The conclusions of the study, which agree with the comments of Olstad (ref. 28), show that, in addition, it is necessary to also insist that the value of h_e be consistent with the condition that the divergence of the radiation flux vector in the outer part of the boundary layer be asymptotic to the value of the divergence of the radiation flux vector for the external flow in the vicinity of the wall. In this manner, the enthalpy solution to the boundary layer energy equation (6) will have asymptotic character and its value on the outer-edge of the boundary layer will be equal to the value of the enthalpy for the radiating external flow in the vicinity of the wall. Thus, the proper value for h_e in eq. (63) is the wall enthalpy for the radiating external flow.

The outer-edge boundary condition which was employed in this investigation is the arbitrary value of h_e given in eq. (63). Of course this boundary condition for the enthalpy is only a first approximation to the proper outer-edge boundary condition discussed in the previous paragraph. However, the resulting enthalpy profiles in fig. 6(a) indicate that this approximation is quite good for the high Eckert number flows considered in the investigation. For the low Eckert number flows investigated, the resulting enthalpy profiles in figs. 6(b) and 8 indicate that this approximation is quite good for a combination of high external flow and low wall emissivities, but only fair for high wall and/or low external flow emissivities.

From figs. 6 and 8, it appears that the first-order approximation for the outer-edge boundary condition is poorest for a combination of low Eckert number, low external flow emissity, and high wall emissivity. Hence, the effect of this approximation on the wall heat flux results will be greatest for the aforementioned emissivity and Eckert number conditions. The quantitative effect of the boundary condition approximation on the heat transfer results has been estimated for the combination of low Eckert number, low external flow emissivity, and high wall emissivity. The estimates yield the following values for the magnitude of the effect of the boundary condition approximation on the heat flux results at these specific Eckert number and emissivity conditions:

4.0%	for	$q_{cw,g}/q_{cwo}$	in fig. 9(b),
1.5%	for	$q_{cw}/q_{cw,g}$	in fig. 10(b),
0.8%	for	$q_{Rw}/q_{Rw,g}$	in fig. 11(b),
2.8%	for	q_{Rw}/q_{cw}	in fig. 12(b),
0.1%	for	q_{tw}/q_{cwo}	in fig. 13(b),
0.7%	for	$q_{tw}/q_{tw,g}$	in fig. 14(b).

REFERENCES

1. Cess, R. D.: Radiation Effects Upon Boundary-Layer Flow of an Absorbing Gas. J. of Heat Transfer, vol. 86, no. 4, Nov. 1964, pp. 469-475.

2. Olstad, Walter B.: Stagnation-Point Solutions for an Inviscid, Radiating Shock Layer. Presented at the 1965 Heat Transfer and Fluid Mechanics Institute (Los Angeles, Calif.), June 21-23, 1965.

3. Sewell, K. G.: The Radiative Properties of Air in Thermodynamic Equilibrium. Rep. 0-71000/2R-26, Ling-Temco-Vought Research Center, July 1962.

4. Howe, John T.; and Viegas, John R.: Solutions of the Ionized Radiating Shock Layer, Including Reabsorption and Foreign Species Effects, and Stagnation Region Heat Transfer. NASA TR R-159, 1963.

5. Koh, J. C. Y.; and DeSilva, C. N.: Interaction Between Radiation and Convection in the Hypersonic Boundary Layer on a Flat Plate. ARS J., vol. 32, no. 5, May 1962, pp. 739-743.

6. Goulard, R.: Fundamental Equations of Radiation Gas Dynamics. The High Temperature Aspects of Hypersonic Flow, Wilbur C. Nelson, ed., The Macmillan Co. (New York), 1964, pp. 529-554.

7. Goulard, R.: Similarity Parameters in Radiation Gas-Dymamics. High Temperatures in Aeronautics, Carlo Ferrari, ed., Pergamon Press, Ltd. (Oxford, England), 1964, pp. 181-210.

8. Unsöld: Physik der Sternatmosphären. Julius Springer (Berlin), 1955.

9. Van Driest, E. R.: Investigation of Laminar Boundary Layer in Compressible Fluids using the Crocco Method. NACA TN 2597, 1952.

10. Anon.: U. S. Standard Atmosphere, 1962. Committee on Extension to the Standard Atmosphere (COESA), Dec. 1962.

11. Neel, C. A.; and Lewis, Clark H.: Interpolations of Imperfect Air Thermodynamic Data - II. At Constant Pressure. Tech. Doc. Rep. AEDC-TDR-64-184, ARO, Inc., Sept. 1964. (Available from DDC as AD-446 386).

12. Dorrance, William H.: Viscous Hypersonic Flow. McGraw-Hill Book Co., Inc., c. 1964.

13. Goulard, Robert: Preliminary Estimates of Radiative Transfer Effects on Detached Shock Layers. AIAA J., vol. 2, no. 3, Mar. 1964, pp. 494-502.

14. Eckert, E. R. G.; and Drake, Jr., Robert M.: Heat and Mass Transfer. Second ed., McGraw-Hill Book Co., Inc., 1959.

15. Tribus, Myron: Thermostatics and Thermodynamics. D. Van Nostrand Company, Inc., c. 1961.

16. Kivel, B.; and Bailey, K.: Tables of Radiation from High Temperature Air. Research Rep. 21, AVCO Res. Lab., 1957.

17. Armstrong, B. H.; Sokoloff, J.; Nicholls, R. W.; Holland, D. H.; and Meyerott, R. E.: Radiative Properties of High Temperature Air. J. Quant. Spectrosc. Radiat. Transfer, vol. 1, 1961, pp. 143-162.

18. Davis, Harry J.: Thermal Radiation from High-Temperature Air. Rep. TR-1225, Harry Diamond Labs., May 1964.

19. Breene, Jr., R. G.; and Nardone, Maria: Radiant Emission from High Temperature Equilibrium Air. Rep. R61SD020, Space Sciences Lab., General Electric Co., May 1961.

20. Thomas, P. D.: Air Emissivity and Shock-Layer Radiation. J. Aerospace Sci., vol. 29, no. 4, April 1962, pp. 477-478.

21. Nardone, Maria; Breene, R. G.; Zeldin, Saydean; Riethof, T. R.: Radiance of Species in High Temperature Air. Rep. R63SD3 (Contract No. AF 04(694)-222), Space Sciences Lab., General Electric Co., June 1963.

22. Archer, Douglas H.: Radiant Emission from High Temperature Equilibrium Air. RM63TMP-44 (DASA 1435), General Electric Co., Oct. 1963. (Available from DDC as AD-431 737).

23. Churchill, D. R.; Hagstrom, S. A.; and Landshoff, R. K. M.: The Calculations of Spectral Absorption in Heated Air. (DASA 1465) Lockheed Missiles and Space Co., Dec. 1963. (Available from DDC as AD-436 885).

24. Gilmore, F. R.: Approximate Radiation Properties of Air Between 2000 and 8000° K. Mem. RM-3397-ARPA (ARPA order no. 189-61), The RAND Corp., Mar. 1964.

25. Bowen, T. Roy: An Approximate Method for Predicting the Radiation from Pure Equilibrium Air. Rep. TN-AMSM1-RNR-63-3, ARPA, April 1964. (Available from DDC as AD-442 216).

26. Ashley, Jr., Ernest N.: Radiant Properties of High Temperature Equilibrium Air (3800 Å to 6500 Å). EG&G Rep. B-2782 (DASA 1506), Edgerton, Germeshausen & Grier, Inc., May 1964. (Available from DDC as AD-607 069).

27. Gilmore, F. R.: The Contribution of Generally-Neglected Band Systems and Continua to the Absorption Coefficient of High-Temperature Air. Mem. RM-4335-PR (Contract No. AF 49(638)-700), The RAND Corp., Oct. 1964. (Available from DDC as AD-607 571).

28. Olstad, Walter B.: Private communication.

29. Ahtye, Warren F.; and Peng, Tzy-Cheng: Approximations for the Thermodynamic and Transport Properties of High-Temperature Nitrogen with Shock-Tube Applications. NASA TN D-1303, 1962.

30. Cohen, Nathaniel B.: Correlation Formulas and Tables of Density and Some Transport Properties of Equilibrium Dissociating Air for Use in Solutions of the Boundary-Layer Equations. NASA TN D-194, 1960.

31. Cohen, Nathaniel B.: Boundary-Layer Similar Solutions and Correlation Equations for Laminar Heat-Transfer Distribution in Equilibrium Air at Velocities up to 41,100 feet per second. NASA TR R-118, 1961.

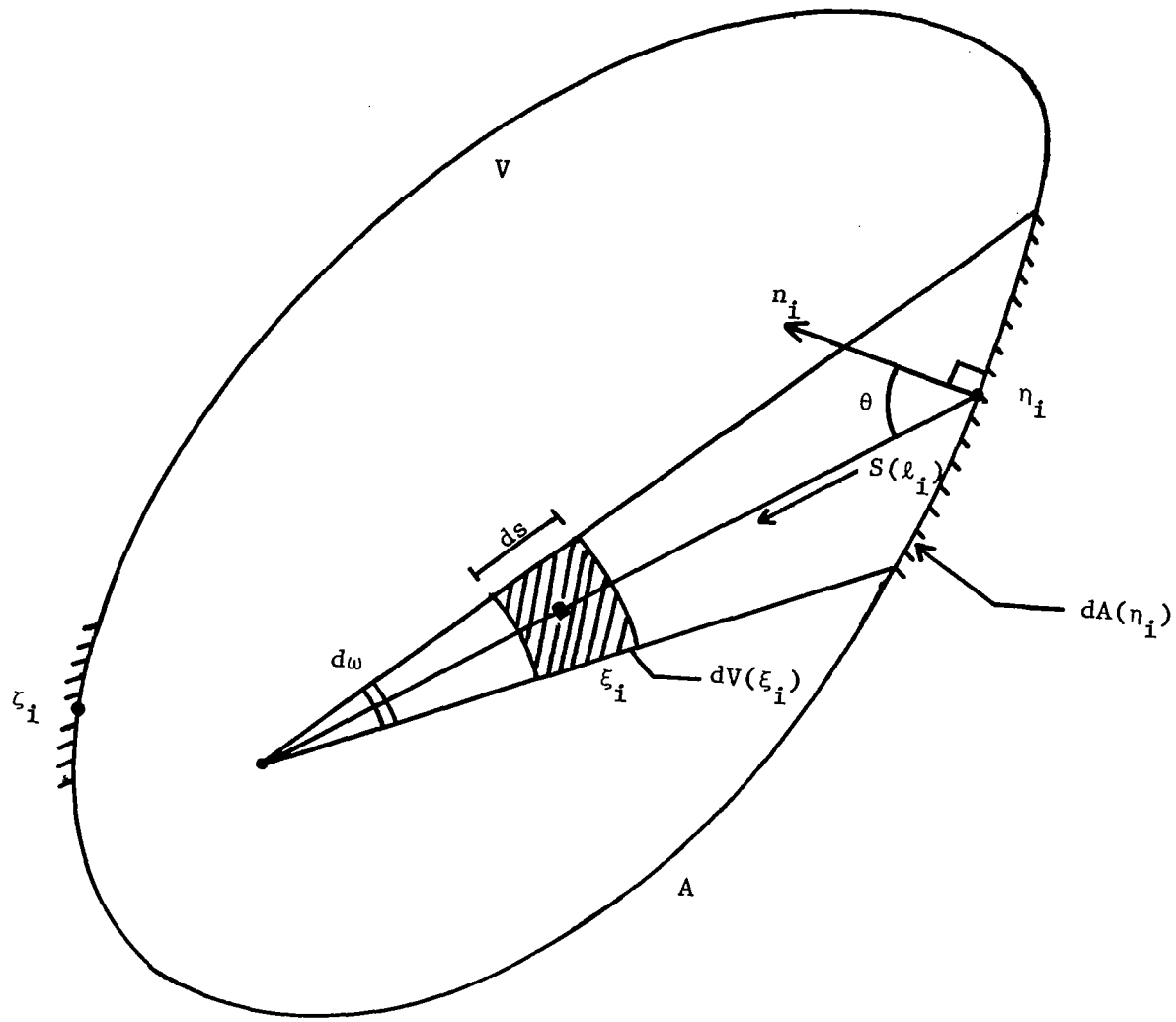

Figure 1.- Radiation contributions to the point x_i from the elementary cone of solid angle $d\omega$ whose axis is the directed line $S(\ell_i)$.

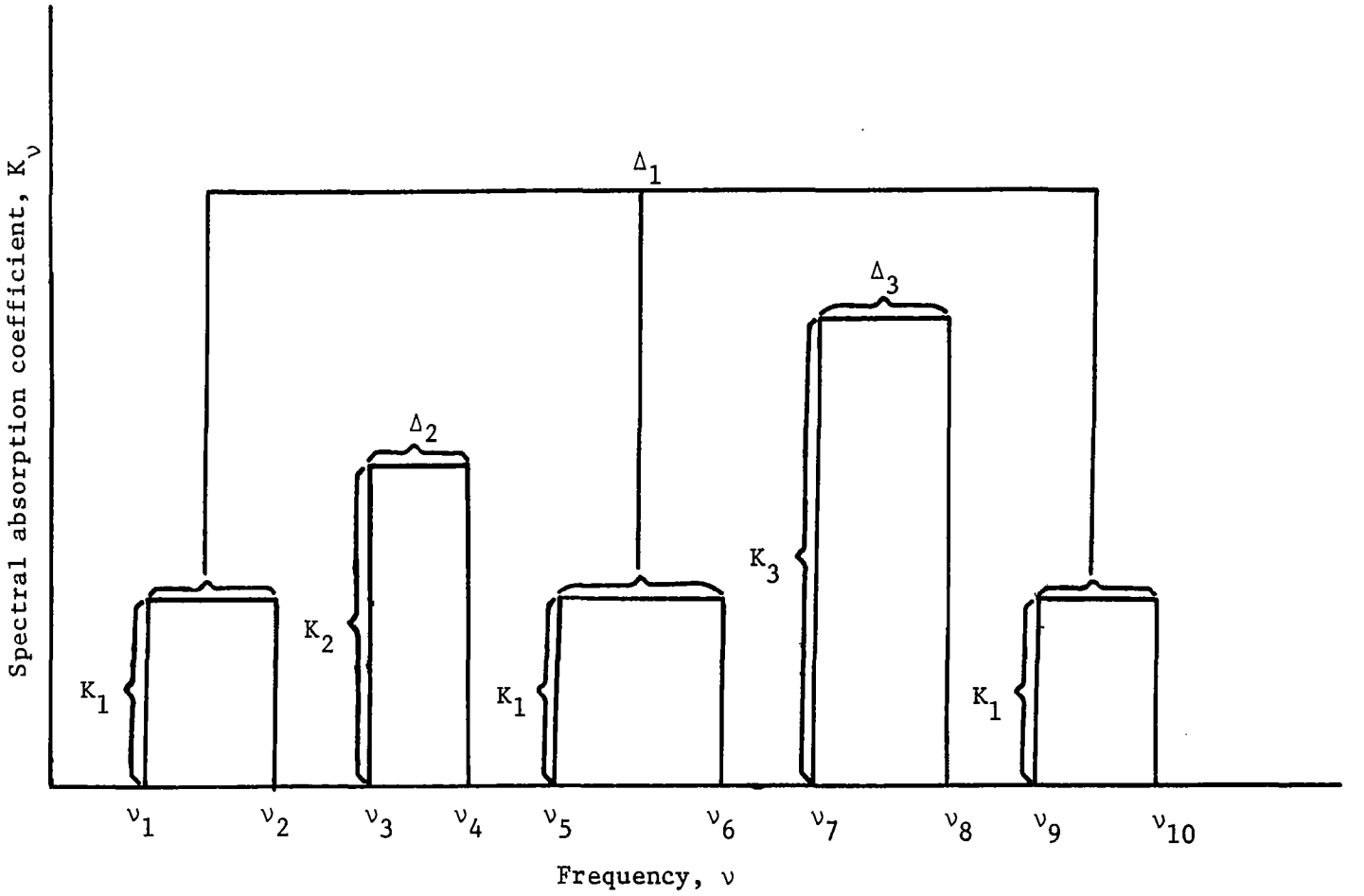

Figure 2.- Example of a nongrey absorption coefficient model obeying eq. (11).

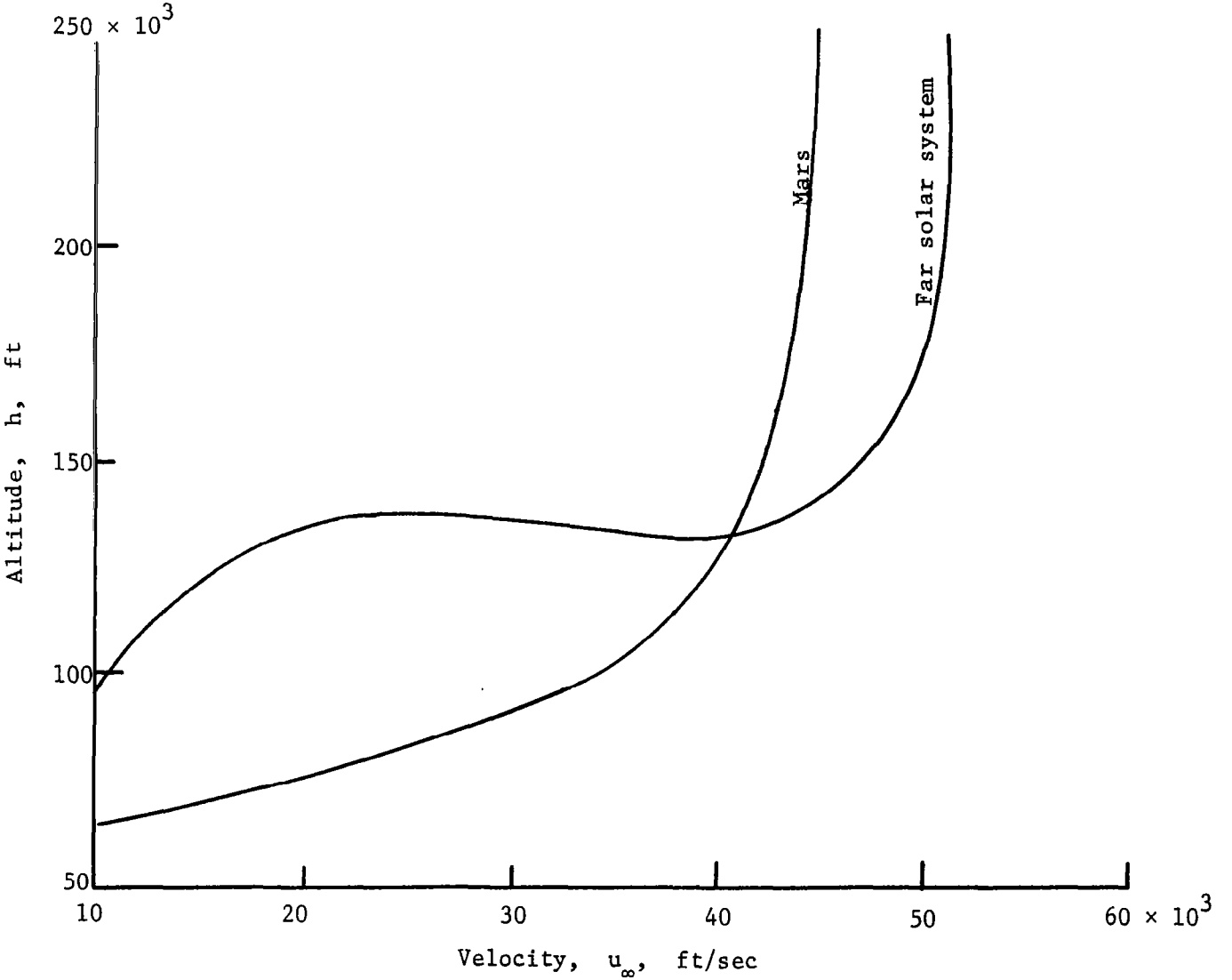

Figure 3.- Flight paths for reentry into the earth's atmosphere from a Mars mission and a far solar system mission as given in ref. 4.

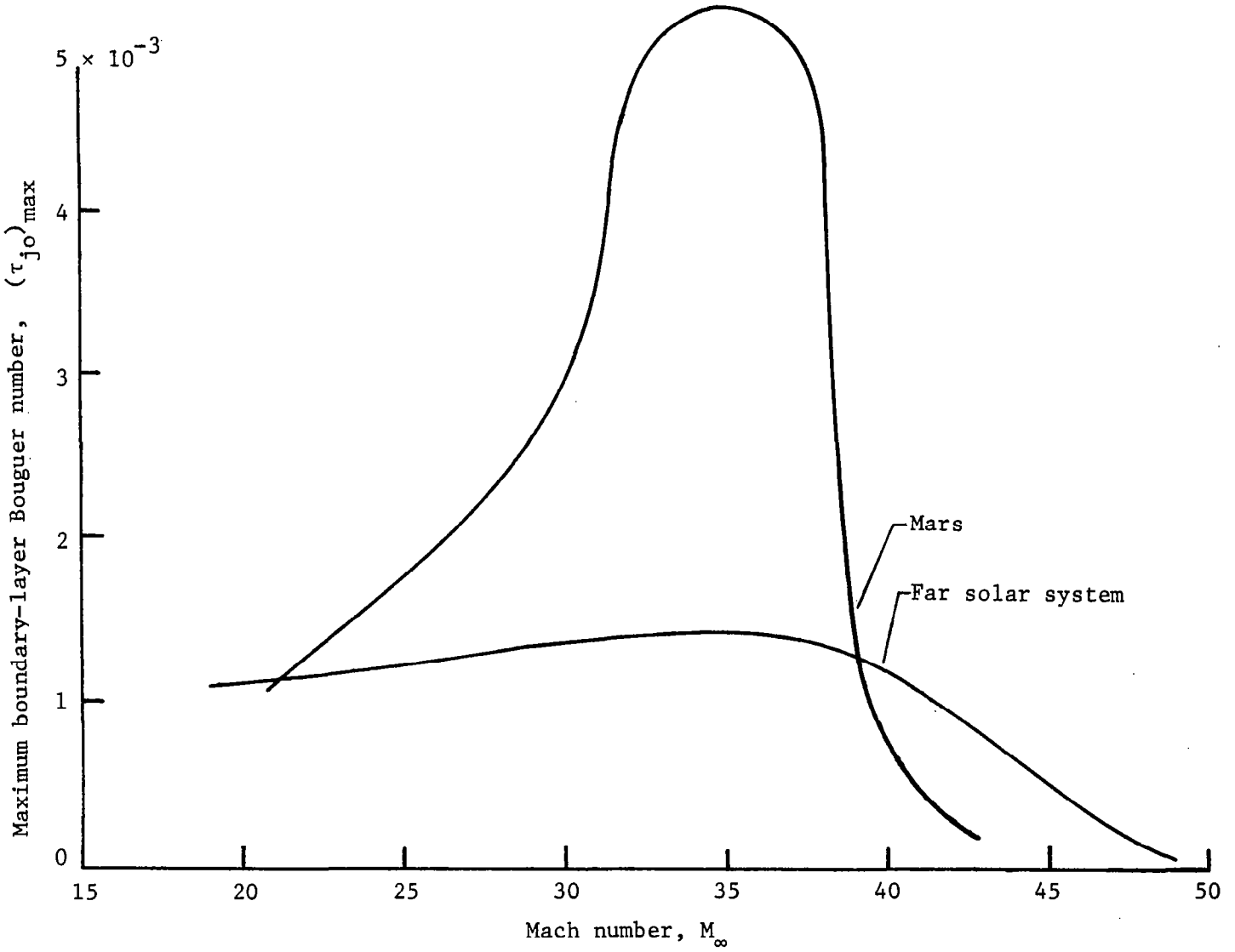

Figure 4.- The maximum boundary-layer Bouguer numbers for a 3 meters long flat plate where the reference thermodynamic states along the typical earth reentry trajectories are taken to be (H_∞, P_∞).

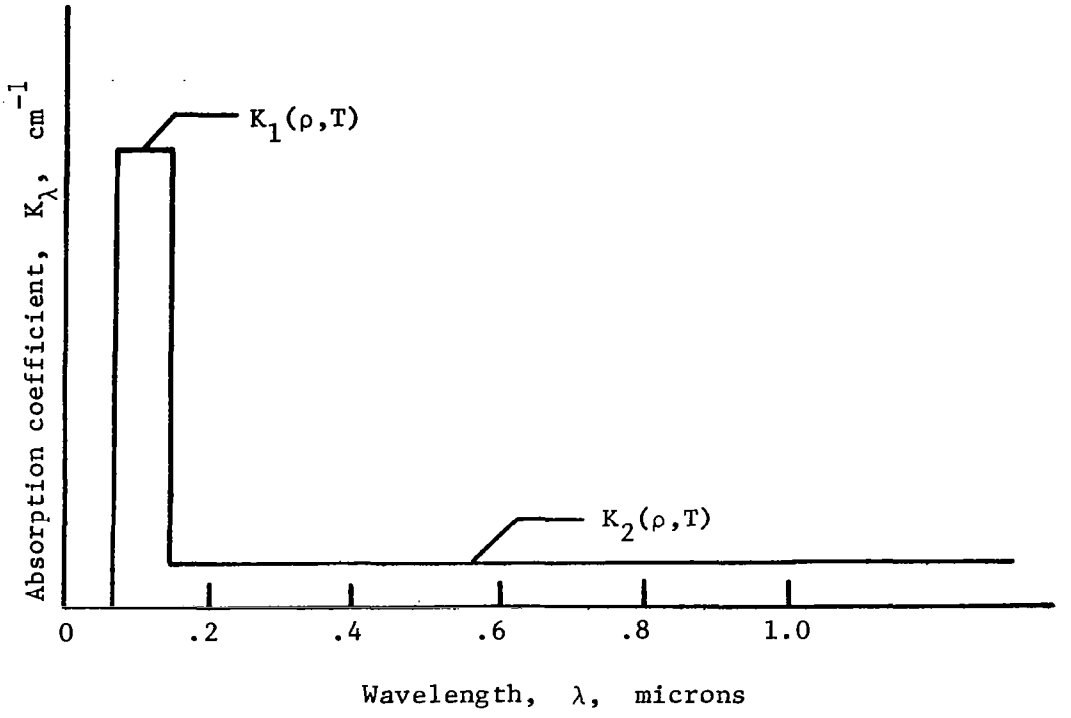

Figure 5.-Step function model of the air absorption coefficient.

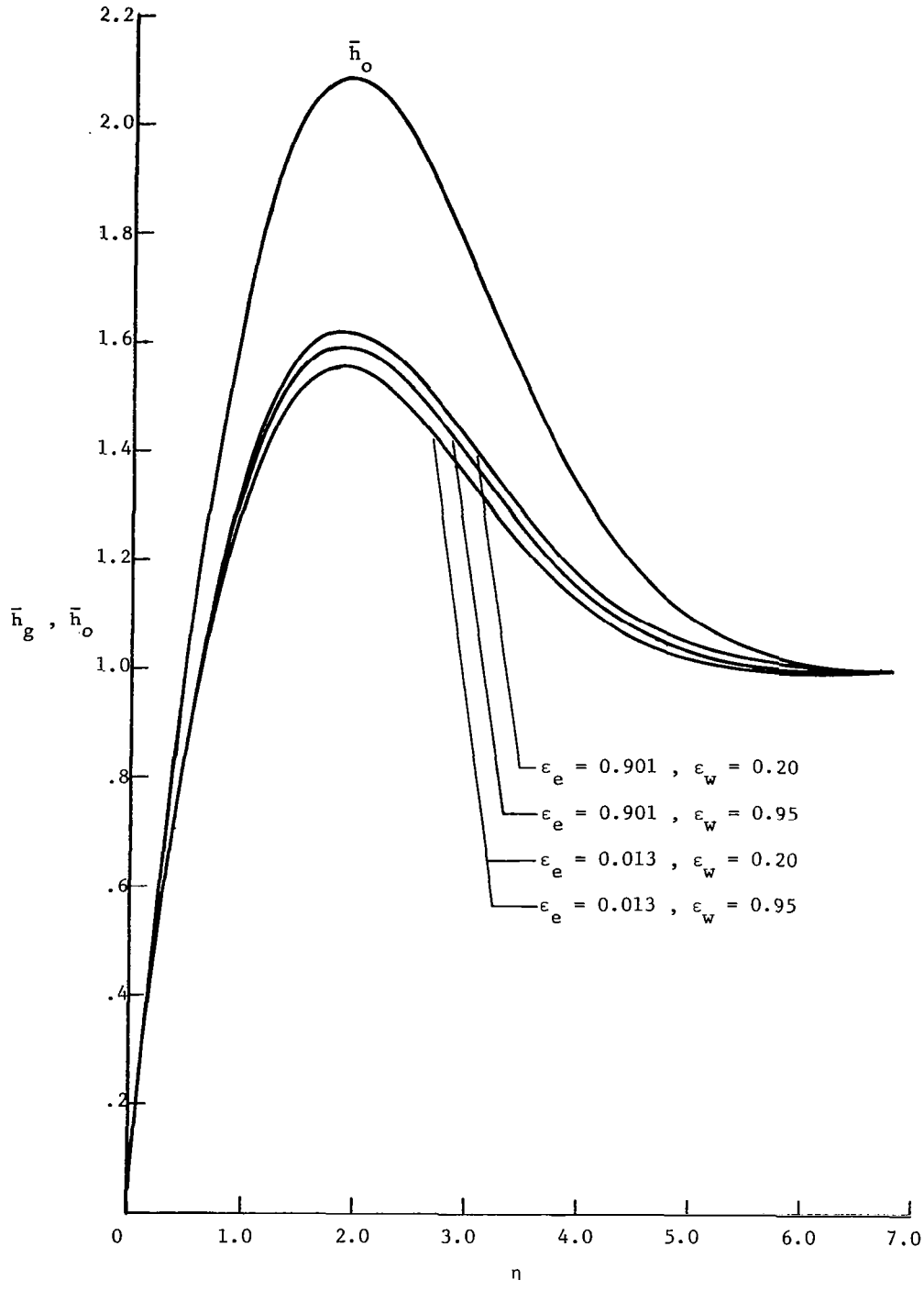

(a) $u_e^2/h_e = 16$, $T_e = 10\ 000°K$, $L = 10$ m

Figure 6.- Enthalpy profiles at $\bar{x} = 1.0$ for the grey radiating air boundary layer on a flat plate; $P_e = 0.1$ atm, $T_w = 2000°$ K.

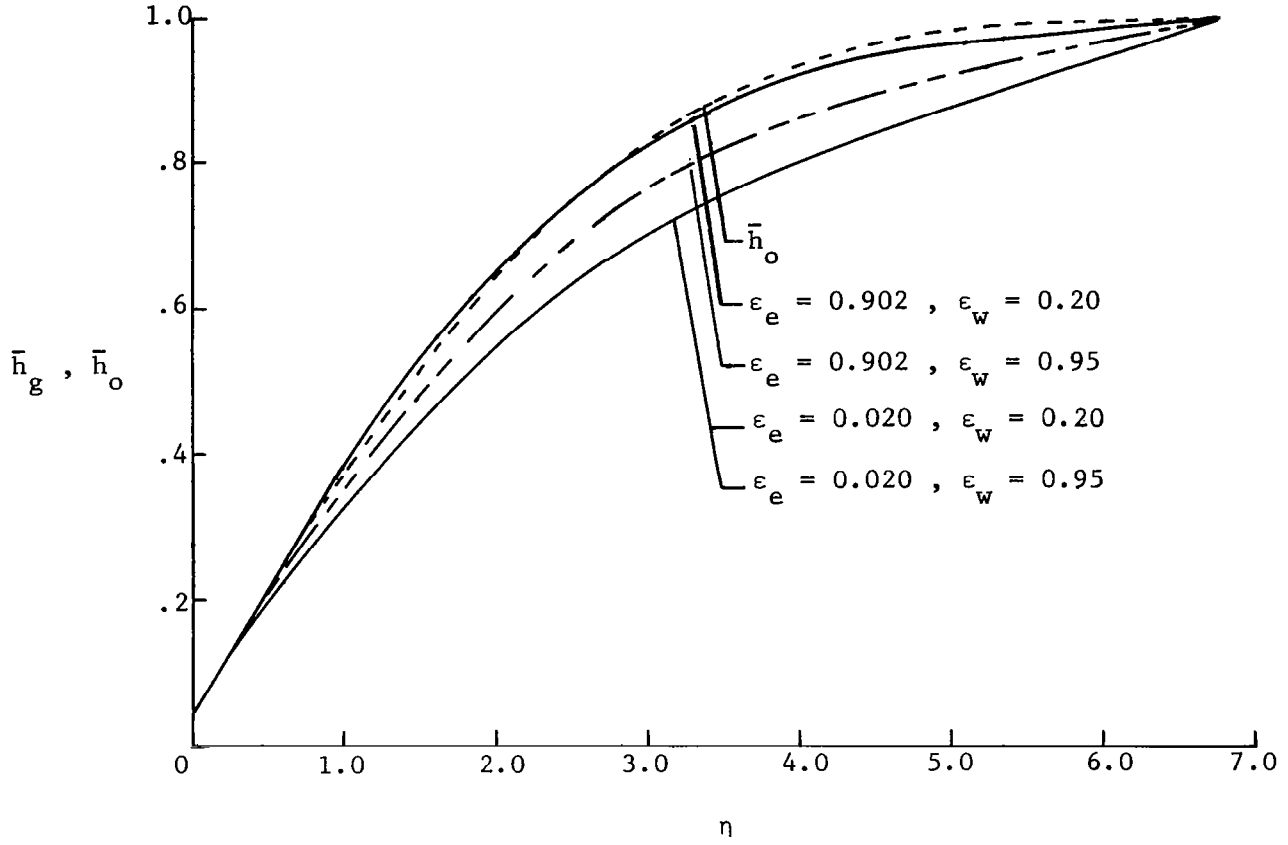

(b) $u_e^2/h_e = 0.7$, $T_e = 12\,000°$ K, L = 3 m

Figure 6.- Concluded.

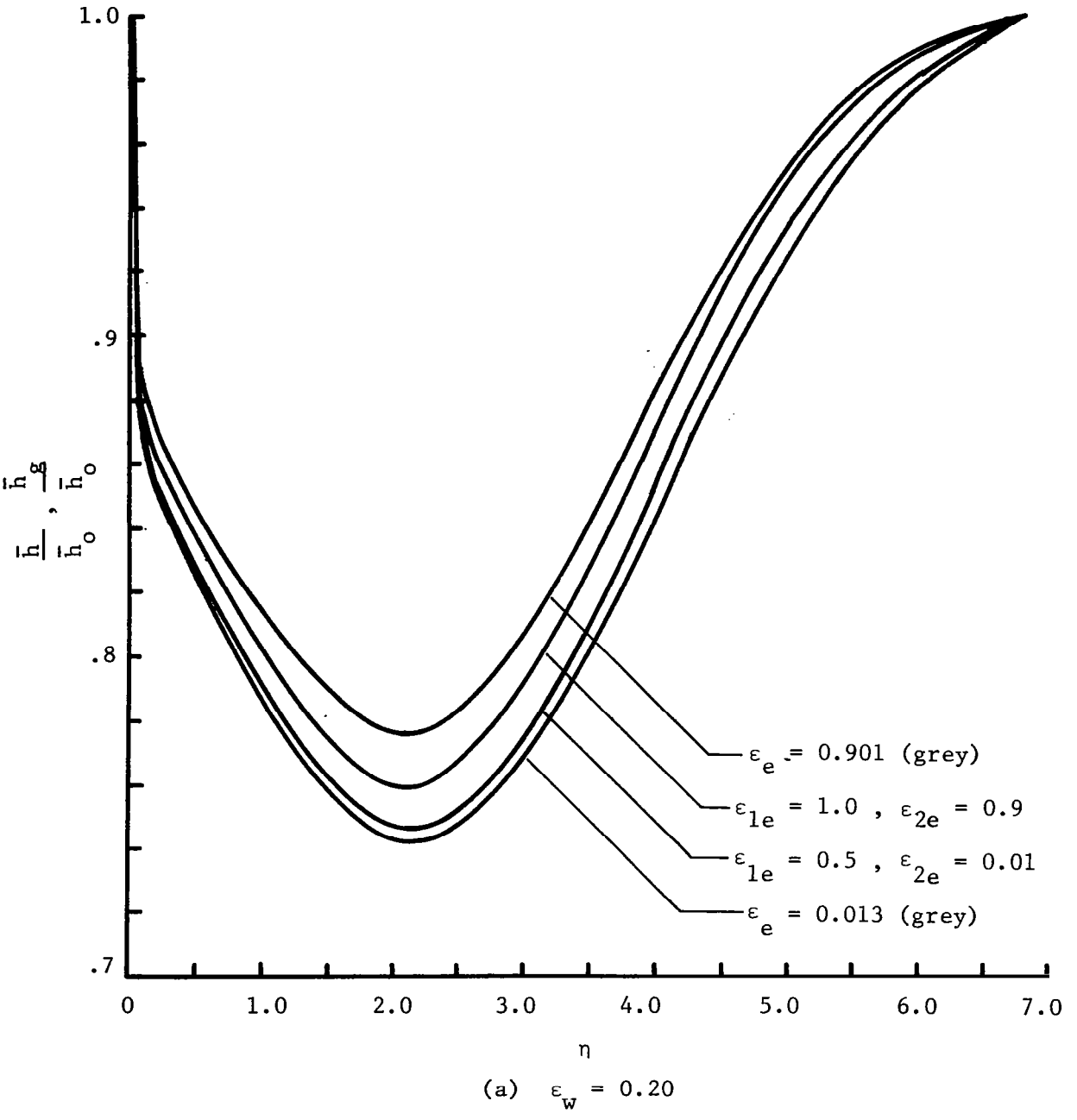

(a) $\varepsilon_w = 0.20$

Figure 7.- Normalized enthalpy profiles at $\bar{x} = 1.0$ for the radiating air boundary layer on a flat plate; $u_e^2/h_e = 16$, $T_e = 10\,000°$ K, $P_e = 0.1$ atm, L = 10 m, $T_w = 2000°$ K.

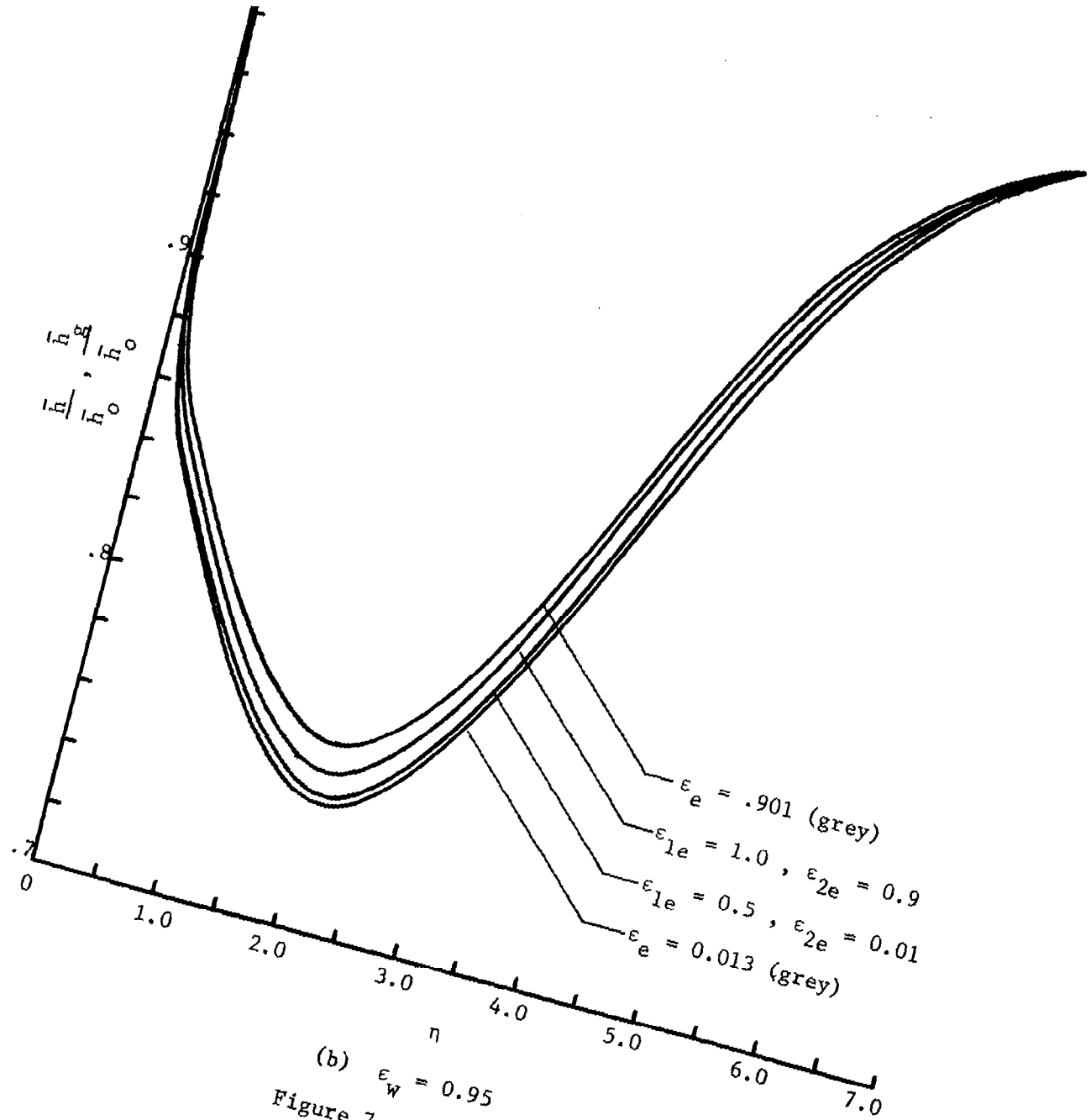

(b) $\varepsilon_w = 0.95$

Figure 7.- Concluded.

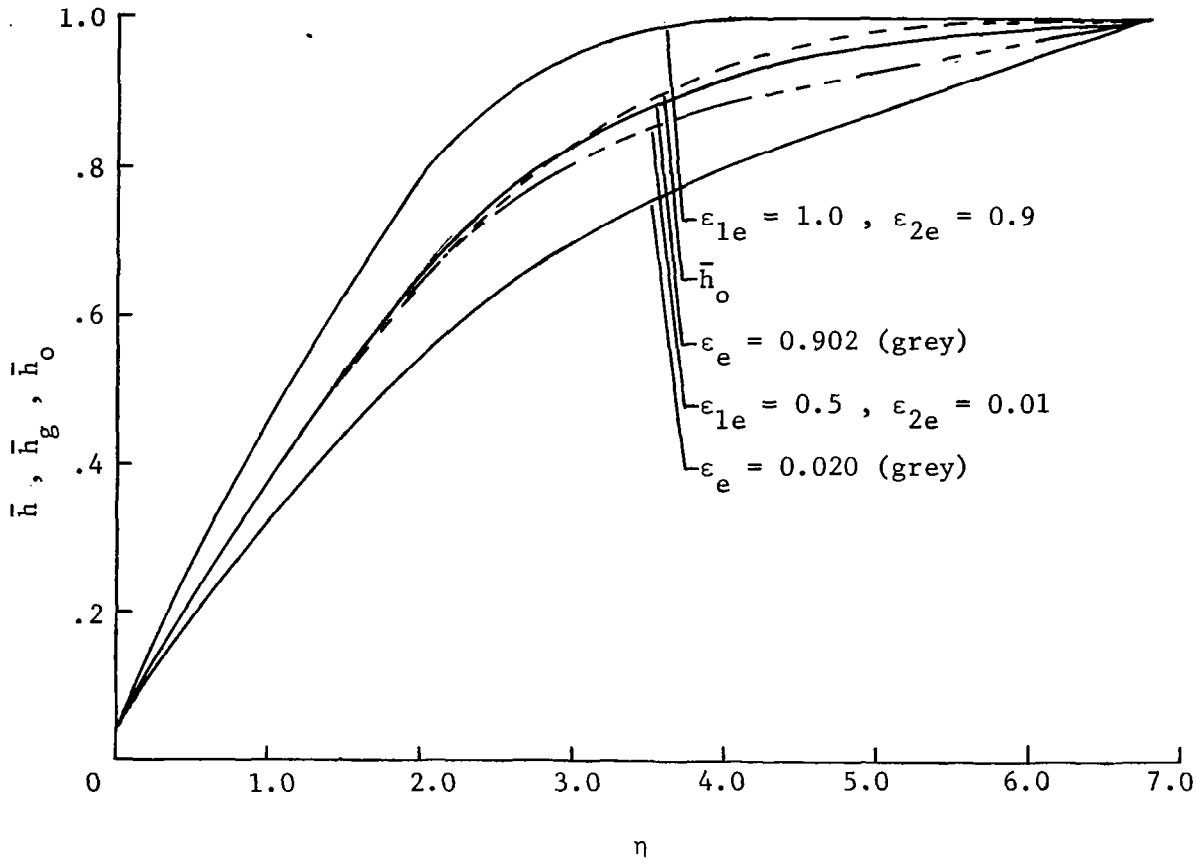

(a) $\epsilon_w = 0.20$

Figure 8.- Enthalpy profiles at $\bar{x} = 1.0$ for the radiating air boundary layer on a flat plate; $u_e^2/h_e = 0.7$, $T_e = 12\,000°$ K, $P_e = 0.1$ atm, L = 3 m, $T_w = 2000°$ K.

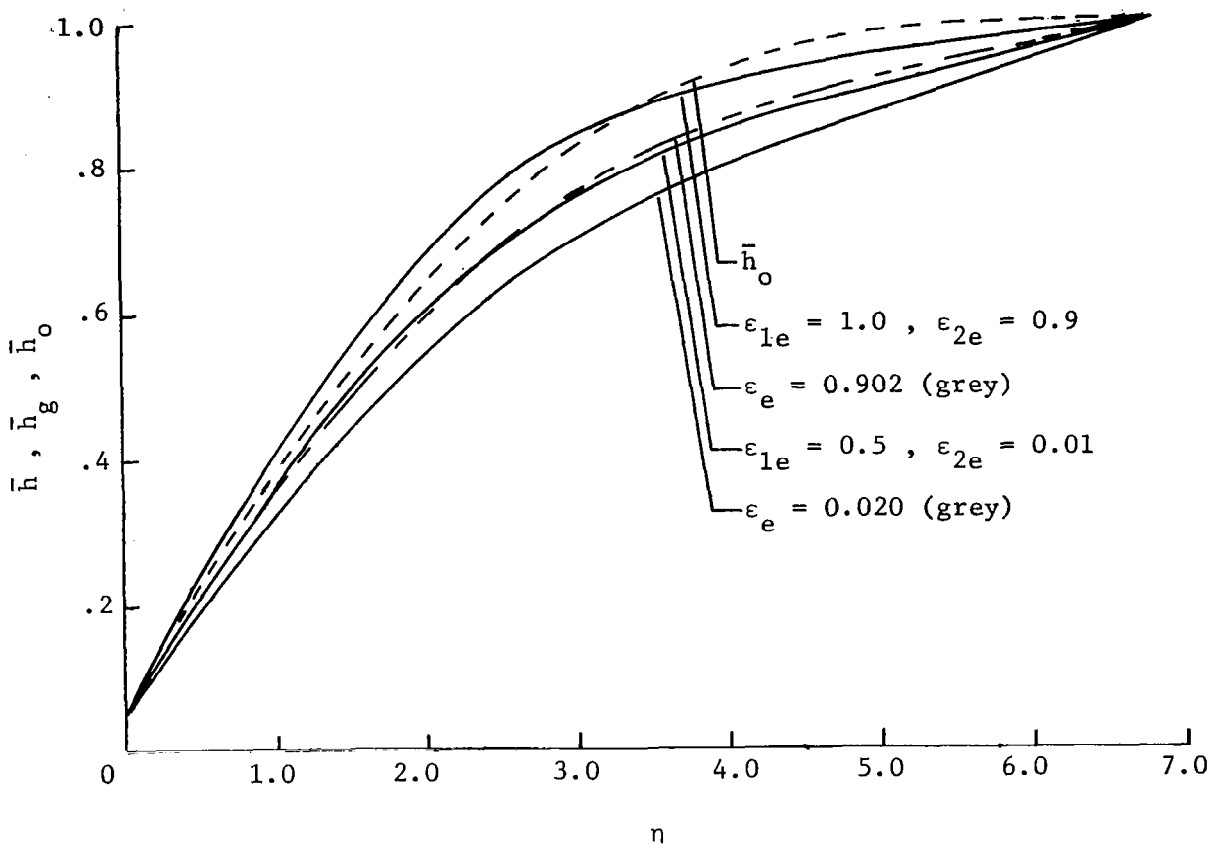

(b) $\varepsilon_w = 0.95$

Figure 8.- Concluded.

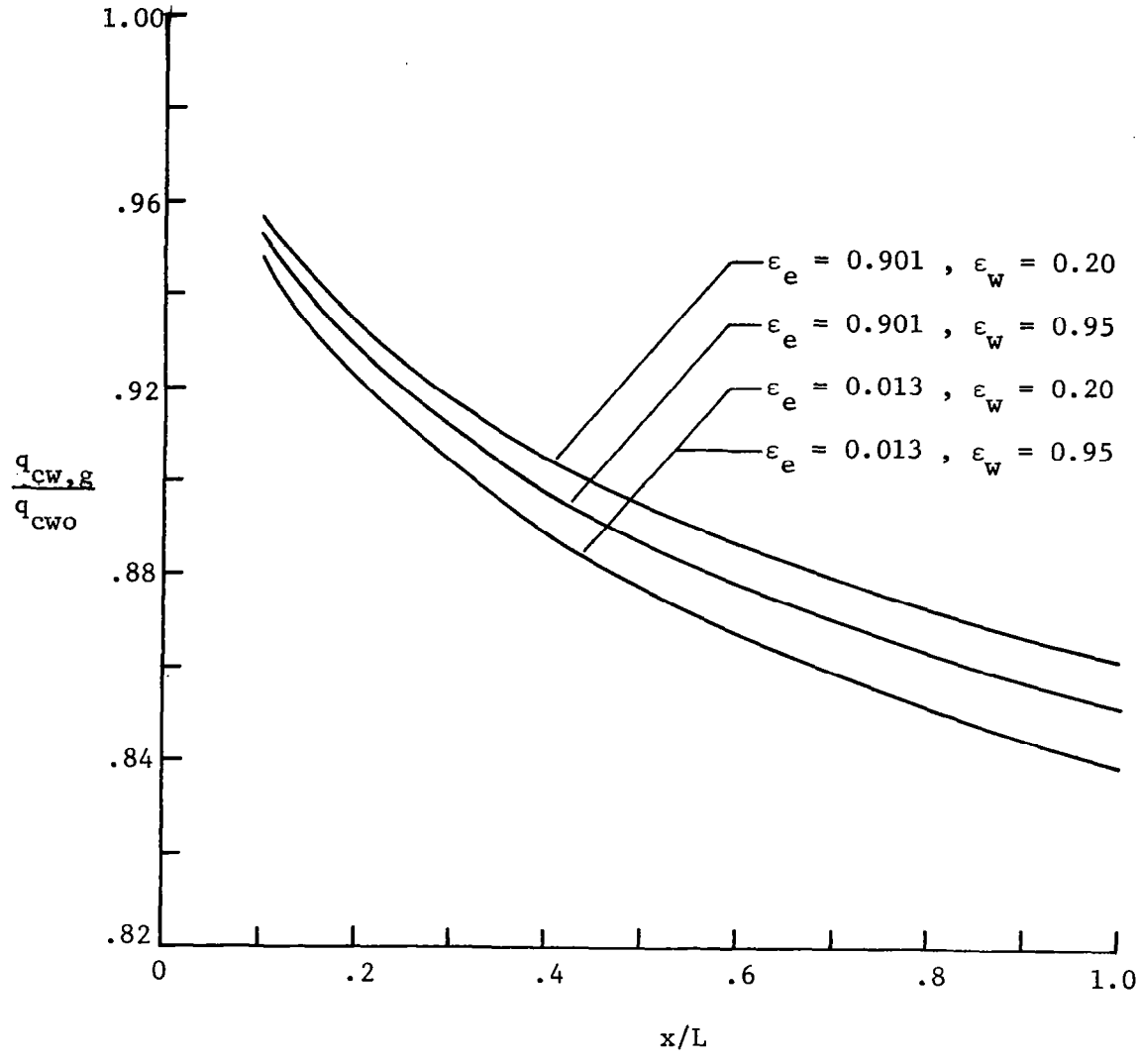

(a) $u_e^2/h_e = 16$, $T_e = 10\ 000°$ K, L = 10 m

Figure 9.- Ratio of the convective wall heat flux for grey radiating air to that for nonradiating air for the flat plate boundary layer; $P_e = 0.1$ atm, $T_w = 2000°$ K.

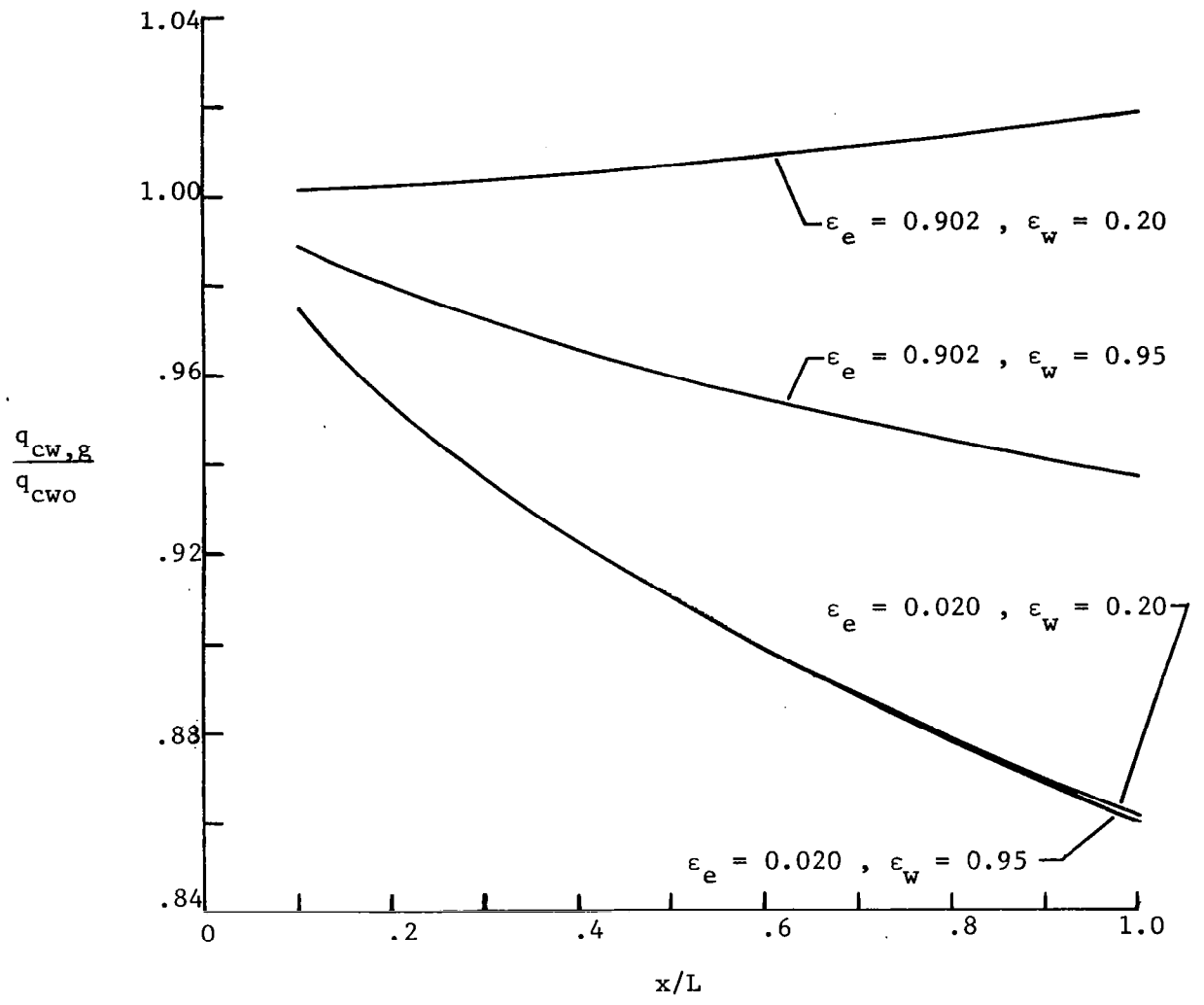

(b) $u_e^2/h_e = 0.7$, $T_e = 12\ 000°$ K, L = 3 m

Figure 9.- Concluded.

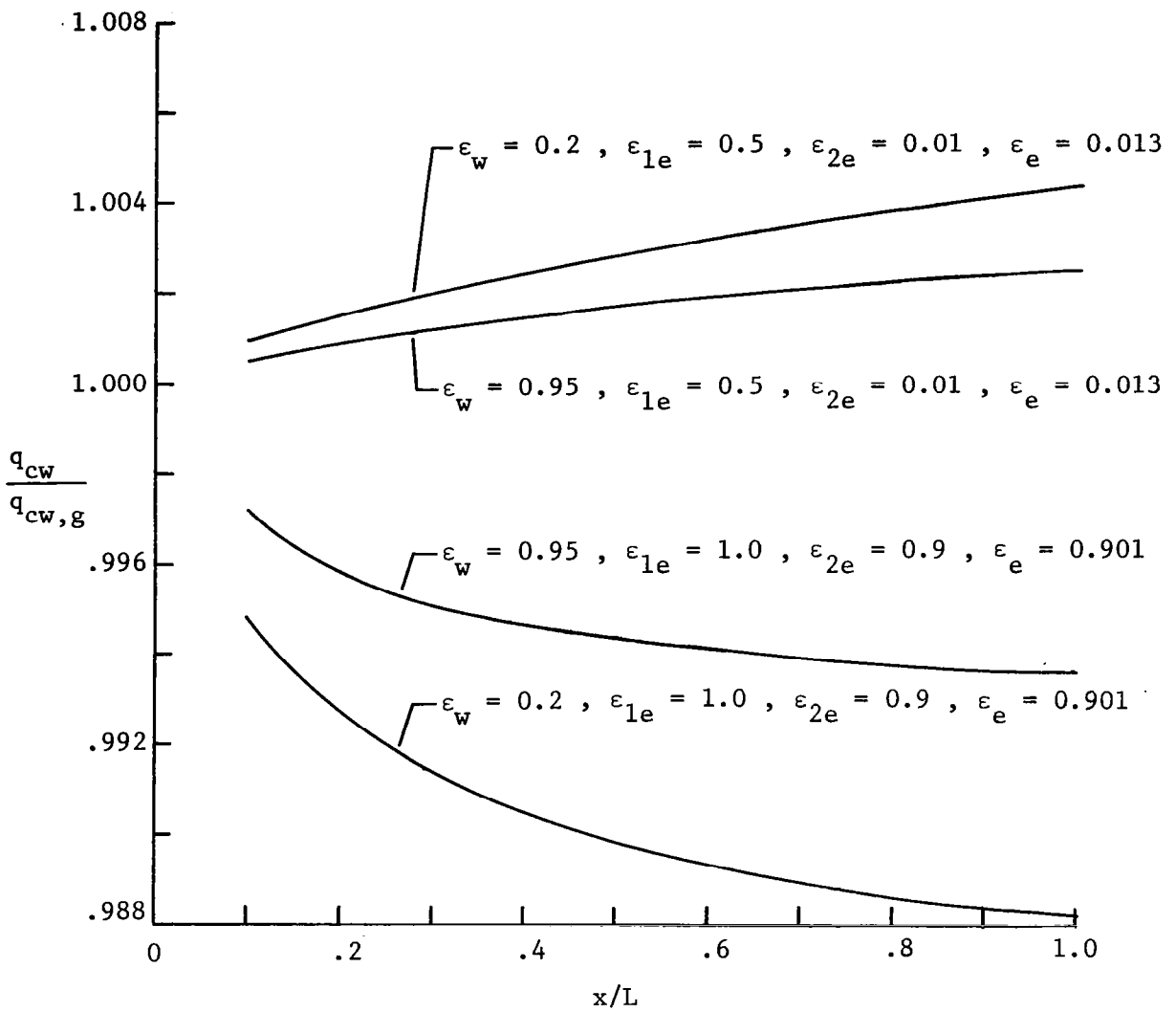

(a) $u_e^2/h_e = 16$, $T_e = 10\ 000°$ K, L = 10 m

Figure 10.- Ratio of the nongrey to grey convective wall heat flux for the radiating air boundary layer on a flat plate; $P_e = 0.1$ atm, $T_w = 2000°$ K.

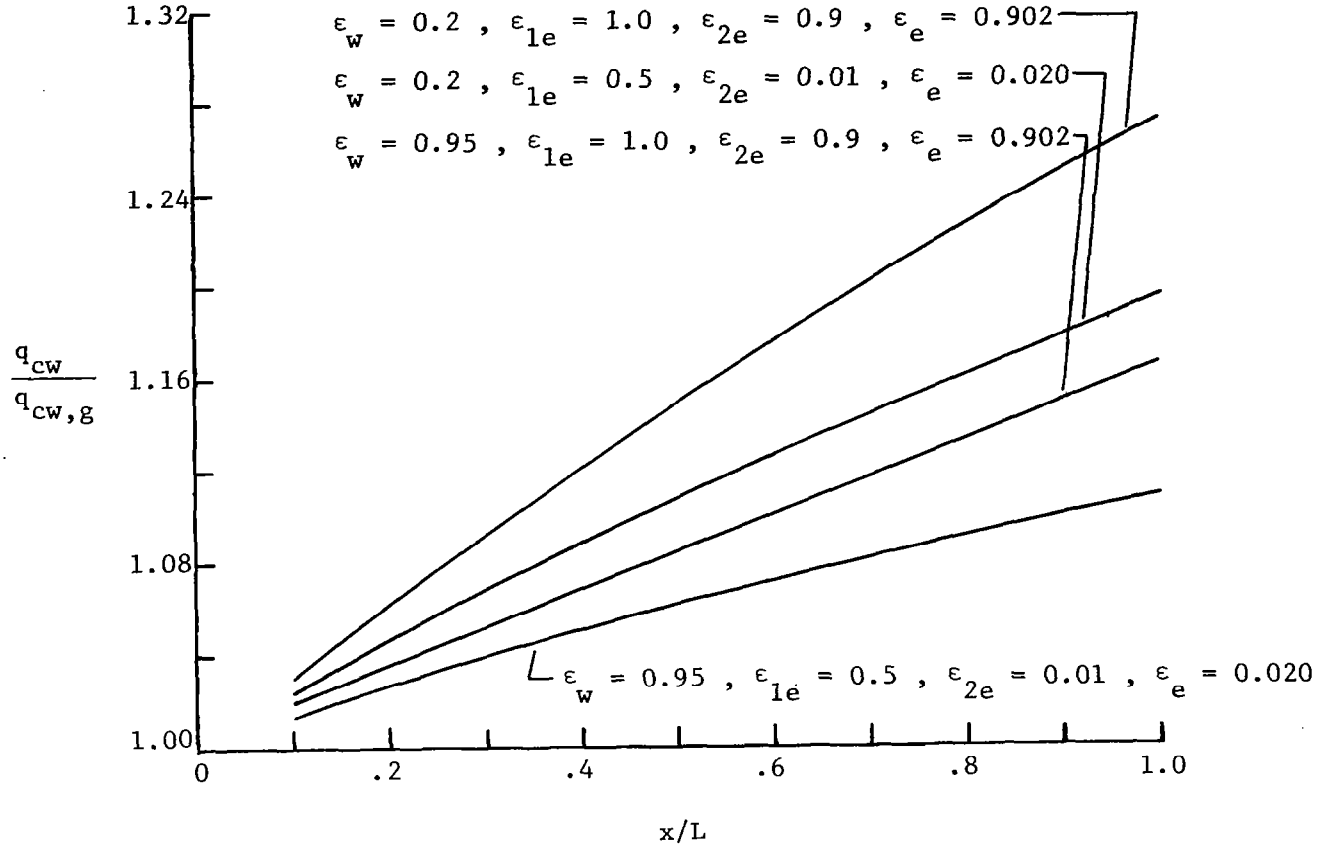

(b) $u_e^2/h_e = 0.7$, $T_e = 12\ 000°$ K, L = 3 m

Figure 10.- Concluded.

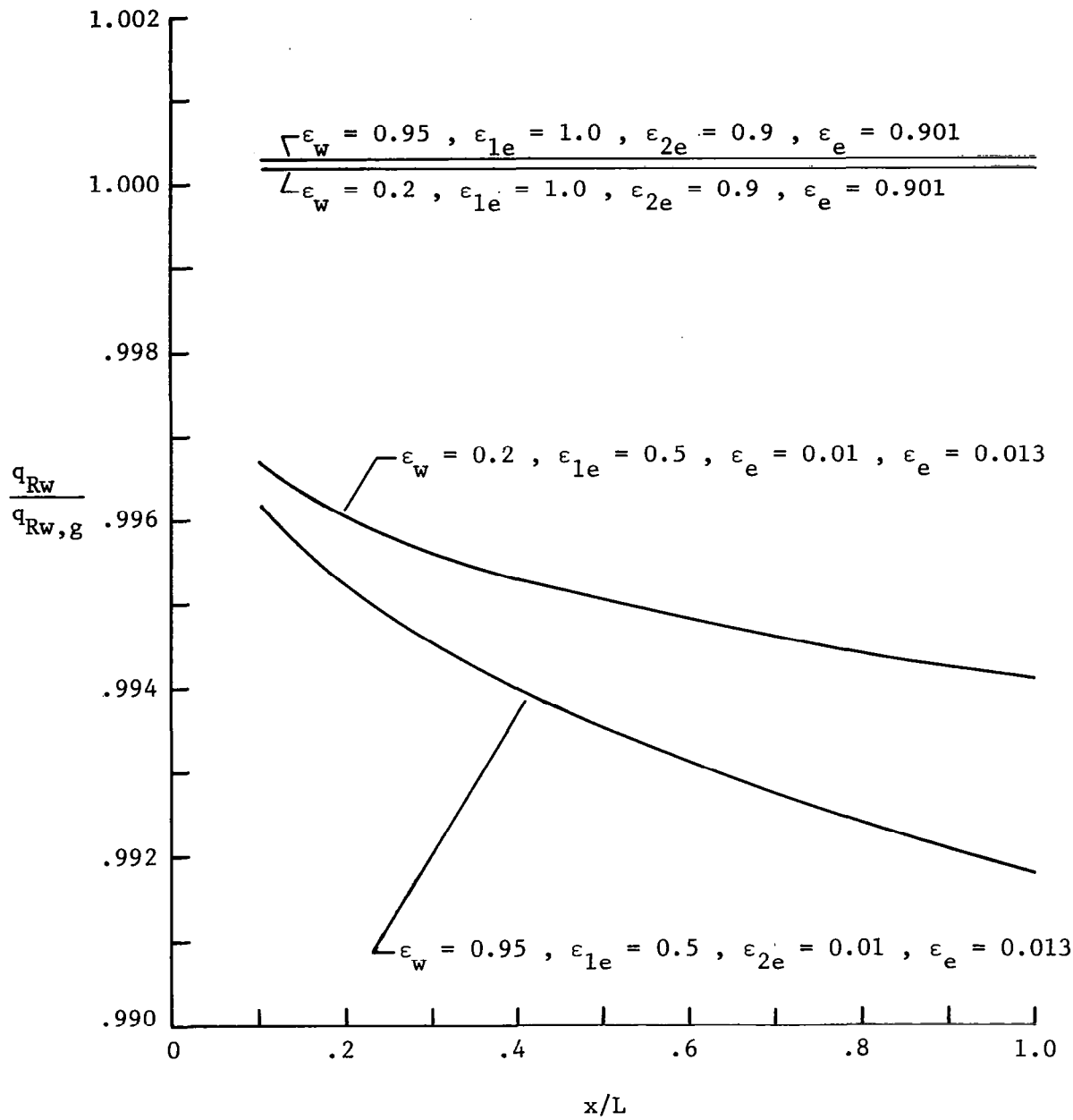

(a) $u_e^2/h_e = 16$, $T_e = 10\ 000°$ K, L = 10 m

Figure 11.- Ratio of the nongrey to grey radiative wall heat flux for the radiating air boundary layer on a flat plate; $P_e = 0.1$ atm, $T_w = 2000°$ K.

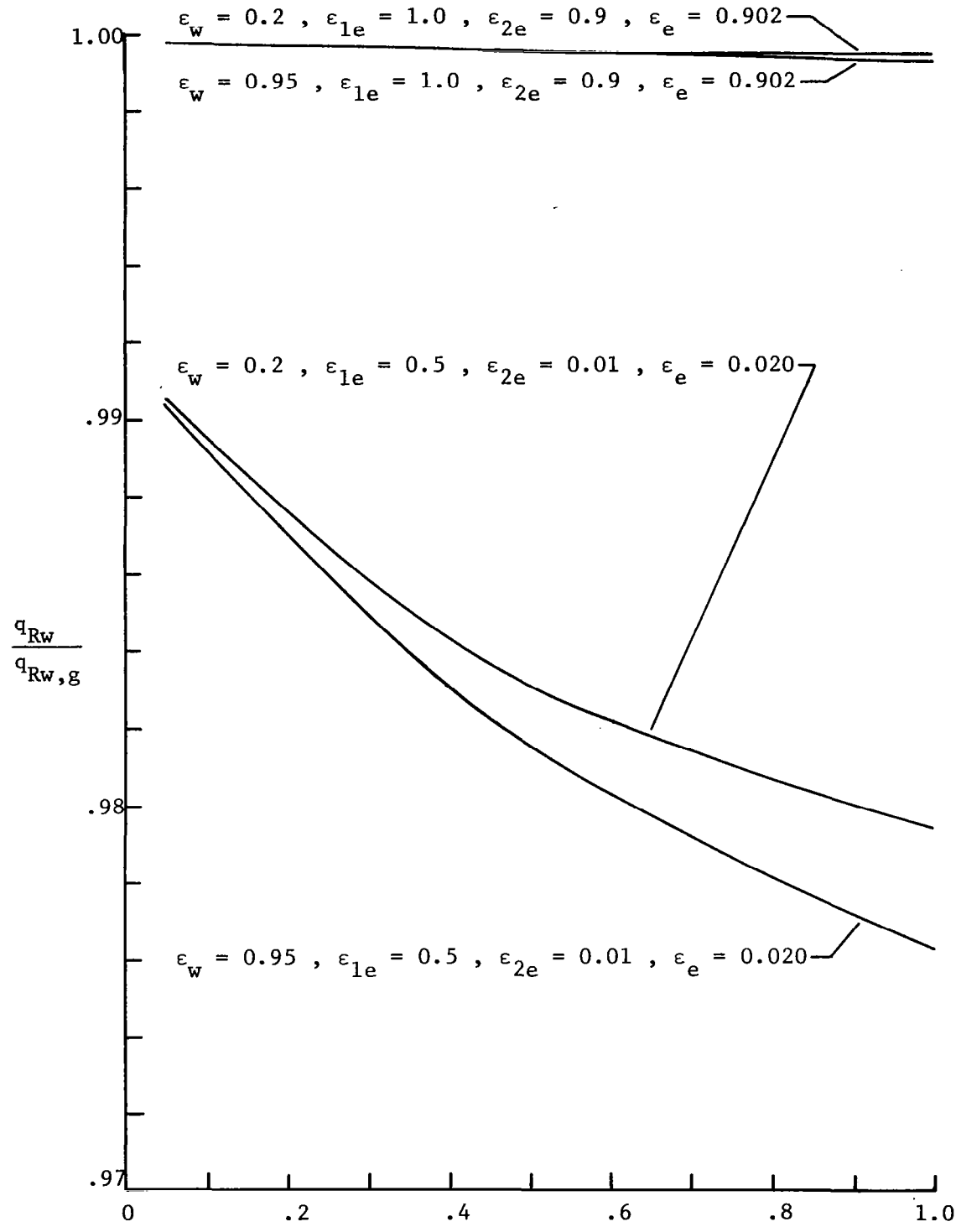

(b) $u_e^2/h_e = 0.7$, $T_e = 12\ 000°$ K, L = 3 m

Figure 11.-Concluded.

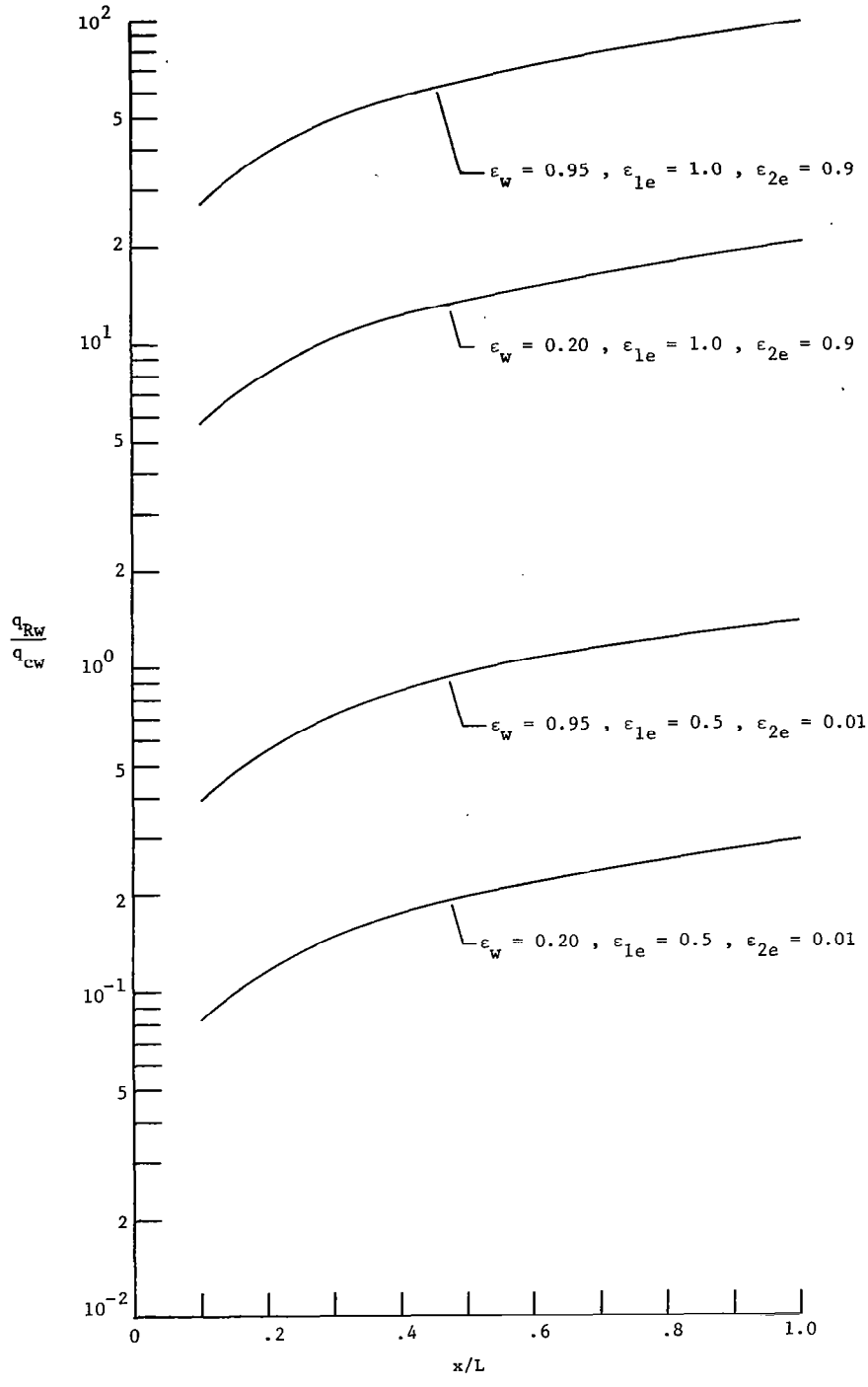

(a) $u_e^2/h_e = 16$, $T_e = 10\ 000°$ K, L = 10 m

Figure 12.- Ratio of the radiative to convective wall heat flux for the nongrey radiating air boundary layer on a flat plate; $P_e = 0.1$ atm, $T_w = 2000°$ K.

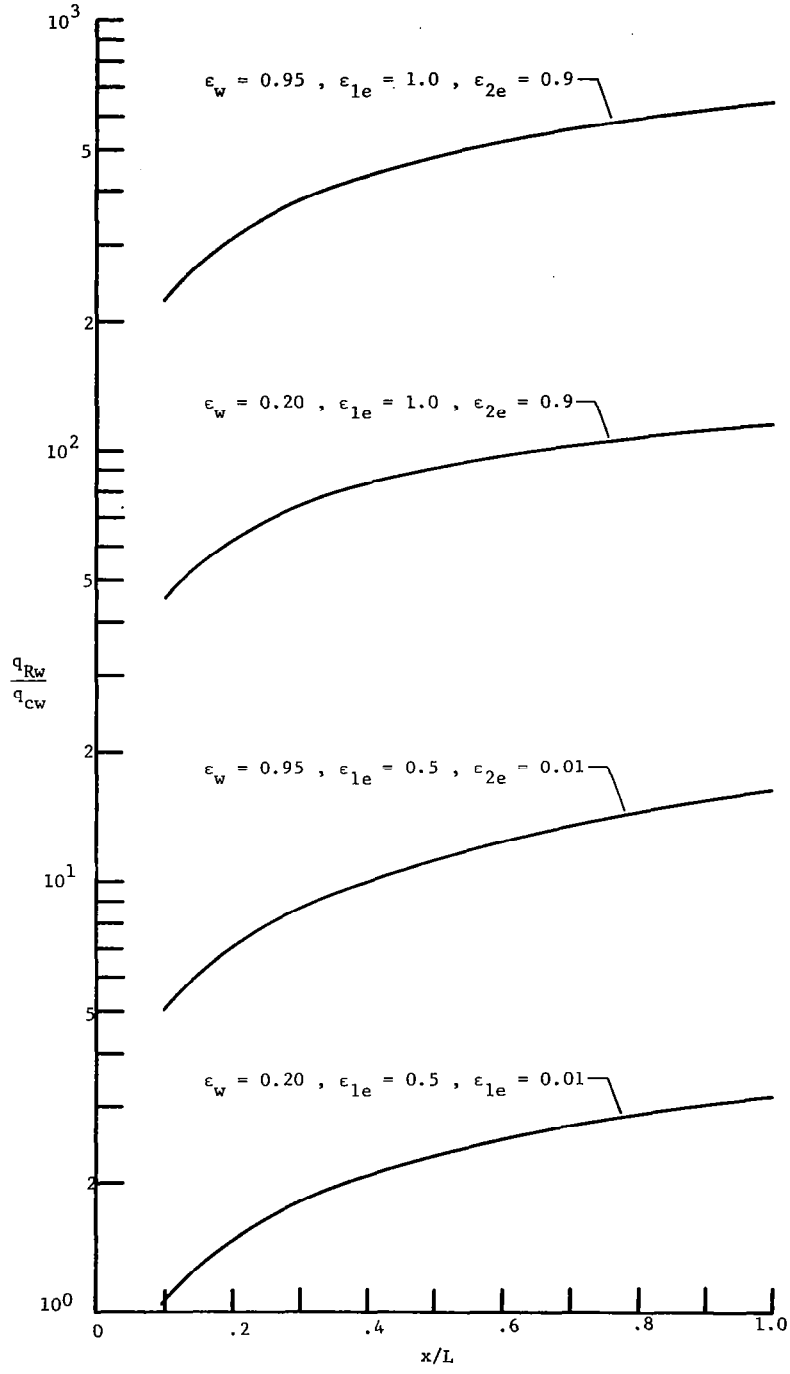

(b) $u_e^2/h_e = 0.7$, $\bar{T}_e = 12\ 000°$ K, L = 3 m

Figure 12.- Concluded.

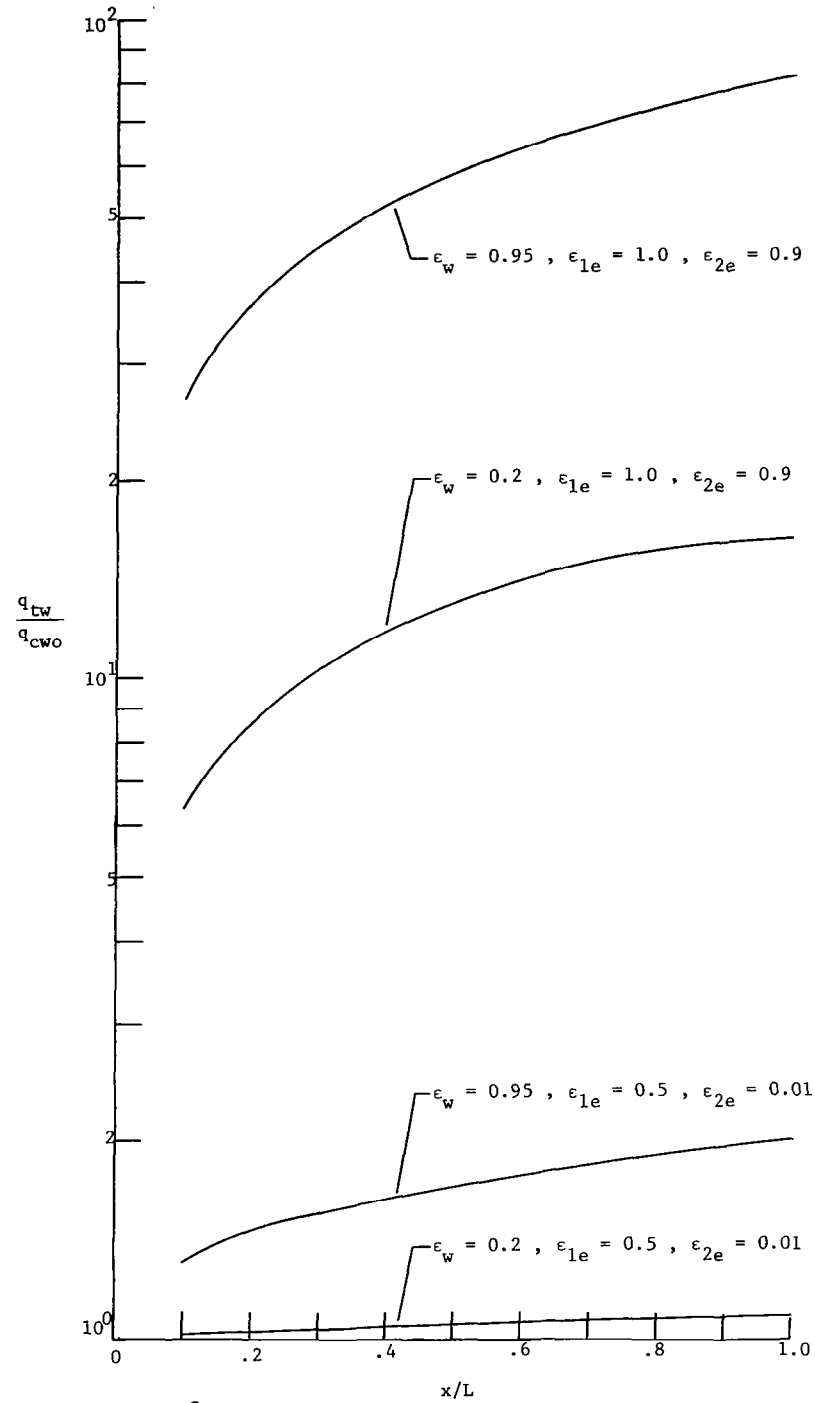

(a) $u_e^2/h_e = 16$, $T_e = 10\ 000°$ K, L = 10 m

Figure 13.- Ratio of the total wall heat flux for nongrey radiating air to the total wall heat flux for nonradiating air for the flat plate boundary layer; $P_e = 0.1$ atm, $T_w = 2000°$ K.

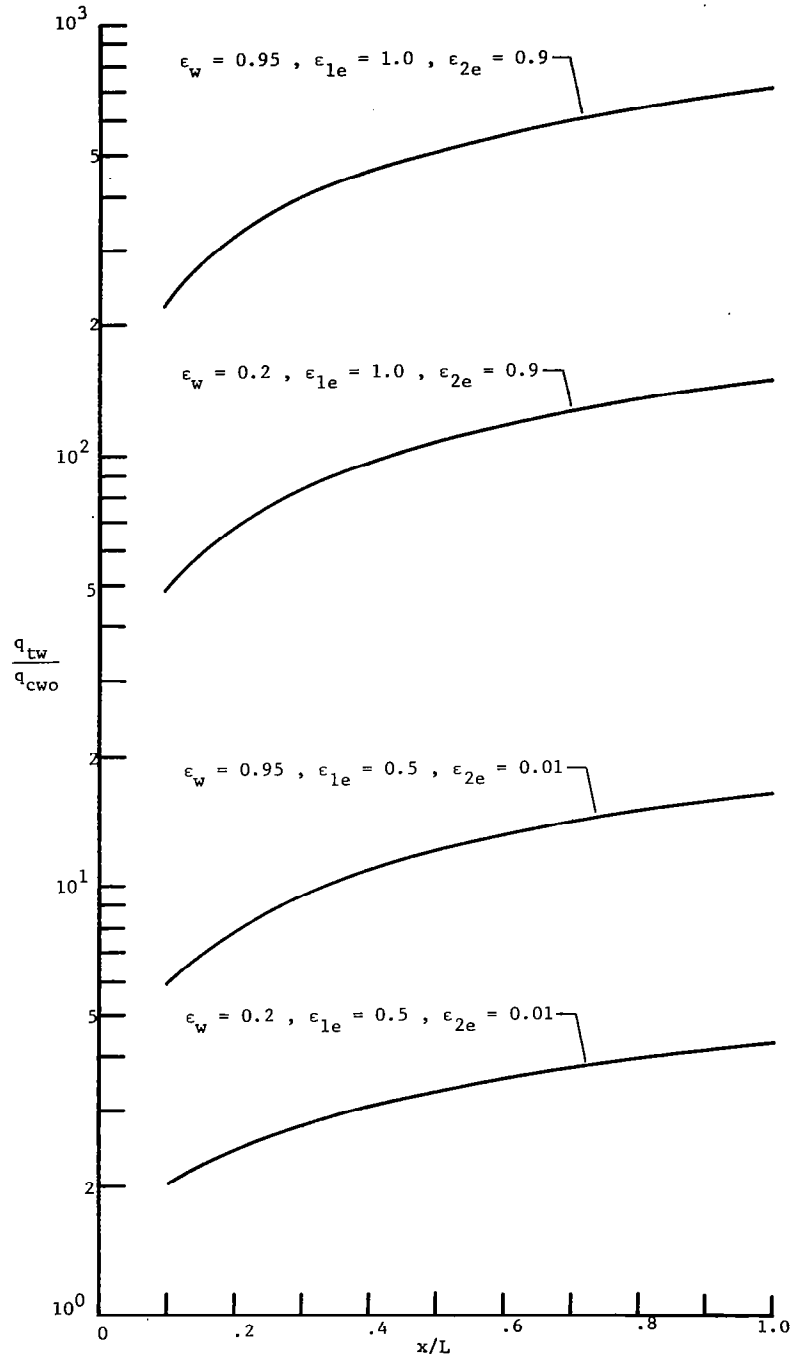

(b) $u_e^2/h_e = 0.7$, $T_e = 12\ 000°$ K, L = 3 m

Figure 13.- Concluded.

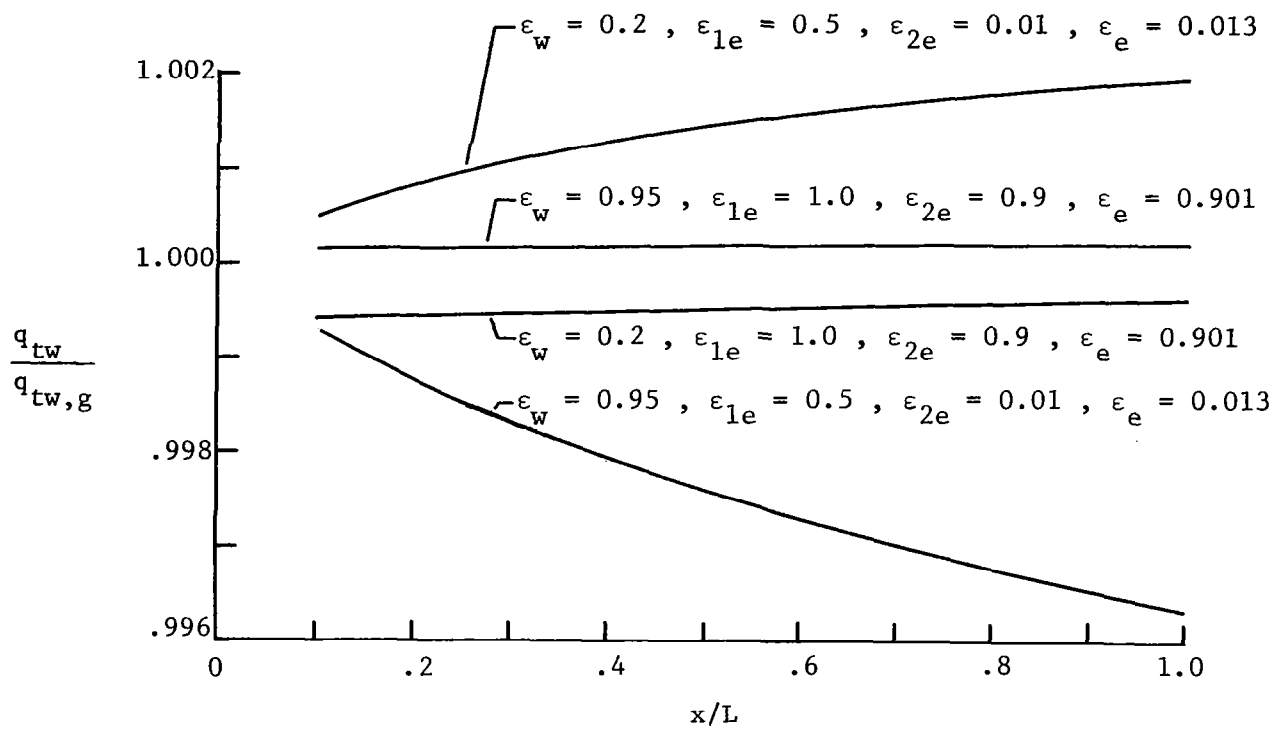

(a) $u_e^2/h_e = 16$, $T_e = 10\ 000°$ K, L = 10 m

Figure 14.- Ratio of the nongrey to grey total wall heat flux for the radiating air boundary layer on a flat plate; $P_e = 0.1$ atm, $T_w = 2000°$ K.

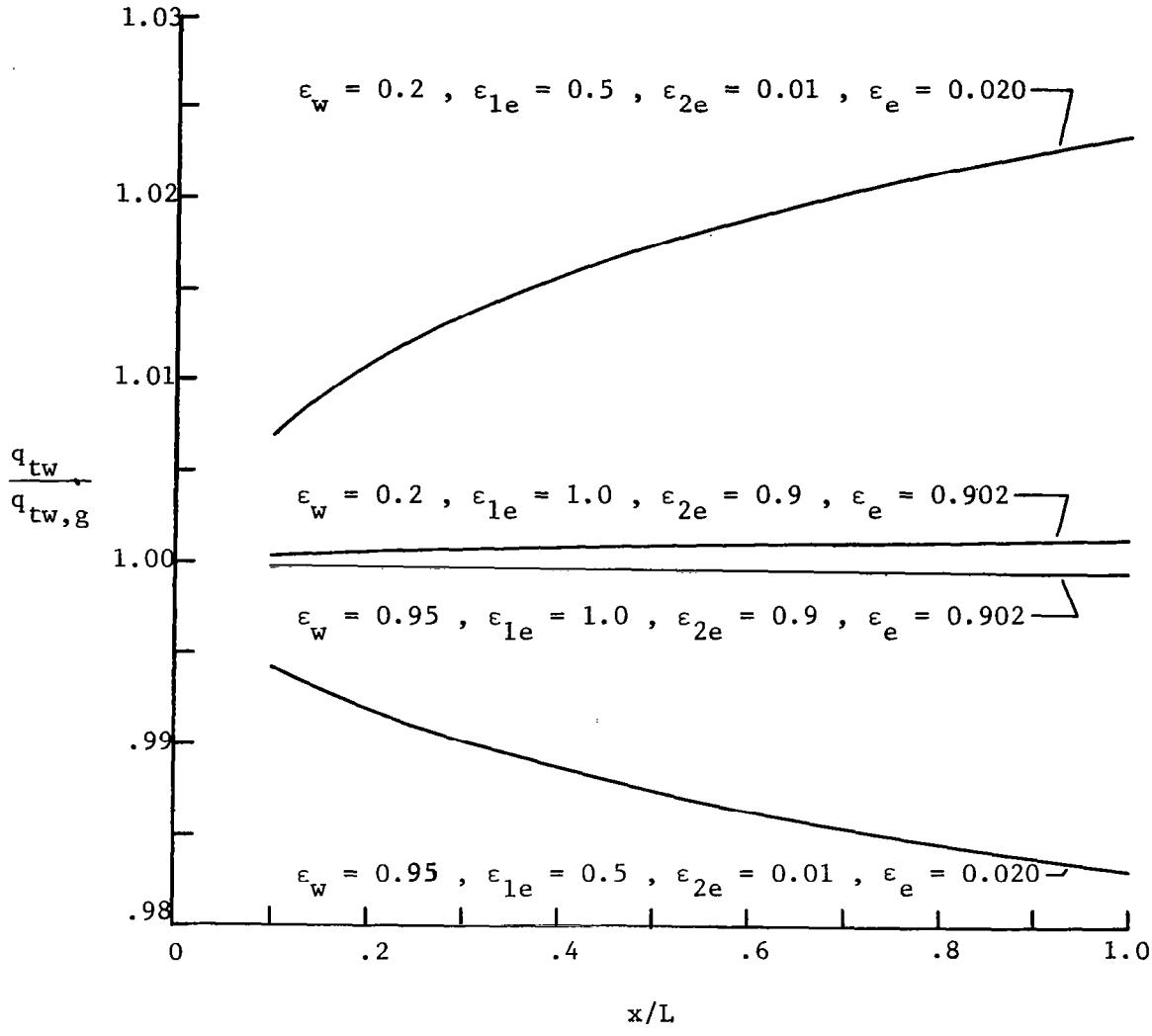

(b) $u_e^2/h_e = 0.7$, $T_e = 12\ 000°$ K, L = 3 m

Figure 14.- Concluded.

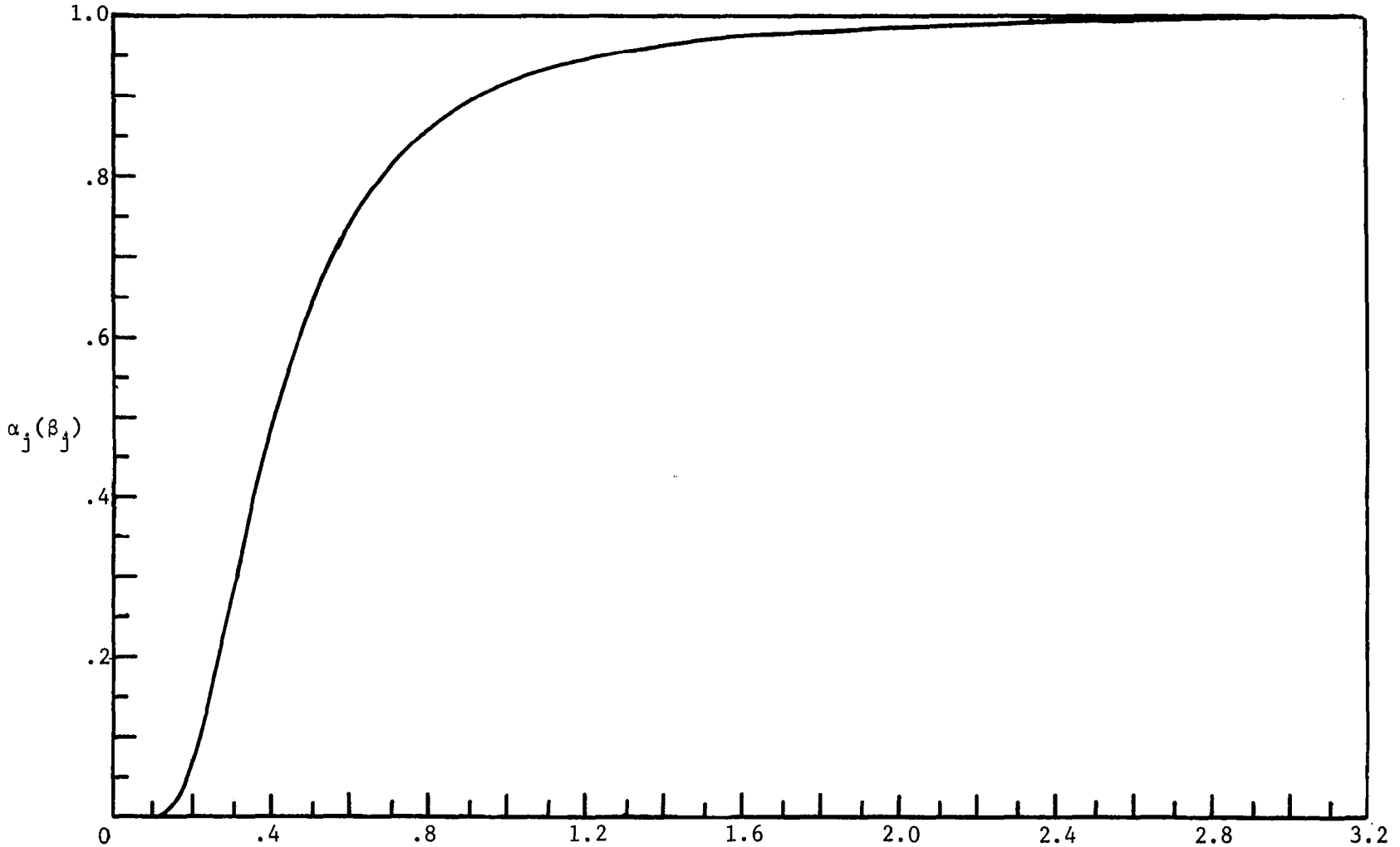

(a) $\lambda_j T \geq 0$

Figure 15.- $\alpha_j(\beta_j)$ as a function of $\lambda_j T$ where the numerical values plotted were taken from ref. 15.

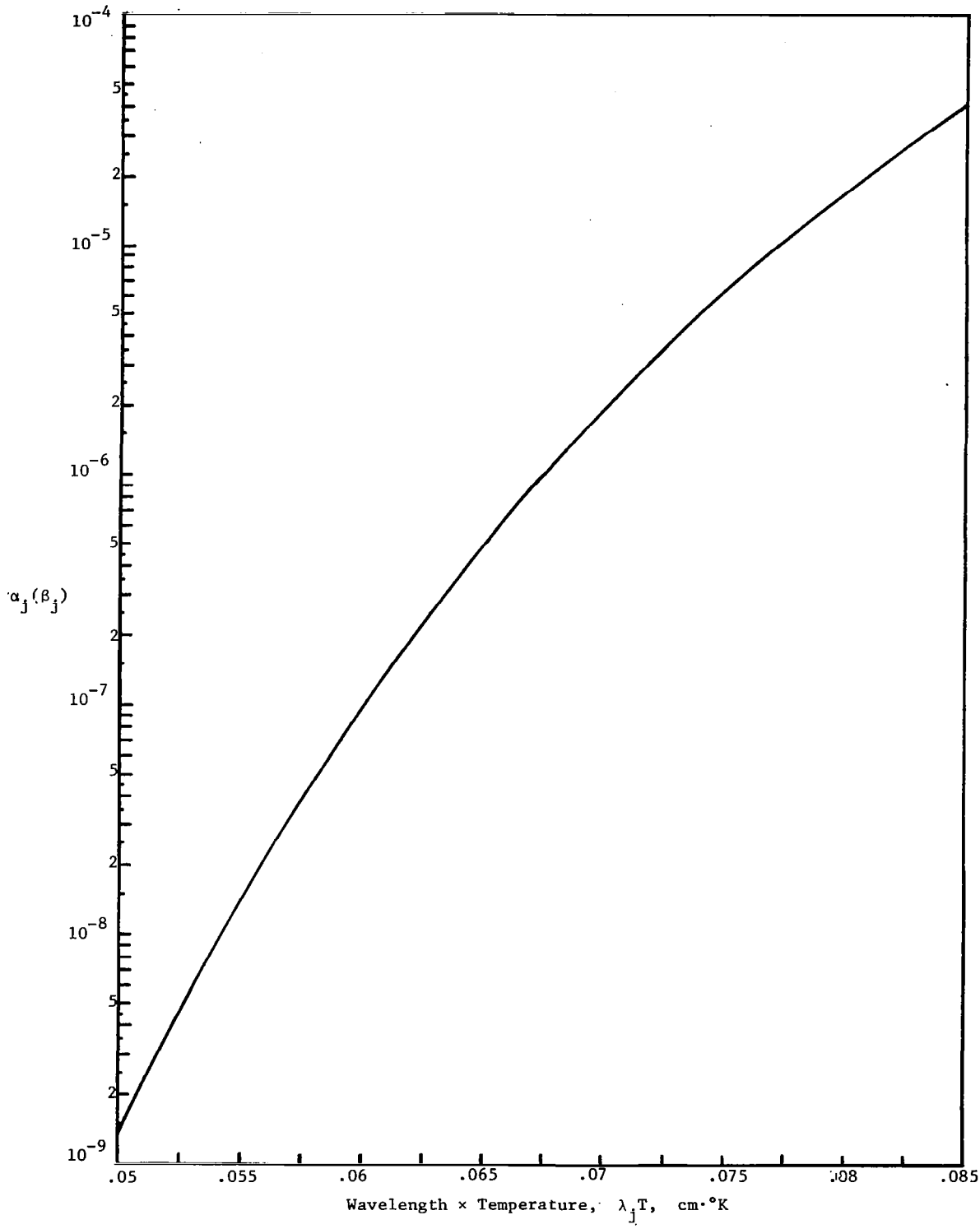

(b) $0.05 \leq \lambda_j T \leq 0.085$

Figure 15.- Continued.

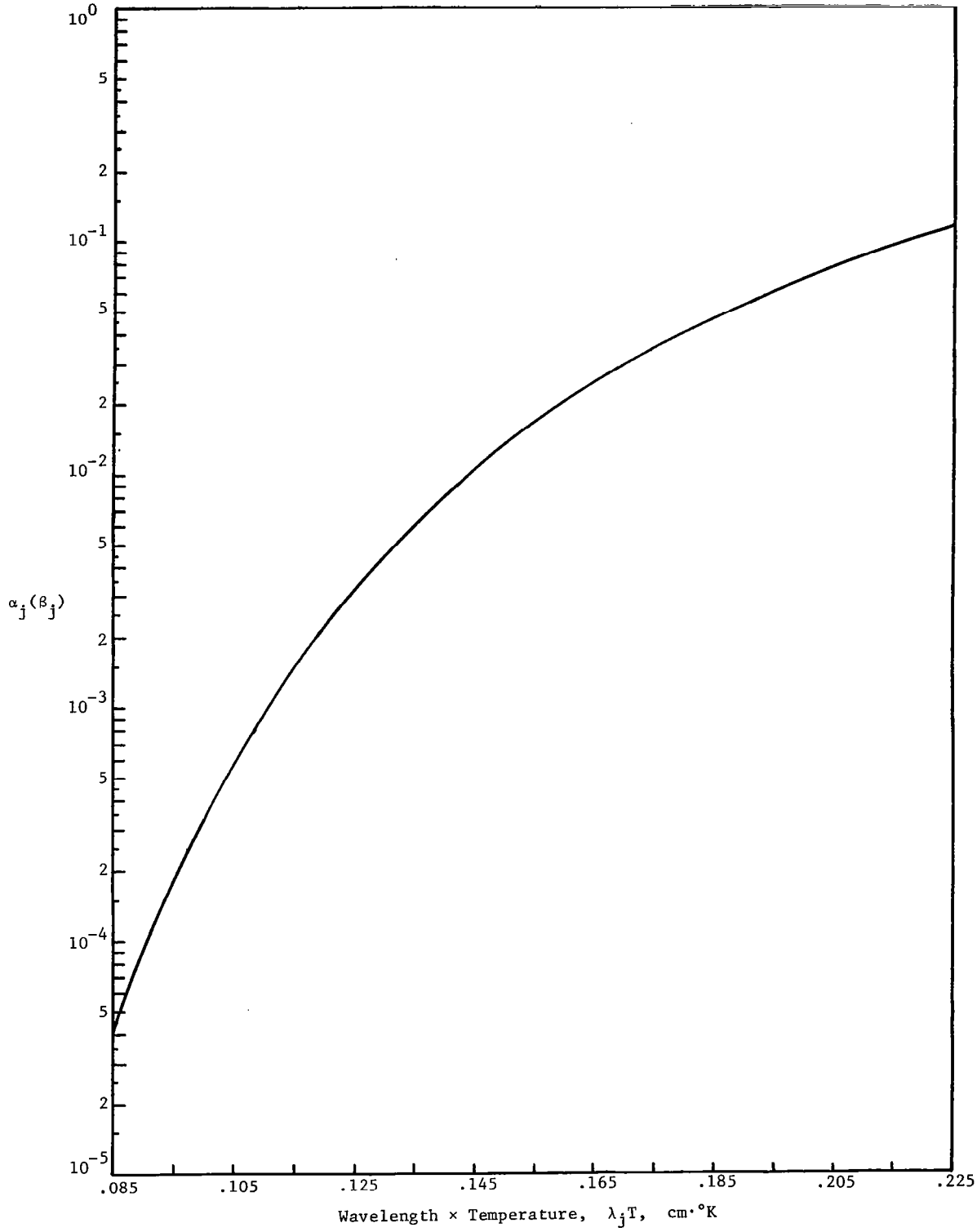

(c) $0.085 \leq \lambda_j T \leq 0.225$

Figure 15.- Concluded.

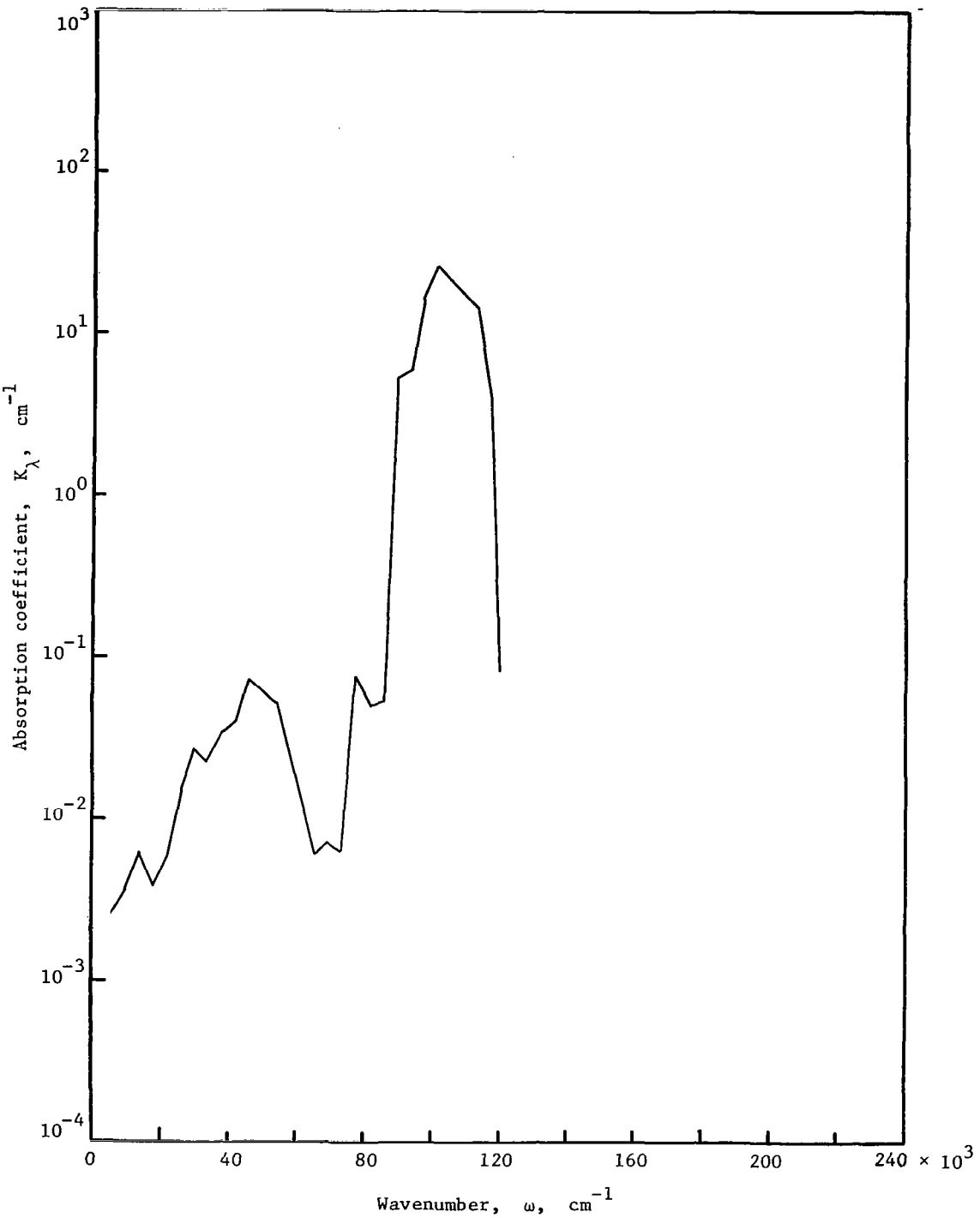

(a) T = 8000° K , $\rho/\rho_{s.l.} = 10^0$

Figure 16.- The linear spectral absorption coefficient of air as derived from ref. 3.

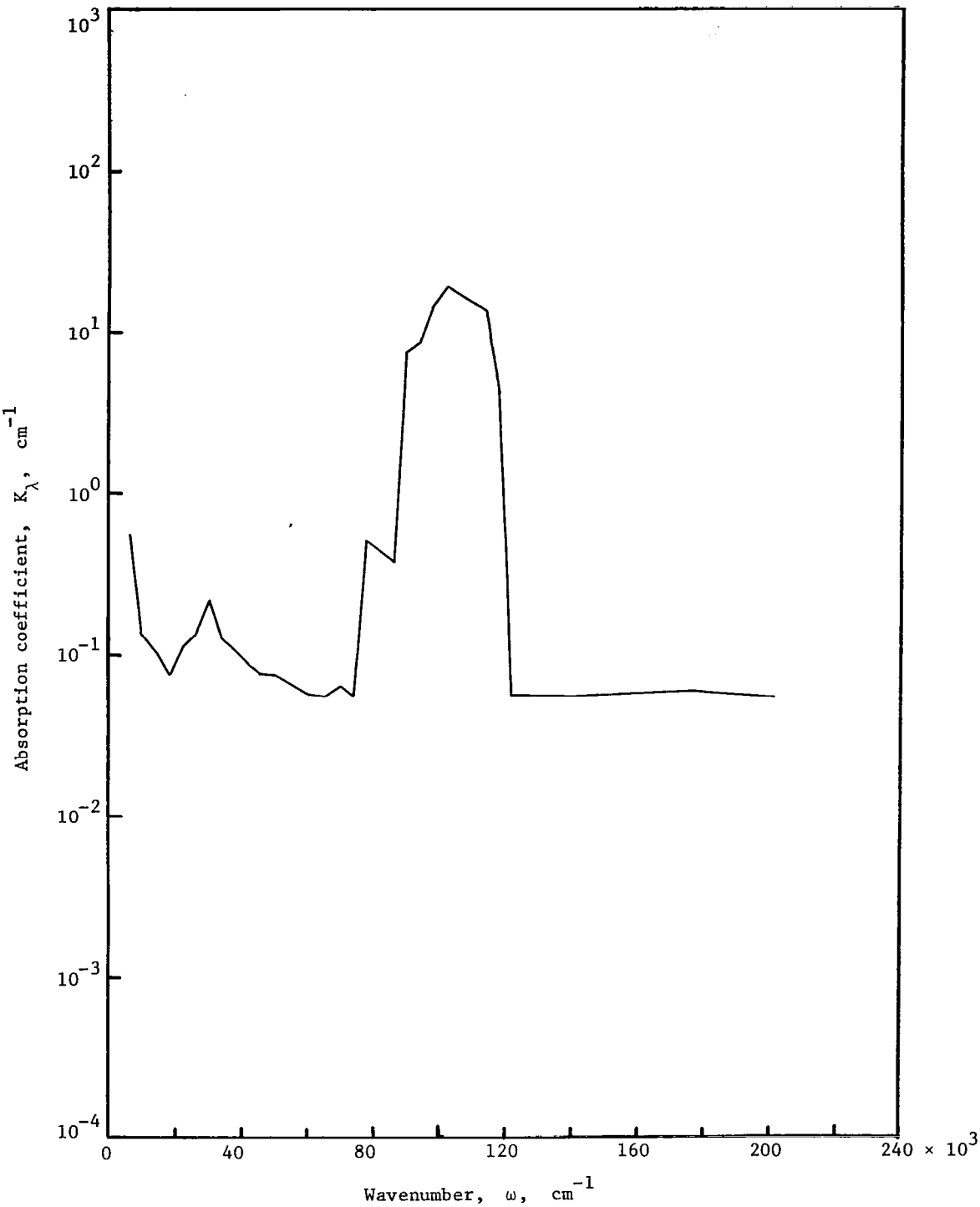

(b) T = 12 000° K , $\rho/\rho_{s.l.} = 10^0$

Figure 16.- Continued.

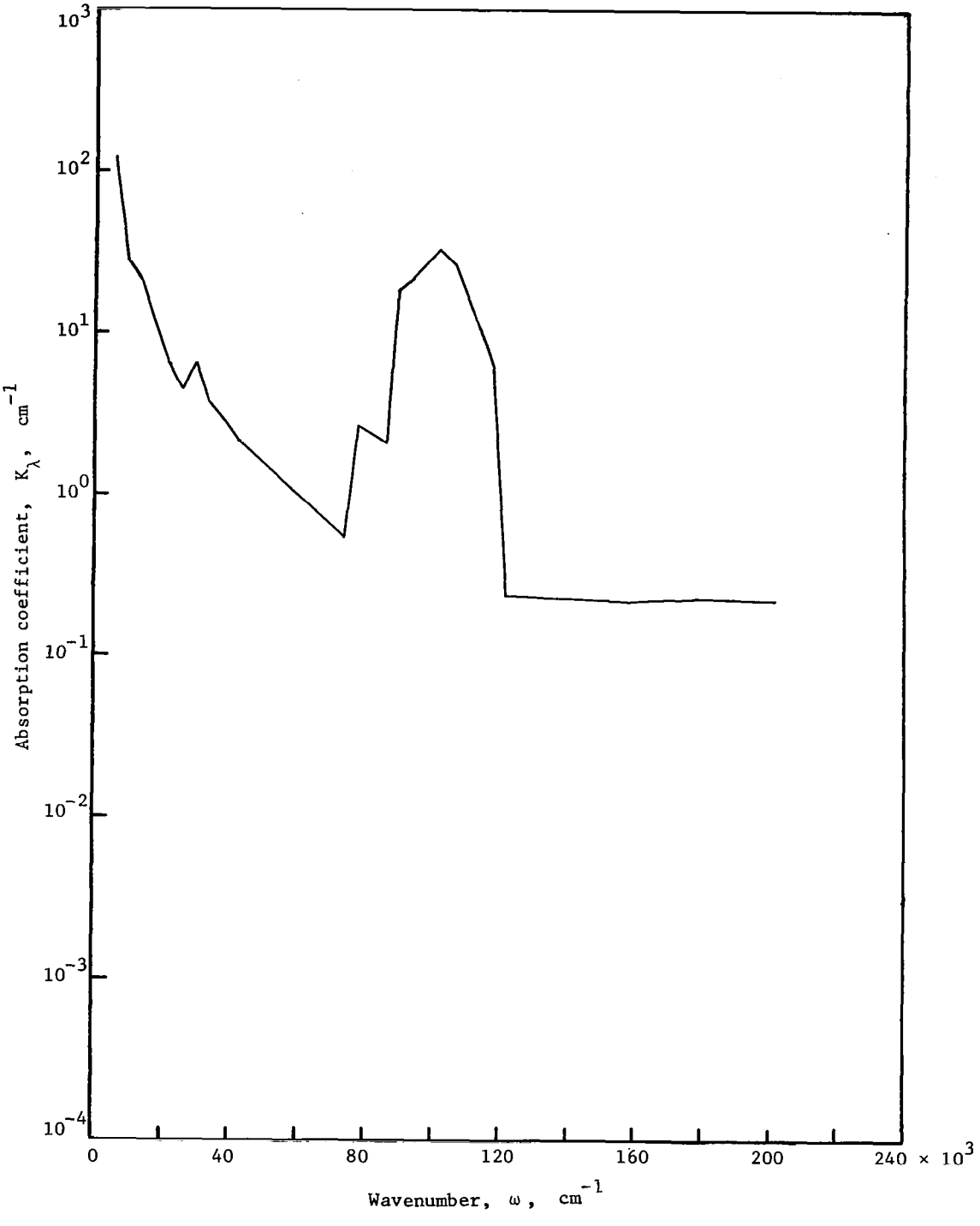

(c) T = 20 000° K , $\rho/\rho_{s.l.} = 10^0$

Figure 16.- Continued.

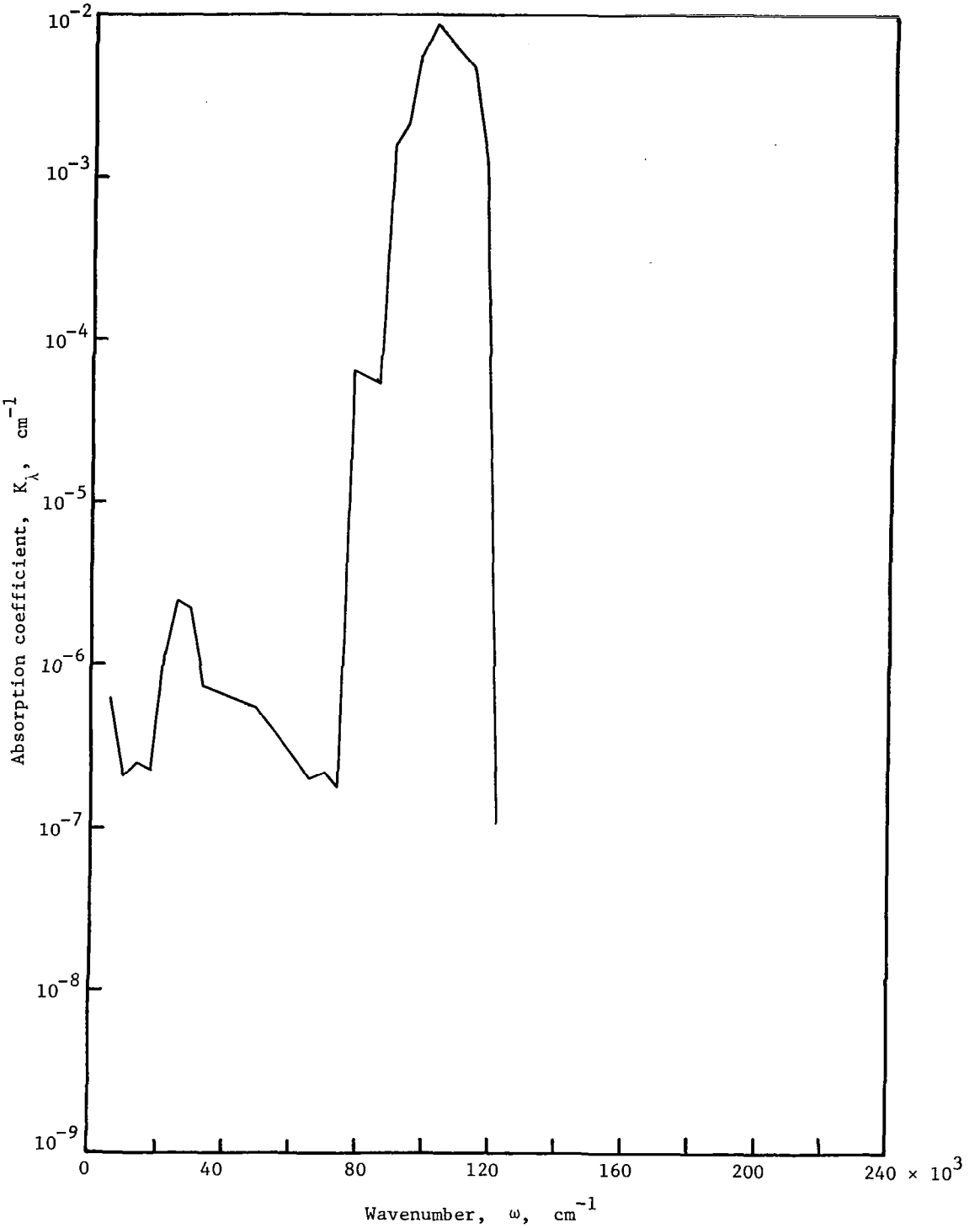

(d) $T = 8000°$ K , $\rho/\rho_{s.l.} = 10^{-3}$

Figure 16.- Continued.

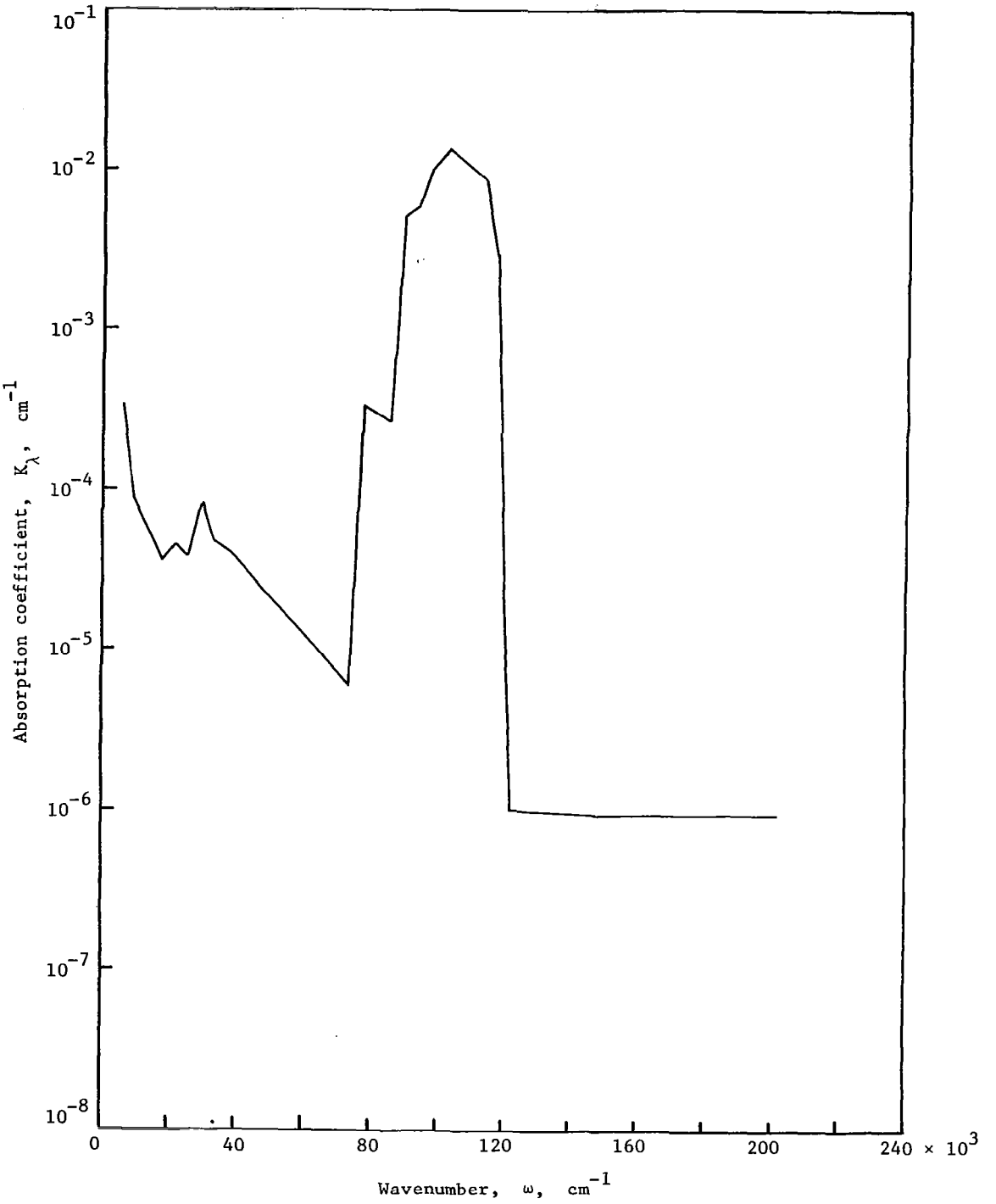

(e) T = 12 000° K , $\rho/\rho_{s.l.} = 10^{-3}$

Figure 16.- Continued.

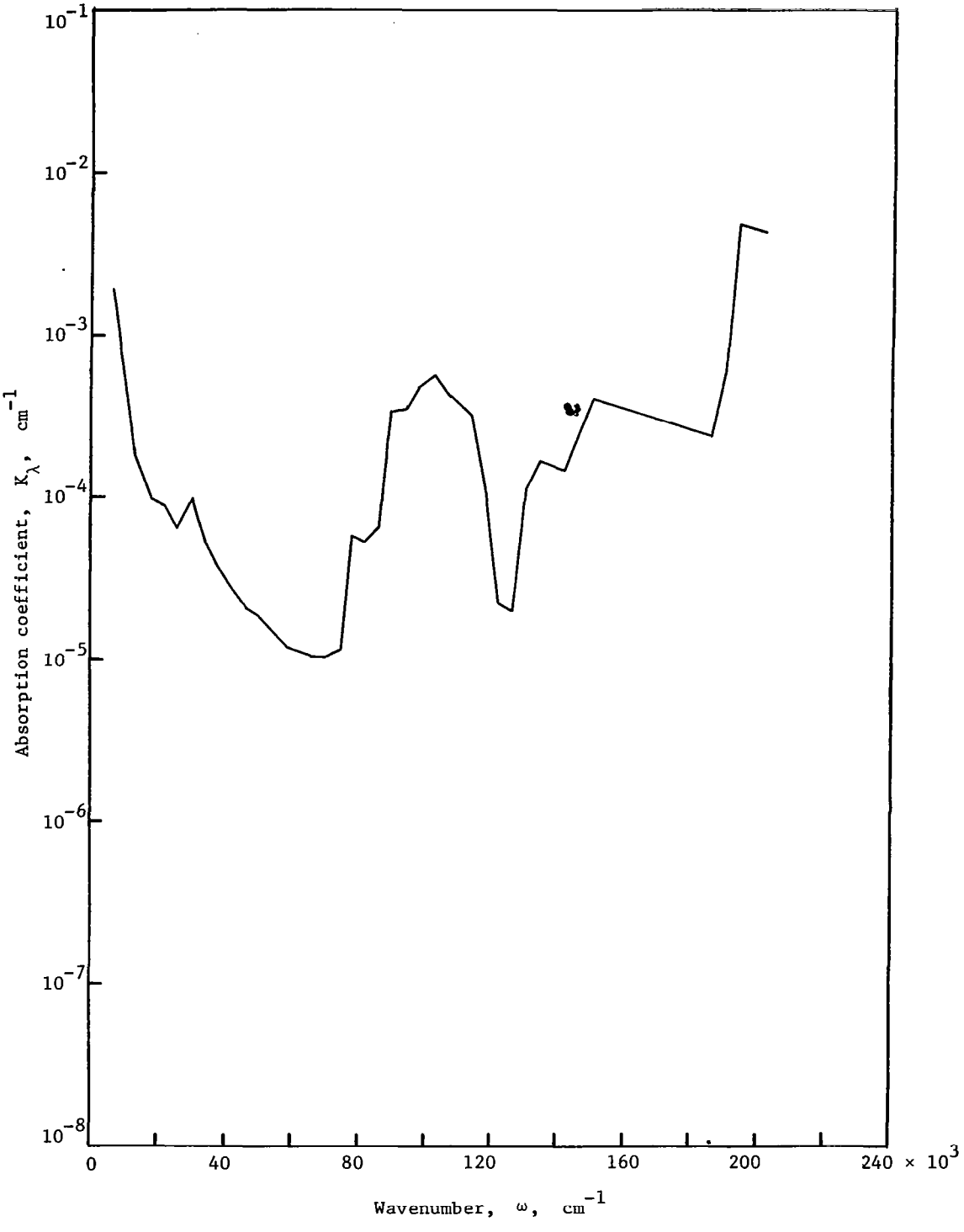

(f) T = 20 000° K , $\rho/\rho_{s.l.} = 10^{-3}$

Figure 16.- Continued.

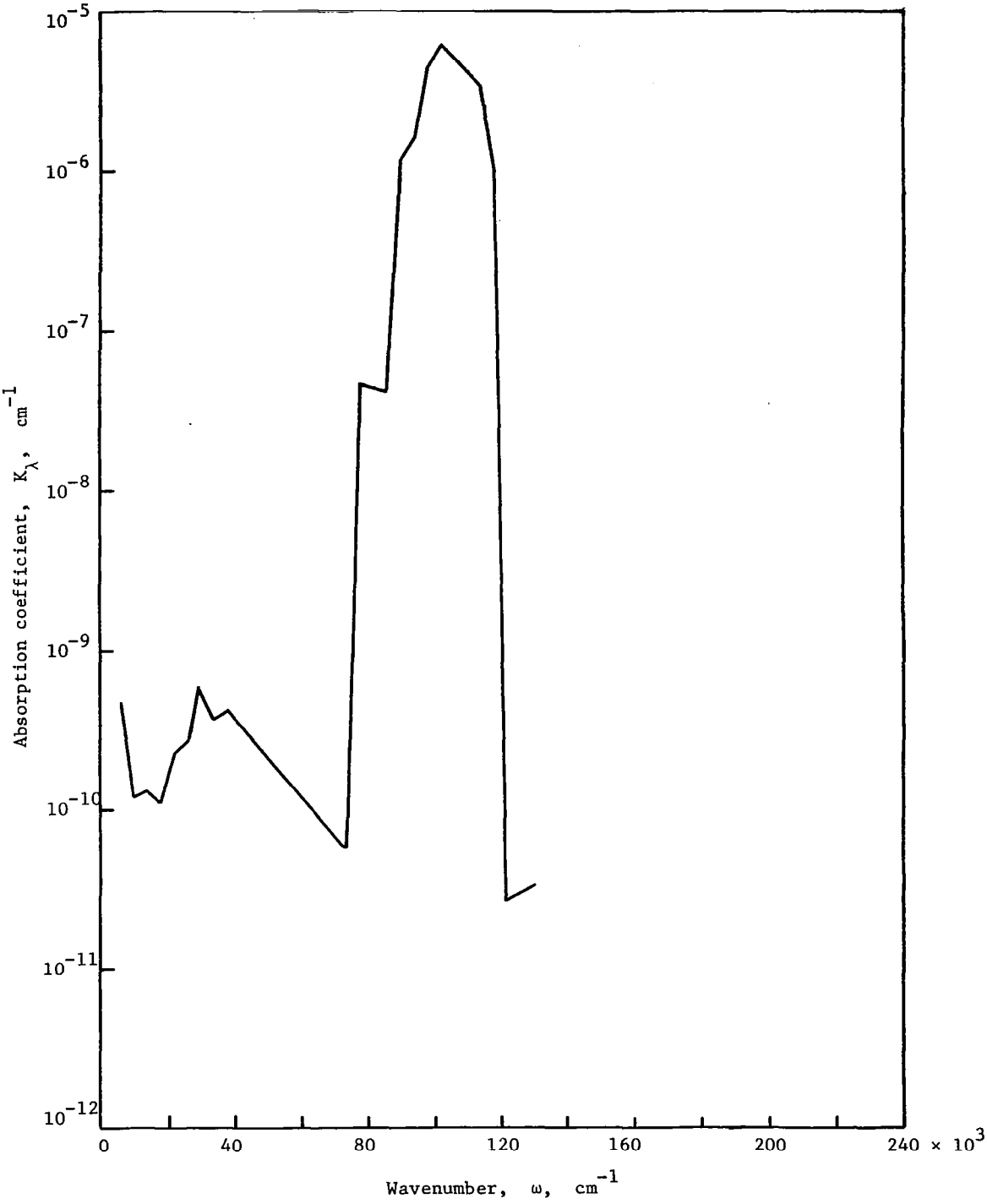

(g) T = 8000° K , $\rho/\rho_{s.l.} = 10^{-6}$

Figure 16.- Continued.

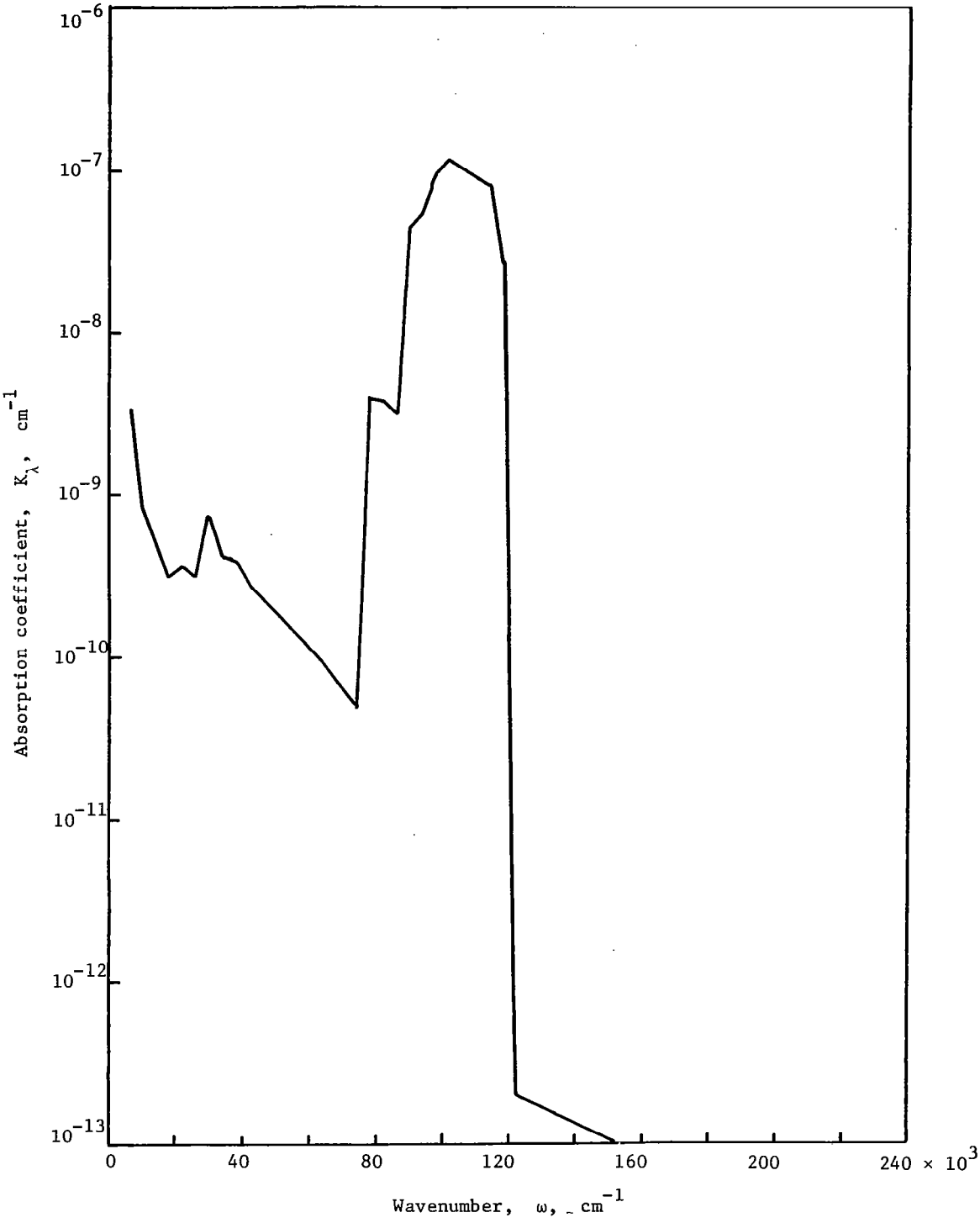

(h) T = 12 000° K , $\rho/\rho_{s.l.} = 10^{-6}$

Figure 16.- Continued.

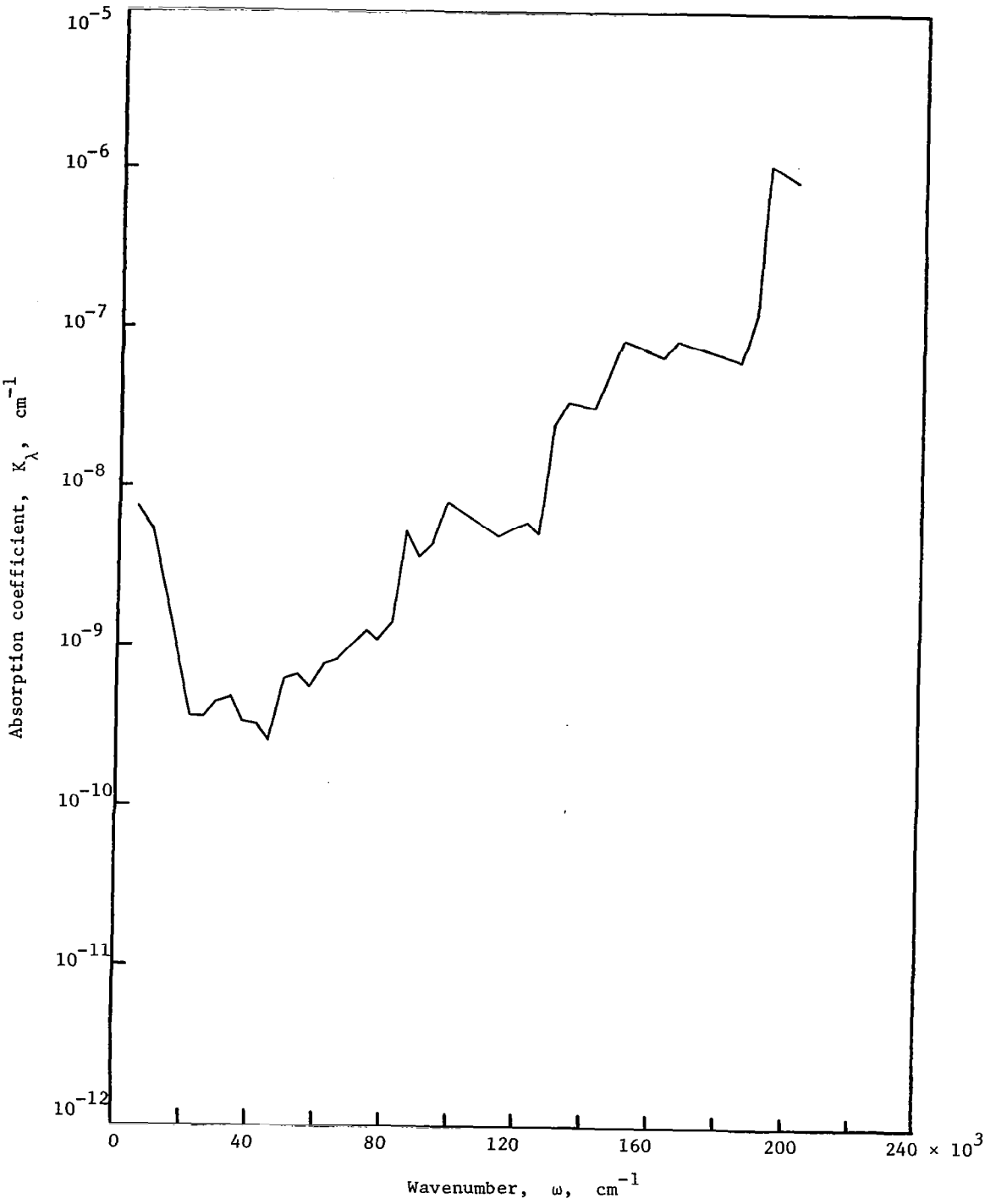

(i) T = 20 000° K , $\rho/\rho_{s.l.} = 10^{-6}$

Figure 16.- Concluded.

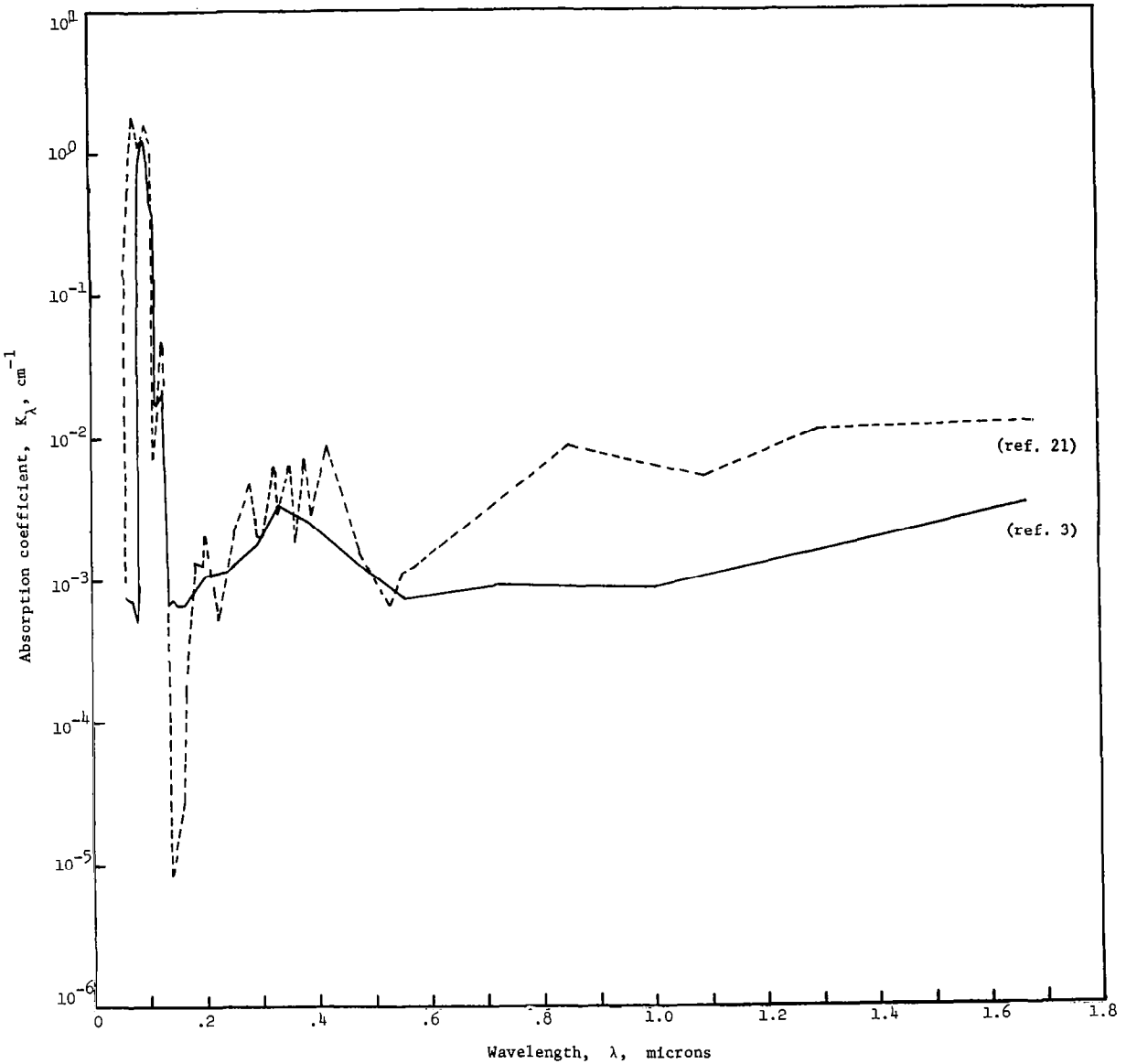

Figure 17.- Comparison of the spectral absorption coefficients derived from refs. 3 and 21, $T = 10\ 000°\ K$, $\rho/\rho_{s.l.} = 10^{-1}$.

NASA-Langley, 1966 CR-576

"The aeronautical and space activities of the United States shall be conducted so as to contribute . . . to the expansion of human knowledge of phenomena in the atmosphere and space. The Administration shall provide for the widest practicable and appropriate dissemination of information concerning its activities and the results thereof."

—NATIONAL AERONAUTICS AND SPACE ACT OF 1958

NASA SCIENTIFIC AND TECHNICAL PUBLICATIONS

TECHNICAL REPORTS: Scientific and technical information considered important, complete, and a lasting contribution to existing knowledge.

TECHNICAL NOTES: Information less broad in scope but nevertheless of importance as a contribution to existing knowledge.

TECHNICAL MEMORANDUMS: Information receiving limited distribution because of preliminary data, security classification, or other reasons.

CONTRACTOR REPORTS: Technical information generated in connection with a NASA contract or grant and released under NASA auspices.

TECHNICAL TRANSLATIONS: Information published in a foreign language considered to merit NASA distribution in English.

TECHNICAL REPRINTS: Information derived from NASA activities and initially published in the form of journal articles.

SPECIAL PUBLICATIONS: Information derived from or of value to NASA activities but not necessarily reporting the results of individual NASA-programmed scientific efforts. Publications include conference proceedings, monographs, data compilations, handbooks, sourcebooks, and special bibliographies.

Details on the availability of these publications may be obtained from:

SCIENTIFIC AND TECHNICAL INFORMATION DIVISION

NATIONAL AERONAUTICS AND SPACE ADMINISTRATION

Washington, D.C. 20546